Real-time UV-Index retrieval in Europe using Earth Observation based techniques: system description and quality assessment

Panagiotis G. Kosmopoulos[1], Stelios Kazadzis[2], Alois W. Schmalwieser[3], Panagiotis I. Raptis[1], Kyriakoula Papachristopoulou[1], Ilias Fountoulakis[1,4], Akriti Masoom[5], Alkiviadis F. Bais[6], Julia Bilbao[7], Mario Blumthaler[8], Axel Kreuter[8,9], Anna Maria Siani[10], Kostas Eleftheratos[11], Chrysanthi Topaloglou[6], Julian Gröbner[2], Bjørn Johnsen[12], Tove M. Svendby[13], Jose Manuel Vilaplana[14], Lionel Doppler[15], Ann R. Webb[16], Marina Khazova[17], Hugo De Backer[18], Anu Heikkilä[19], Kaisa Lakkala[20], Janusz Jaroslawski[21], Charikleia Meleti[5], Henri Diémoz[4], Gregor Hülsen[2], Barbara Klotz[8], John Rimmer[16], Charalampos Kontoes[1]

[1]National Observatory of Athens, Athens, Greece
[2]Physikalisch-Meteorologisches Observatorium Davos, World Radiation Center, Davos Dorf, Switzerland
[3]University of Veterinary Medicine, Vienna, Austria
[4]Environmental Protection Agency of Aosta Valley, Aosta, Italy
[5]Indian Institute of Technology Roorkee, India
[6]Aristotle University of Thessaloniki, Greece
[7]Valladolid University, Valladolid, Spain
[8]Innsbruck Medical University, Innsbruck, Austria
[9]Luftblick OG, Innsbruck, Austria
[10]Sapienza University of Rome, Rome, Italy
[11]National and Kapodistrian University of Athens, Athens, Greece
[12]Norwegian Radiation and Nuclear Safety Authority, Bærum, Norway
[13]NILU - Norwegian Institute for Air Research, Kjeller, Norway
[14]National Institute for Aerospace Technology, Torrejón de Ardoz, Spain
[15]German Weather Service, Offenbach, Germany
[16]University of Manchester, Manchester, UK
[17]Public Health England, London, UK
[18]Royal Meteorological Institute of Belgium, Bruxelles, Belgium
[19]Finnish Meteorological Institute, Helsinki, Finland
[20]Finnish Meteorological Institute, Sodankylä, Finland
[21]Institute of Geophysics, Polish Academy of Sciences, Warsaw, Poland

Correspondence to: P.G. Kosmopoulos (pkosmo@noa.gr)

Abstract. This study introduces an Earth observation (EO)-based system which is capable of operationally estimating and continuously monitoring the ultraviolet index (UVI) in Europe. The UVIOS (i.e. UV-Index Operating System) exploits a synergy of radiative transfer models with high performance computing and EO data from satellites (Meteosat Second Generation and Meteorological Operational Satellite-B), and retrieval processes (Tropospheric Emission Monitoring Internet Service, Copernicus Atmosphere Monitoring Service and the Global Land Service). It provides a near-real-time now-casting

and short-term forecasting service for UV radiation over Europe. The main atmospheric inputs for the UVI simulations include ozone, clouds and aerosols while the impacts of ground elevation and surface albedo are also taken into account. The UVIOS output is the UVI at high spatial and temporal resolution (5 km and 15 minutes, respectively) for Europe (i.e. 1.5 million pixels) in real-time. The UVI is empirically related to biologically important UV dose rates and the reliability of this EO-based solution was verified against ground-based measurements from 17 stations across Europe. Stations are equipped with spectral, broadband or multi-filter instruments and cover a range of topographic and atmospheric conditions. A period of over one year of forecasted 15-min retrievals under all sky conditions were compared with the ground–based measurements. UVIOS forecasts were within ±0.5 of measured UVI for at least 70% of the data compared at all stations. For clear sky conditions the agreement was better than 0.5 UVI for 80% of the data. A sensitivity analysis of EO inputs and UVIOS outputs was performed in order to quantify the level of uncertainty in the derived products, and to identify the covariance between the accuracy of the output and the spatial and temporal resolution, and the quality of the inputs. Overall, UVIOS slightly overestimated UVI due to observational uncertainties in inputs of cloud and aerosol. This service will hopefully contribute to EO capabilities and will assist the provision of operational early warning systems that will help raise awareness among European Union citizens of the health implications of high UVI doses.

Keywords. Ultraviolet Index; Earth Observation; Radiative Transfer; High Performance Computing; Clouds; Aerosols; Ozone; Solar Zenith Angle; Ground Elevation; Surface Albedo

1 Introduction

Human exposure to ultraviolet (UV) radiation (<400 nm) has both beneficial and harmful effects (Andrady et al., 2015; Juzeniene et al., 2011; Lucas et al., 2006). Overexposure to UV radiation (UVR) has a number of implications, such as the acute response of erythema, the risk of skin cancer and a number of eye diseases (snow blindness, cataract). Nevertheless, exposure to solar UVB radiation (290-315 nm) is the main mechanism for the synthesis of Vitamin D in the human skin (Holick, 2002; Webb and Engelsen, 2008; Webb et al., 2011). Low levels of the Vitamin D are associated with depression of the immune system and there is evidence that is linked to a number of medical implications (Lucas et al., 2015).

The UV index was introduced by WHO/WMO in 1994 (WMO, 1995), as a simple method of informing the general public about the erythema effective (sun-burning) UV. It is a unitless, scaled version of erythemally-weighted UV determined by multiplying the erythema weighted irradiance (in W/m^2) by 40 m^2/W (Fioletov et al., 2010 ; Vanicek et al., 2000; WHO, 2002).

The response of UV radiation to climatic changes is of great concern (Bais et al., 2019; Bais et al., 2018; McKenzie et al., 2011). According to the latest work of Bais et al. (2019) greater values of UV are expected by the end of 21st century, relative to the present decade, at low latitudes, while at higher latitudes UV will decrease but these projections are associated with high uncertainty (up to 30%).

There are many factors affecting UV irradiance reaching Earth's surface (Kerr and Fioletov, 2008). The dependence of UV irradiance on astronomical and geometrical parameters is generally well understood, and in many cases the changes are periodical (e.g., (Blumthaler et al., 1997; Gröbner et al., 2017; Larkin et al., 2000; Seckmeyer et al., 2008)). Atmospheric gases play a crucial role in attenuating UV irradiance, specifically NO_2 is a major absorber in the UV (e.g., Cede et al. (2006)), while O_3 is the main absorber at lower (UVB) wavelengths. Other gases that have significant absorption in the UV include SO2 (Fioletov et al., 1998) and HCHO (Gratien et al., 2007), but their –usually- smaller atmospheric abundances, result in minor effects to incoming UV (with major exceptions such as volcanic incidents). Aerosols are another important parameter controlling UV irradiance levels at the surface (e.g., Kazadzis et al. (2009b)). Aerosol optical depth (AOD) that quantifies the attenuation of the direct solar beam by aerosols is a parameter varying with wavelength. Single scattering albedo (SSA), which determines the scattering ratio to total extinction, is also a spectrally variant parameter. Several recent studies based on surface UV irradiance measurements or calculations reveal the enhanced absorption by aerosols in the UV relative to the visible spectral range. Finally, a number of studies have highlighted the importance of using representative SSA in the UV spectral region, instead of interpolating SSA at visible wavelengths to the UV, or directly using SSA at visible wavelengths, options that systematically overestimate UV irradiance (Corr et al., 2009; Fountoulakis et al., 2019; Kazadzis et al., 2016; Mok et al., 2018; Raptis et al., 2018).

All the aforementioned parameters are particularly important under cloud free conditions. The cloudy sky complicates the propagation of solar radiation, predominantly in the troposphere, through multiple cloud - radiation interactions. Nonetheless, UVR is less affected than the total solar radiation by clouds (e.g., Badosa et al. (2014)). Bais et al. (1993) quantified that for the city of Thessaloniki the change from 0 to 8 oktas for cloud coverage corresponds to 80% reduction in the UVR and pointed out that there is very low wavelength dependence of UVR attenuation by cloud cover. Although, the transmittance of clouds does not vary significantly with wavelength, some studies (Mayer et al., 1998; Seckmeyer et al., 1996) have found that the diffuse component of the surface UVR is affected by clouds in a spectrally dependent way, due to more efficient scattering and absorption of shorter UV wavelengths, in case of large air masses. In cases of partially cloudy sky but unobscured sun, UVR tends to be higher than in clear sky conditions (e.g., Badosa et al. (2014)), as is the case for total solar radiation. For short timescale analysis the variability of UVR introduced by clouds should be considered.

Solar UV irradiance at the surface increases with increasing surface albedo. This increment affects the UV radiant exposure, which becomes crucial for outdoor human activities (Schmalwieser and Siani, 2018; Schmalwieser, 2020; Siani et al., 2008). Measurements and computations of effective surface albedo for heterogeneous surfaces reveal its strong spectral dependence, with snow-covered surfaces having significantly higher values of albedo for short wavelengths compared to total solar radiation (Blumthaler and Ambach, 1988; Kreuter et al., 2014). Stronger enhancement of the UV relative to visible radiation over highly reflective surfaces is also due to the more effective multiple scattering of shorter wavelengths in the atmosphere.

Any systematic changes in any of the parameters described in previous paragraphs have the potential to lead to changes for UVR. These changes vary significantly throughout the globe and are attributed to different possible drivers (Bernhard and Stierle, 2020; Fountoulakis et al., 2018; McKenzie et al., 2019). Fountoulakis et al. (2020a) gives a review of recent

publications concerning UV trends since 1990s, and associated factors, summarizing these as positive trends for South and Central Europe and negative trends at higher latitudes, and recognizing the important role of aerosols and cloud coverage for these trends. Chubarova et al. (2020) found a long term increase of 3% per decade in UV at Northern Eurasia for the 1979-2015 period. For the northern mid-latitudes Zerefos et al. (2012) showed that the long-term (1995-2006) positive trend in total ozone wasn't enough to compensate for, let alone reverse, the UVB increase attributed to tropospheric aerosol decline (brightening effect). Since 2007, a slowdown or even a possible turning point in the positive UVB trend was detected, which was attributed to the continued upward trend in total ozone overwhelming the aerosol effect (Zerefos et al., 2012). By contrast, the long-term variability of UVB irradiance over northern high latitudes was determined by ozone and not by aerosol trends, as shown by Eleftheratos et al. (2015) who found a statistically significant negative trend of -3.9% per decade for the UVB irradiance during the time period 1999-2011, in agreement with statistically significant increase of spaceborne measured total ozone by about 1.5% per decade (ozone recovery) for the same area.

The continuous monitoring of the UV index is currently performed by about 160 stations from 25 countries around Europe (Schmalwieser et al., 2017), with all monitoring instruments having the potential to provide other effective doses such as the effective dose for the production of vitamin D in human skin (e.g., Fioletov et al. (2009)).

There are three types of instruments for UV irradiance measurements; those measuring the integral of UV irradiance (broadband sensors) tailored to a specific response, narrow band instruments such as filter radiometers with coarse spectral resolution, and instruments performing high resolution spectral measurements – the most versatile but most challenging and least robust instruments. Concerning the current UV monitoring measurement accuracy; The European reference UV spectroradiometer (QASUME) is a traveling instrument which provides a common standard through inter-comparison on-site (Gröbner et al., 2005; Hülsen et al., 2016). During the period 2000-2005 the QASUME visited 27 spectroradiometers sites. Out of the 27 instruments, 13 showed deviations of less than 4% relative to the QASUME reference spectroradiometer in the UVB (for 15 instruments in the UVA) for solar zenith angles below 75°. The expanded relative uncertainty (coverage factor k=2) of solar UV irradiance measurements by QASUME, for SZA smaller than 75º and wavelengths longer than 310 nm, was 4.6% in 2002 – 2014 (Gröbner and Sperfeld, 2005), and has been 2 % since 2014 (Hülsen et al., 2016). For broadband instruments, the current instrument uncertainties are summarized in (Hülsen et al., 2020; Hülsen et al., 2008). In 2017, 75 broad-band instruments measuring the UV index, the UVB or/and the UVA irradiance participated in the solar UV broadband radiometer comparison in Davos Switzerland. Using the instrument/user calibration factors, the differences between the datasets by the broad-band instruments and the reference (QASUME) dataset were within ±5 % for 32 (43 %) of the instrument datasets, ±10 % for 48 (64 %), and exceeded ±10 for % 27 (35 %).

Although ground-based monitoring of solar UVR is more accurate than satellite retrievals, ground based stations are sparse, and the only way for continuous monitoring of the UVR on a global scale is through satellites. In recent decades instruments on-board satellites have provided the necessary data for estimates of UV irradiance reaching the Earth surface on a global scale (Herman, 2010) and hence satellite-derived UVR climatological studies have been conducted (Vitt et al., 2020; Verdebout, 2004). The satellite UV irradiance record started with the Total Ozone Mapping Spectrometer (TOMS) on-board Nimbus-7 in

1978 and continued with Ozone Monitoring Instrument (OMI) on-board NASA's satellite EOS-Aura. The OMI retrieval algorithm for surface UVR estimates was based on the experience gained from TOMS (Levelt et al., 2018; Levelt et al., 2006). The early surface UVR retrieval algorithms from satellite data didn't account for the enhanced aerosol absorption in the UV spectral range, resulting in overestimated values (Krotkov et al., 1998). A lot of scientific effort has been put into correcting the products (Arola et al., 2009). TROPOspheric Monitoring Instrument (TROPOMI) onboard Sentinel – 5 Precursor (Lindfors et al., 2018) is the current satellite instrument that provides the surface UVR product on a daily basis with global coverage, including 36 UVR parameters. As the aforementioned instruments were installed onboard polar orbiting satellites, providing global spatial coverage, the temporal resolution of the data is daily since there are only one or two overpasses per day for every point. Geostationary satellites provide continuous (in time) measurements over wide areas. The geostationary meteorological satellites Meteosat monitor the full Earth Disk including Europe and their frequent data acquisition of rapidly changing parameters e.g., cloud is essential for estimating daily UV doses (Verdebout, 2000).

Comparison of OMI surface UV irradiance estimates with ground-based measurements for Thessaloniki, Greece showed that OMI irradiances overestimate surface observations for UVB wavelengths by between ~1.5% to 13.5% in contrast to underestimated satellite values for UVA wavelengths (Zempila et al., 2016). Results from the validation of TROPOMI surface UV radiation product showed that most of the satellite data agreed within ± 10 % with ground-based measurements for snow-free surfaces (Lakkala et al., 2020). Larger differences between satellite data and ground-based measurements were observed for sites with non-homogeneous topography and non-homogeneous surface albedo conditions. The differences between ground-based and satellite UVR data are mostly due to uncertainties in the input parameters to the satellite algorithm used to retrieve the UV irradiance at the surface. Based on a recent study of Garane et al. (2019) a mean bias of 0-1.5% and a mean standard deviation of 2.5 – 4.5 % was found for the relative difference between TROPOMI total ozone column (TOC) product and ground based quality assured Brewer and Dobson TOC measurements.

In this study we introduce a novel UV-Index Operating System, called UVIOS, which is able to efficiently combine information on geophysical input parameters from different modelled and satellite-based data sources in order to provide for the European region the best possible UV-Index (UVI) estimates operationally and in real-time. The reliability of the UVIOS input and output parameters was tested for the year 2017 against ground-based measurements and an analytical sensitivity analysis was performed in order to quantify the uncertainties and to provide information about the limitations and about the optimum operating conditions of the proposed system.

In Section 2 we describe the UVIOS and the input data sources, while Section 3 presents the ground-based measurements used as well as the evaluation methodology. Section 4 analyses the results in terms of model performance and factors that affect the UVIOS retrievals and the overall accuracy. Finally, Section 5 summarizes the findings and the main conclusions of this study and provides a brief description of the future plans with this system.

2 The UV Index operating system (UVIOS)

2.1 System description

The UVIOS system is a novel model that uses real-time and forecasted atmospheric inputs based on satellite retrievals and modelling techniques and databases in order to nowcast and forecast the UVI with a spatial resolution of 5 km and a temporal resolution of 15 minutes. The UVIOS calculation scheme is based on the libRadtran library of radiative transfer models (RTM) (Mayer and Kylling, 2005) within which all the available inputs (i.e. solar elevation, cloud and aerosol optical properties, ozone) can be integrated in real-time into the radiative transfer code and calculate the UVI for each pixel. Afterwards, post processing correction for the elevation of each location and the surface albedo is also performed. In order to be able to simulate the UVI for 1.5 million pixels in real-time we use pre-determined spectral solar irradiance LUTs based on the Libradtran RTM, in combination with high performance computing (HPC) architectures that speed up the process of choosing and interpolating/extrapolating the right combinations from the LUTs (Kosmopoulos et al., 2018; Taylor et al., 2016). The result is the retrieval of UVI for 1.5 million pixels covering the European domain in less than 5 minutes after receiving all necessary input parameters.

As mentioned the UVIOS architecture does not include a clear sky model and the subsequent calculation of individual sources of UV attenuation, but instead it directly uses the following parameters: solar zenith angle (SZA), the aerosol optical depth (AOD) and other aerosol optical properties (e.g., single scattering albedo (SSA), asymmetry parameter, and Ångström exponent (AE)), the total ozone column (TOC), the cloud optical thickness (COT), as well as the surface elevation (ELE) and the surface albedo (ALB) as RTM inputs. Table 1 presents the EO data used as inputs for the UVI real time simulations, their description and sources. The Meteosat Second Generation (MSG) cloud microphysics includes the nowcasted cloud optical thickness (COT) at 550 nm, and cloud phase (CPH) obtained at a spatial and temporal resolutions of 5 km (average, depending on latitude) and 15 minutes, respectively. Typical values of other cloud properties (e.g., cloud height, cloud thickness) have been assumed based on the cloud type (information which is also available from MSG) (for more detailed information see Taylor et al. (2016). The 1-day forecast CAMS aerosol optical depth (AOD) at 550 nm is obtained at a spatial and temporal resolutions of 40 km and 3 h, respectively and the monthly aerosol optical properties obtained from Aerocom (Kinne, 2019) includes asymmetry parameter, single scattering albedo (SSA) and Ångström exponent (AE) at 1^o x 1^o (latitude x longitude) spatial resolution. Solar elevation is taken from the Astronomical model (NREL) (5 km – 15 minutes) (Reda and Andreas, 2008) and climatological surface albedo (ALB) is retrieved from Copernicus Global Land Service (CGLS) (1 km – 12 days) (Carrer et al., 2010). Surface elevation (ELE) is obtained from the Digital Elevation Model (DEM) of NOAA (NOAA, 1988). The Tropospheric Emission Monitoring Internet Service (TEMIS) 1-day forecast of total ozone column (TOC) is at a spatial resolution of 1^o x 1^o – 1 day with assimilated ozone fields from GOME-2 (METOP-B) (Eskes et al., 2003). We have to mention also here that the selection of the RTM inputs has been decided based on their real-time availability.

2.2 Real-time processing concept

The LUT approach, despite its large size (almost 2.5 million spectral RTM simulations for clear and all sky conditions) (Kosmopoulos et al., 2018), still provides estimates at discrete input parameters values. To overcome this mathematical issue, we performed a multi-parametric interpolation technique to correct the input-output parameter intervals. This solution is computationally more costly than a continuous function-approximation model, i.e. a Neural Network (NN) model (Kosmopoulos et al., 2018), but the accuracy improvement is significant. Indicatively, using a test set of 1 million RTM simulations for UVI from the developed LUT, we applied the NN developed in Kosmopoulos et al. (2018) and found a mean execution time of around 144 seconds followed by a mean absolute error (MAE) of 0.0321, while by using the proposed UVIOS multi-parametric interpolation exploiting the HPC and distributed computing benefits we found for the same test set an execution time of 295 seconds with a MAE of 0.0001. The inclusion of many parameters (in this study we incorporated eight, i.e. AOD, SZA, TOC, COT, ELE, ALB, AE, SSA) with small step sizes dramatically increase the LUT size, followed by high computing requirements for the multi-parametric interpolation/extrapolation procedures.

For the UVIOS simulations performed in this study, a 32-core UNIX server was used equipped with 256 Gb of RAM and 12 Tb of storage system working in a RAID10 architecture. The combination of the HPC with the analytical LUTs, which were developed by using the libRadtran RTM, allow a high speed multi-parametric interpolation and polynomial reconstruction (Gal, 1986) to increase accuracy between the LUT records following a mathematical equation relating the UVIOS outputs to the EO inputs.

An example of the UVIOS input output data is presented in Figure 1 through a flowchart illustration of the modelling technique scheme. The inputs, including the solar and surface elevation, albedo, aerosol, ozone forecasts and the cloud observations as described in Table 1, are fed to the real-time solver that results in spectrally weighted output of UVI for the European region. Figure 2 shows the memory usage and error statistics for a range of different LUT sizes. The LUT error decreases as the LUT size increases, regardless of the function being approximated. The LUT sizes in Figure 2 fit into cache on our HPC environment, thus performance in terms of processing speed and overall output accuracy vary only slightly between the table sizes shown. In our case, UVIOS shows that LUT transformation can provide a significant performance increase without incurring an unreasonable amount of error, provided there is sufficient memory available. We note that the cache size is a critical factor for LUT performance, while under a HPC environment practically there is no limit. Such techniques can be implemented in hardware with distributed computing that operates in parallel to provide optimum performance.

Since UVIOS can produce massive UVI outputs of the order of 1.5 million simulations in less than 5 minutes following the proposed simulation and computing architecture, this means that it can be used for both operational applications and real-time estimations. The exact use of UVIOS depends only on the available input data sources. For this study both nowcasts (clouds) and forecasts (ozone, aerosol) were used as inputs to the system. The nowcasts represent the continuous monitoring dimension (i.e. what is happening now) in terms of cloud microphysics data every 15 minutes retrieved in real-time by the geostationary satellite MSG. The forecasts represent the future estimations (day ahead in our study) of aerosol optical properties and total ozone column based on deterministic approaches (ECMWF) and assimilated satellite data for better accuracy. As a result, UVIOS under cloudless conditions operates as a forecast system since it uses forecasted inputs and provides the clear-sky UVI

forecasts operationally. By adding the nowcast cloud information as input to UVIOS (i.e. all sky conditions), the whole procedure will follow the time steps of MSG cloud microphysics data collocated and synchronized with the forecast data. So, following the proposed operation method of this study, the UVIOS can be used as a UVI forecast system for cloudless conditions or as a UVI nowcast system for all sky conditions.

2.3 Input data description

The Cloud Optical Thickness (COT) data from Meteosat was used, whose retrieval algorithm is based on 0.6 and 1.6 micron channel radiances of Meteosat's Spinning Enhanced Visible and InfraRed Imager (SEVIRI). MSG products have been described in Derrien and Le Gléau (2005) and the MétéoFrance (2013) technical report. The COT impact uncertainty on UVI deals with the MSG COT reliability and accuracy and hence introduces errors into the UVIOS simulations (Derrien and Le Gléau, 2005; Pfeifroth et al., 2016). In addition, comparison principles of (point) station UVI measurements with a 5 km MSG COT matrix are possibly responsible for at least part of the observed deviations (e.g., Kazadzis et al. (2009a)). For instance, when a MSG pixel is partly cloudy, the ground measurements of UVI could fluctuate more than 100%, depending on whether the sun is visible or whether clouds attenuate the direct component of the solar irradiance. The result is that in cases of partly covered MSG pixels and in the absence of clouds between the ground measurement and the sun, the ground truth UVI would be much higher than the UVIOS one. Of course, the presence of small clouds which have not been identified by MSG and cover (part of) the sun disk, is plausible as well, consequently causing an overestimation of the modelled UVI (Koren et al., 2007). Furthermore, sensors onboard geostationary satellites suffer from the parallax error, which contributes to the spatial errors of the images and the overall uncertainty of the products (Bieliński, 2020; Henken et al., 2011). The error depends on the altitude of the cloud and the viewing angle (parallax errors are more significant for high viewing angles).

UVIOS calculations at high solar zenith angles (>70 deg) are retrieved assuming cloudless skies since the MSG COT product is not available in these conditions, facing reliability issues (Kato and Marshak, 2009). This has an effect on the quality of the UVIOS overall performance at high solar zenith angles, where there is no cloud information as input to the model in order to quantify the consequent impact on UVI. However, such measurements under high solar zenith angles are accompanied with very low UVI levels (<1) both in the performed RTM simulations and in the ground-based measurements. This inconsistency, even if does not affect UVIOS UVI results associated with dangerous effects on human health, nevertheless it is still affected by the rest of input parameters (i.e. ozone, aerosol etc) mitigating the UVIOS uncertainty in the absence of cloud information under such high solar zenith angles. There is more discussion in the next section on how we use these data for the UVIOS validation.

For the total aerosol optical depth, we used 1-day forecast data from the Copernicus Atmospheric Monitoring Service (CAMS) as the basic input parameter. These forecasts are based on the Monitoring Atmospheric Composition and Climate (MACC) analysis and provide accurate data of aerosol optical depth (AOD) at 550 nm with a time step of 1 h and spatial resolution of 0.4°. For aerosol single scattering albedo properties climatological values from MACv2 aerosol climatology (Kinne, 2019)

was utilized. Monthly means of single scattering albedo at 310nm were acquired from global gridded data at a 1º x 1º spatial resolution. Also, in order to derive the Angstrom exponent, monthly means of AOD at 340nm and 550nm were used. The calculated Ångström exponent was then applied to the 550 nm AOD (from CAMS) in order to get AOD in the UV.

The surface albedo data were obtained from the Copernicus global land service (CGLS: Geiger et al., 2008; Carrer et al., 2010). As a global surface ALB product is not available in the UV region, for this study we have used the climatological product of CGLS (in the visible range) (Lacaze et al., 2013) as follows: based on the findings of Feister and Grewe (1995), we used a UV albedo of 0.05 for non-snow cases and a UV ALB equal with CGLS when CGLS exceeded 0.5 (snow cover). The total ozone column forecasts were obtained from Tropospheric Emission Monitoring Internet Service (TEMIS) which is a near- real time service which uses the satellite observations of total ozone column by the Global Ozone Monitoring Experiment (GOME) and SCIAMACHY assimilated in a transport model, driven by the European Centre for Medium-Range Weather Forecasts (ECMWF) forecast meteorological fields (Eskes et al., 2003). The elevation data was obtained from the 5-minute Gridded Global Relief Data (ETOPO5) database, which provides land and seafloor elevation information at a 5-minute latitude/longitude grid, with a 1-meter precision in the region of Europe and is freely available from NOAA (NOAA, 1988). An analytical description of the above geophysical parameters including their specifications and resolution can be found in Table 1, followed by the corresponding references for more technical details. Figure 3 shows an example of the input-output UVIOS parameters. An extensive validation of the MACC analysis and forecasting system products were performed by Eskes et al. (2015). The aerosol optical properties were validated against 3-year (Apr. 2011 – Aug. 2014) near real time level 1.5 AERONET measurements and for AOD at 550 nm an overall overestimation was exhibited. Due to dedicated validation activity of the MACC service a validation report that covers the time period of this study (Eskes et al., 2018) is also available, presenting an overall positive modified normalized mean bias during 2017, ranging from 0 to 0.4, with the same range of values over the study region (Europe). This overestimation of AOD at 550 nm may explain some of the UVI underestimation under clear sky conditions (see section 4.2.2).

3 Ground measurements and evaluation methodology

3.1 Ground-based measurements

In order to validate the UVIOS results 17 ground based stations were selected, for which measurements of the UVI were available during 2017. The stations are shown in Fig. 4. Comparisons were performed with a 15-minute step. The ground based measurements were obtained from spectrophotometers (Brewer), spectroradiometers (Bentham), filter radiometers (GUV) and broadband instruments (SL501 and YES) as Table 2 shows. Note that UV data in table 2 has been calibrated, processed and provided directly by the responsible scientists for each station. References wherein more information for the data quality of particular instruments can be found are also provided. Brewer spectrophotometers measure the global spectral UV irradiance with a step of 0.5 nm, and a resolution which is approximately 0.5 nm (usually between 0.4 and 0.6 nm). Depending on their

type the spectral range is usually 290-325 nm (MKII, MKIV) or 290-363 nm (MKIII,). Since Brewer spectrophotometers measure the spectrum up to a wavelength which is shorter than 400 nm, extension of the spectrum up to 400 nm in order to calculate the UV index is usually achieved using empirical methods (e.g., (Fioletov et al., 2003; Slaper et al., 1995)). The additional uncertainty in the UVI due to the latter approximation is well below the overall uncertainty in the measurements. Bentham spectroradiometers measure the whole UV spectrum (290 – 400 nm) with step and resolution which can be determined by the operator. The spectra from AOS and LIN (measured by Bentham spectroradiometers) used in this study have been recorded with a step of either 0.25 or 0.5 nm and a resolution of ~ 0.5 nm. The Brewer Spectrophotometer measures the total column of ozone using the differential absorption method, i.e. measuring the direct solar irradiance at four wavelengths and then comparing the intensity at wavelengths that are weakly and strongly absorbed by ozone (Kerr et al., 1985). Brewer TOC measurements are used in the present document to validate the TEMIS forecasts. The Ground-based Ultraviolet (GUV) instrument is a multichannel radiometer that measures UV radiation in five spectral bands having central wavelengths as 305, 313, 320, 340 and 380 nm. However, in addition to UV irradiances, other data that can be obtained from GUV instruments are total ozone and the cloud optical depth (Dahlback, 1996; Lakkala et al., 2018). GUV measurements are used for LAN station of Norway. At stations AKR, INN and VIE, the surface UV was measured using Solar Light (SL) 501 radiometers. It provides direct observation of UV index with a frequency of one minute. The Yankee Environmental System (YES) has been used for VAL station.

The low latitude stations include AKR, ARE, ATH, ROM, THE, and VAL. AKR has minimum altitude of 23 m and VAL has maximum altitude of 705 m above sea level. The middle latitude locations are AOS, DAV, INN, BEL, LIN, MAN, UCC, and VIE among which the minimum altitude is 10 m in LAN and maximum altitude is in DAV at 1610 m above mean sea level. HEL, LAN, and SOD represent the high latitude zone, with HEL having an altitude of 48 m and SOD an altitude of 185 m above mean sea level (Table 2). A summary of basic climatic information for the validation locations was obtained from the Köppen climate classification (Chen and Chen, 2013) and it is summarized here. THE, AKR, ARE, ROM, ATH and VAL have a Mediterranean climate comprising of mild, wet winters and dry summers. MAN experiences maritime climate (cool summer and cool, but not very cold, winter). AOS, UCC, LAN, BEL, HEL, LIN and VIE experience humid continental climate with warm to hot summers, cold winters and precipitation distributed throughout the year. DAV and INN experience boreal climate characterised by long, usually very cold winters, and short, cool to mild summers. SOD has subarctic climate having very cold winters and mild summers.

3.2 Evaluation methodology

The time series period covers the whole year 2017 at 15-min intervals, following the MSG available time steps. A synchronization between the UVIOS simulations and the ground-based measurements was performed in order to match the 15-min intervals of UVIOS to the measured data. The UVIOS data availability is 93%, while for the ground stations it reaches almost 79% enabling a direct UVI data comparison of 77% of the 2017 time steps. For the comparison we used the closest

instrument measurements to the 15-min intervals with a maximum deviation of 3 minutes in order to avoid solar elevation and cloud presence mismatches. Additionally, the UVIOS comparisons included measurements up to 70 degrees SZA. The rationale for this cutoff was that UVIOS retrievals at high SZA are retrieved as cloudless as COT is unavailable from MSG. In addition, the comparison is also impacted by limitation of the horizon of ground-based sites (e.g., Davos, Innsbruck, Aosta) where the diffuse component and in some cases the direct component of solar UV irradiance are affected by obstacles (mountains) on the horizon. The contribution of this mainly diffuse irradiance to the total budget is a function of solar elevation and azimuth (day of the year) and also cloudiness. Although UVIOS simulations were corrected for changing UVI with respect to altitude (see Section 3.2.3), the correction cannot be perfect for higher altitude stations. The reason is that it is not possible to take into account all different factors (aerosol load and properties, atmospheric pressure, surface albedo) (e.g., Blumthaler et al., 1997; Chubarova et al., 2016) which affect the change of UVI with altitude. This explains some of the deviations in the results as the UVIOS retrieves UVI assuming a flat horizon. Clear sky conditions were defined as the UVIOS retrieval where MSG COT equals to zero. Further discussion on the uncertainties introduced by this choice is mentioned in the cloud effect section.

Most of the comparisons have been performed using the absolute (mean bias or median) UVI differences (model – measurements). In addition, median values of the percentage differences (100* (model – measurements)/measurements) have been used. UVIOS estimations were also evaluated in terms of mean bias and root mean square error (MBE and RMSE, respectively), defined as follows:

$$\mathrm{MBE} = \bar{\varepsilon} = \frac{1}{N}\sum_{i=1}^{N} \varepsilon_i \qquad (1) \qquad\qquad \mathrm{RMSE} = \sqrt{\frac{1}{N}\sum_{i=1}^{N} \varepsilon_i^2} \qquad (2)$$

Where $\varepsilon_i = x_f - x_o$ are the residuals (UVIOS errors), calculated as the difference between the simulated values (x_f) and the ground-based values (x_o), and where N is the total number of values. MBE quantifies the overall bias and detects whether the UVIOS overestimates (MBE>0) or underestimates (MBE<0). RMSE quantifies the spread of the error distribution. Finally, the correlation coefficient (r), as well as the coefficient of determination (R^2) were used to represent the proportion of the variability between modeled and measured values.

4 Results

4.1 Overall performance of the UVIOS system

Fig. 5 presents a density scatterplot of the UVIOS simulations for all stations as compared to the ground-based measurements, in which a pattern of shaded squares represents the counts of the points falling in each square and which shows a correlation coefficient (r) of 0.94. For a more detailed view of the UVIOS performance, Fig. 6 depicts a Taylor diagram with the overall model accuracy for all ground stations under all sky and clear sky conditions as a function of the correlation coefficient, normalized standard deviation and RMSE. For both clear sky and all sky conditions, the results are similar. The absolute

differences between the UVIOS and the measured UVI are within ± 0.5, and the correlation coefficients are between 0.85 and 0.99 for all stations. The RMSE is for most stations less than 0.5. Under all sky conditions the RMSE is higher relative to the RMSE for clear skies for MAN, DAV and SOD, which is probably due to misclassification of cloudy pixels (see also the Appendix A section). Relative differences can be misleading as they may correspond to very small absolute differences without physical meaning, especially for low levels of the UVI. Thus, we focused on absolute differences in order to have a more representative assessment of the actual effect (UV Index) and its results. The differences were categorized to low (less than 0.5), moderate (0.5 - 1) and high (more than 1). In the Appendix A, relative differences are also discussed.

In Table 3, U1.0 and U0.5 represent the percentage of cases with absolute differences between modelled and ground based UVI measurements within 1 and 0.5, respectively, for all comparisons between the 15-minute model retrievals and the corresponding ground-based measurements. As shown in Table 3, for all stations and for both, clear- and all sky conditions, differences were within 0.5 UVI for at least 70% of the cases. Under clear sky conditions, AOS, BEL, HEL, LAN, LIN, SOD and THE had above 90% of U0.5 cases, while others have 75-90% of U0.5 cases. All stations but DAV had above 90% of U1.0 cases for clear skies, while the correlation coefficients for most of the stations were above 0.9 (exceptions are ATH and MAN). For all-skies differences were within 1 UVI for 90% of the cases for all stations with the correlation coefficients exceeding 0.9 for most of them (exceptions are DAV, MAN and SOD). Median differences for all skies for every station were well within $\pm$0.2 UVI, with the 25-75 percentiles being within $\pm$0.5 UVI and the 5-95 percentiles within $\pm$1 UVI. For clear skies the corresponding values are $\pm$0.1, $\pm$0.4 and $\pm$0.8 respectively. In the following sections we try to investigate the factors that contribute to the differences between UVIOS and ground-based measurements.

4.2 Factors affecting UVIOS retrievals

4.2.1 Ozone effect

All the available collocated Total Ozone Column (TOC) measurements for the stations used in UVIOS evaluation have been obtained from the WOUDC (https://woudc.org/) database. In this database 8 out of 17 UVIOS evaluation stations (AOS, ATH, DAV, MAN, ROM, SOD, THE and UCC) were found, providing TOC ground-based measurements. TOC comparison has been performed by calculating daily means of ground-based measurements and the TOC from TEMIS. In order to quantify the effect of the uncertainty of the forecasted TOC used as input at UVIOS we have calculated the mean differences of the forecasted and measured TOCs and used a radiative transfer model to investigate their effect on UVIOS retrieved UVI. Table 4 shows the mean differences in D.U. from TEMIS TOC (used as inputs in UVIOS) as compared to the WOUDC ground-based measurements for one year of comparison data. It is seen that for the stations AOS, DAV, MAN and UCC the values of the TEMIS observations are higher as compared to the ground-based measurements (by 7.6, 1.9, 5, and 2.9 DU respectively) while for the other stations TEMIS observations are lower (by 0.9, 5.4, 9.9, and 2.2 DU for ATH, ROM, SOD, and THE respectively). The negative bias is seen to be highest for ROM station (-9.9) and the positive bias is highest for AOS station (7.6). Part of the large differences over the complex terrain sites can be explained by the difference between the actual altitude

of the station and the average altitude of the corresponding grid points of TEMIS. For example, for AOS the average altitude of the pixel is 2000 m while the real altitude of the station is 570 m, resulting in an underestimation of the tropospheric column of ozone by TEMIS. In general, differences can be explained by the combined effects of uncertainties in TOC retrieval from satellite and ground-based platforms (Rimmer et al., 2018; Boynard et al., 2018; Garane et al., 2018). Figure 7 shows the effect of this TOC bias on the calculated UVIOS. As seen in Table 4, there is a mix of small underestimation and overestimation cases in the TOCs used within UVIOS, with average absolute differences of 4-5 DU. Worst TOC UVIOS inputs were found in AOS and ROM (7.6 and -9.9 DU) leading to maximum (at 30 degrees SZA) differences in UVI of -0.22 and 0.3 for AOS and ROM, respectively. In general, in most of the cases UVI mean differences are less than 0.1. It has to be noted that the TOC differences have a larger impact when expressed in percent at higher SZAs, while in Figure 7 higher absolute differences for low SZA's are associated with higher UVIs at these SZAs. Detailed comparisons for each station are shown in the Appendix A figures.

4.2.2 Aerosol effect

Aerosol optical depth measurements used for the UVIOS aerosol input evaluation have been collected from the AERONET-NASA web site (Giles et al., 2019) for 12 out of our total 17 stations (AKR, ARE, ATH, DAV, HEL, LIN, ROM, SOD, THE, UCC, VAL and VIE. AERONET (level 2, version 3) values of AOD at 500 nm were interpolated at 550nm using the AERONET derived 440-870nm Angstrom exponent for each individual measurement. In order to compare those measurements with CAMS forecasted AOD used for the UVIOS their daily means were derived. The comparison of forecasted and measured daily means was based on all available data due to gaps in the AERONET time series. The AOD MBE and RMSE statistical scores are shown in Table 5 in absolute units and correlation coefficient as well. All the stations have a mean positive bias up to 0.071 except UCC which is showing a mean negative bias of 0.007. The comparison of all individual stations with CAMS data used as inputs on UVIOS showed that under all cases CAMS AOD is higher than that from AERONET with a mean difference of 0.07 at 550nm. The correlation between the modeled and the measured values varies from 0.10 for VIE to 0.91 for ARE with most of the stations showing the correlation coefficient above 0.7. As in the case of the TOC, AOD CAMS data are forecasts from the previous day and real time WOUDC or AERONET level 2.0 data do not exist. Although real time TOC (and in due course AOD in the UV) is available from Eubrewnet (López-Solano et al., 2018; Rimmer et al., 2018), it is only for particular locations and not for the whole European domain. Thus, the only choice in providing for a real time UV Index for Europe is using the CAMS (for AOD) and the TEMIS (for TOC) data.

In order to evaluate the effect of AOD on UVI, UVI differences between the UVIOS using both AOD datasets (CAMS and AERONET) as UVIOS inputs were analyzed. Figure 8 shows the mean bias error of the CAMS – AERONET AOD impact on UVI for all stations with available ground based AOD data as a function of SZA together with the uncertainty range ($\pm$ 1 σ). It can be seen that UVIOS with CAMS AOD input underestimates UVI compared to the UVIOS with AERONET data, except for the UCC station. This is consistent with CAMS overestimations of AOD compared to the AERONET measurements,

except for the station UCC as shown in Table 5. Higher aerosol levels in the atmosphere tend to lower the UVI. Highest difference in UVI is observed for the stations HEL, SOD, VIE. Since, the aerosol level at the stations HEL and SOD is very low, the percent difference between the AOD from CAMS and AERONET is larger for these stations (although the absolute difference is similar) relative to stations with higher AOD, leading to higher differences in the UVI. Aerosol content for VIE is higher than HEL and SOD but still within 0.2 which might be the reason for the higher UVI difference. In terms of SZA, it is observed that the mean bias decreases with an increase in the SZA as the values of UVI also decrease with SZA and the most deviation is for station VIE which is consistent with the poor correlation between the CAMS forecasted input and the measurements for this station as seen from Table 5.

The use of single scattering albedo in the UV region is a difficult task and many studies have shown that such measurements need extra effort and it is not possible to perform them worldwide (Arola et al., 2009; Kazadzis et al., 2016; Raptis et al., 2018). The monthly values of the single scattering albedo used in UVIOS for the UV region were derived from the MACv2 database at the 310 nm wavelength (Kinne, 2019). Fig 9 shows the intra annual variability of SSA for the 17 stations. For all stations, SSA values range from 0.76 to 0.93, with most of them having SSA values between 0.83 to 0.93, and relatively small variability. In contrast, there are stations like ARE, BEL, INN, LIN, VIE and THE which have relatively smaller SSA values (0.76-0.9) and greater variability than the other stations.

4.2.3 Albedo effect & surface elevation correction

Surface albedo at UV wavelengths is small (2 – 5%) for most types of surfaces (Feister and Grewe, 1995; Madronich, 1993) except for features like sand (with a typical albedo of ~0.3) and snow (up to 1 for fresh snow) (Meinander et al., 2013; Myhre and Myhre, 2003; Vanicek et al., 2000; Henderson-Sellers and Wilson, 1983). Renaud et al. (2000), found an enhancement of about 15 to 25% in UVI for clear-skies and snow conditions due to the multiple ground-atmosphere reflections and this relative increment was about 80% larger for overcast conditions. The combined effect of aerosols and snow lead to an enhancement of about 50% in UVI in cloud-free condition for moderately polluted atmospheres (Badosa and Van Weele, 2002). Fig. 10 (a) presents the effect of surface albedo on the UVI percentage difference (i.e. for various albedo values under clear sky conditions) as a function of SZA, while Fig. 10 (b) shows the effect of surface elevation on UVI as a function of the percentage difference for various total ozone columns. It is observed that the UVI percentage difference increases almost linearly with albedo for a particular SZA and the variation is found to be almost identical for all SZA. This indicates that the UVI percentage difference is independent of the SZA and increases with surface albedo. The UVI percentage difference is found also to increase almost linearly with the increase in elevation for a particular total ozone column. The percentage difference is similar for all ozone columns up to 1km, after which the differences with ozone column become more apparent. That is, at a particular elevation, the percentage difference is higher for less total ozone column. A 1% fluctuation (decline or increase) in column ozone can lead to about a 1.2% fluctuation (increase or decline) in the UV Index (Fioletov et al., 2003; Probst et al., 2012). Indicatively, the average maximum surface elevation correction in terms of UVI for the DAV station (due to UVIOS input deviation from

to actual elevation) was of the order of 1.6 (15%), while for INN and AOS it was 0.5 and 0.6 respectively (6%) and for the VAL station close to 0.8 (8%).

Uncertainties introduced in UVIOS from the use of a constant surface albedo value of 0.05 for non-snow conditions are quite low. For the case of albedo values used for snow conditions based on the CGLS monthly mean product uncertainties can be related to: the small difference of UV and visible albedo values; the fact that the CGLS provides an albedo of a certain area around the station that does not necessarily coincide with the "effective" albedo area affecting UV measurements; and finally that the monthly albedo product represents a monthly average while a real time CGLS product represents the last 12 days (dynamically changing albedo). In order to investigate this last point, we have compared the UV effects from the use of the two albedo datasets for DAV station, where the average difference between an example ground-based dataset and UVIOS was found to be 0.14 UVI (Gröbner, 2021). In Fig. 11, the effect of surface albedo correction is shown for the Davos station, for a period with snow cover and low percentage cloudiness. The climatological and the dynamically changing albedo are presented in terms of percentage differences between modelled and ground measurements as a function of SZA. In the case of climatological albedo, most of the percentage difference between forecasted and the measured UVI value is found to vary from -30% to 10% for SZA between 20° to 70°, showing more underestimation than overestimation from the UVIOS simulations. Similarly, in the case of dynamically changing albedo, most of the percentage difference between forecasted and the measured UVI value is found to vary from -20% to 10% for SZA between 20° to 70°. The mean percentage difference between the results using the two different albedo inputs is -2.76% in terms of accuracy improvement. However, beyond 70 degree SZA, there is a huge variation in the percentage difference with mostly underestimations from the UVIOS simulations (not shown in Fig. 11).

4.2.4 Cloud effect

For the evaluation we used measurements at SZA lower than 70 degrees, based on the lack of cloud input from MSG for higher SZAs. The lack of MSG data results in an overestimation of UVIOS in high SZAs and the UVI is systematically overestimated for long periods during winter at high latitude regions when SZA does not get below 70 degrees during the day. However, based on the simulations performed by UVIOS, this overestimation is low in terms of absolute UVI and does not usually exceed 0.2 UVI because maximum UVIs at such SZAs rarely exceed UVI=1.

COT retrieved from the MSG satellite has been used as input for the UVIOS together with typical optical properties of the clouds as discussed in Sect. 2.1. The evaluation of all stations for cloudless and cloudy conditions can be seen in Figure 12 that shows the relative frequency distribution of all stations (colours) and the mean (black line) for cloudless (upper plot) and cloudy conditions (lower plot). Mean bias error of the modeled by UVIOS and measured UVI for all- and clear sky conditions and the percentage of clear sky time steps data is presented in Figure 13. The mean bias for clear sky conditions is found to be less than that for the all sky conditions for the stations AKR, ATH and THE (having most days of the year being cloudless as the clear sky percentage is above 70%). The MBE for DAV, LIN and MAN is less for clear sky relative to all sky conditions

even though most days of the year are cloudy (clear sky annual percentage less than 45%) at the particular stations. While, stations BEL, HEL, INN, LAN, SOD, UCC and VIE, that have mostly cloudy skies throughout the year (clear sky annual percentage less than 50%), are having more MBE for clear sky conditions than the all sky condition. This can be due to the erroneous classification of a cloudy sky as clear sky, which is also discussed in the following section. MBE is also larger for AOS and ARE which have mostly clear skies throughout the year. Stations ROM and VAL have comparatively much smaller MBE for clear sky conditions.

As shown in Table 6 there are 45.4% of cases with underestimations and 54.6% cases with overestimations for cloudless conditions (COT=0). For all the other cases, overestimations (62.5%) are more predominant than underestimations (37.5%). The difference in the modelled and the measured values goes beyond ± 1 UVI for only 5.1% cases for cloudless conditions and 14.7% for all other cases. In general, under cloudy conditions, UVIOS shows an overestimation for UVI in contrast to the ground measurements. One explanation for the overestimations could be the erroneous determination of COT from MSG above the ground-based stations, giving cloud input that can be overestimated or underestimated. The results show that there is a general tendency for a small underestimation of MSG COT that leads to a systematic but small UVIOS UVI overestimation under cloudy conditions. Another possible explanation is the spatial representativeness of MSG COT. The MSG COT determination is available at 5 by 5 km pixels that may differ from the actual situation of the cloud prevailing above the station, especially in broken cloud conditions and in case when it blocks the direct radiation from the sun. Moreover, for lower solar elevations, the direct sun irradiance can be blocked by cloud in neighbouring pixels. The first effect has been explored in the relative frequency distribution of Figure 12 that shows a higher number (~ 63%) of data on the right of the zero UVI difference vertical line for cloudy skies. When comparing data outside the 0.5 and 1 difference limits we also see that 1 – 4 times more data show a UVIOS overestimation as compared to the clear sky case. This shows that in general there is a small (in UVI terms) but significant UVIOS overestimation for non-zero COT conditions. Moreover, for clear skies, as determined from the MSG, we observe a less pronounced UVIOS overestimation that corresponds to the fact that even if MSG defines the situation as completely cloudless, in reality there may be some cases where clouds near the ground-based station affect the measured UVI. This effect is easier to understand when showing these differences as a function of solar zenith angle which is explored through Figure 14. It is observed that the absolute difference between the modelled and the measured values decreases with increasing solar zenith angle and most of the difference lies within ± 4 UVI. The seasonal variation of the percentage UVI difference as a function of SZA shows that while absolute UVI is small in winter the percentage difference is higher compared to other seasons.

Figure 15 (a) shows the shadow volume at the surface level of a cloud, relative to the SEVIRI angle view, as a function of cloud height and SZA, highlighting the ray tracing in the presence of clouds and the accompanied angular dependence due to the 3D geometry. 15 (b) shows the scatter of the UVI difference under clear sky conditions for all stations as a function of SZA. It is observed that there is an obvious pattern of scattered data for UVI differences higher than 1.5 compared with the ones for differences less than -1.5. These data represent UVIOS overestimation for UVI retrievals due to the underestimation of the cloudiness just above the stations. These data illustrate the well-known spatial representativeness issues whereby a COT

value for a satellite grid is not fully representative of a point measurement station. In addition, absolute and percentage relative differences are shown in Fig. 15 (c) and (d) respectively for SZA up to 65 degrees. The differences between the UVIOS and the ground-based UVI decreases in absolute level but increases in percent with an increase in SZA. This is due to the decrease of UVI with increasing SZA. Modelled and the measured UVI difference is close to zero both for mean and median values. For SZA below 30 degrees, differences are 0 to -0.2, while 20 to 80 percentiles range from -0.6 to -0.2. Percentage difference increases with SZA as absolute UVI decreases with the 20 to 80 percentiles showing differences between -10% and 10%.

5. Conclusions and future plans

In this study, a fast RTM model of UVI, the so-called UVIOS, using inputs of the SZA, aerosol optical depth, total ozone column, cloud optical depth, elevation and surface albedo that implicitly includes temporal effects and the effect of cloud and aerosol physics, allows for the generation of high-resolution maps of UVI. Ground based measurements of UV are the most accurate way to determine this important health related parameter. However, such stations are sparse and hence, satellite observations can be used in order to have a nowcasted UV service. To date, polar orbiting satellites like TOMS, OMI and recently TROPOMI provided a global UV dataset with a major disadvantage being the temporal resolution (one measurement per day). This, combined with the large temporal variability of clouds can lead to huge deviations from reality when a single daily measurement is included. Geostationary satellite, MSG, have been used in order to try to improve on such limitations using cloud information every 15 minutes.

Comparison of the forecasted and the ground-based measurements indicated that at least 70% and 80% of comparisons were within 0.5 UVI difference for all sky condition and clear sky, respectively. The mean differences between TEMIS TOC and the ground measured TOC from the WOUDC for one year of comparison data showed that TEMIS tends to slightly overestimate the TOC for some stations along with underestimating it for other stations. While, in general, in most of the cases UVI mean differences are less than 0.1, the TOC differences have a larger impact in percent UVI differences at higher SZAs. Such small differences can also be the result of daily TOC variation not captured in TEMIS.

CAMS AOD seems to be slightly overestimated as compared with AERONET data that leads to a UVIOS underestimation. CAMS data are found to overestimate the AOD from AERONET measurements with a mean difference of 0.07 at 500 nm. All the stations have a mean positive bias up to 0.071 except one station that had a mean negative bias of 0.007. The analysis of the impact of the mean bias error of the CAMS – AERONET AOD impact on UVI for all stations showed that the mean bias decreases with an increase in the SZA as the values of UVI also decreases with SZA. The greatest deviation is for station VIE which is consistent with the poor correlation between the CAMS forecasted input and the measurements for this station. The real time data provision approach of UVIOS requires using a maximum of one-day ozone and aerosol forecast using the TEMIS and CAMS service respectively. Uncertainties in the used SSA increase the overall uncertainty of the simulated UVI, especially for high levels of atmospheric aerosols. However, as systematic SSA measurements in the UV region are not available, quantification of these uncertainties were not possible.

Cloudy conditions show high percentage differences but low UVI differences, and have a general tendency to lead to a UVIOS overestimation. It was found that 45.4% of cases have underestimations while 54.6% cases have overestimations for the cloudless conditions, while overestimations (62.5%) were more predominant than underestimations (37.5%) for all the other cases. In general, UVIOS showed an overestimation for UVI in contrast to the ground measurements under cloudy conditions with the difference in the modeled and the measured values going beyond ±1 for 5.1% cases for cloudless conditions and 14.7% for all other cases. At individual stations the results for cloudless sky conditions, which are the most important for health related issues, showed good agreement. In general, ~85% of all and 95% of cloudless cases are within 1 UVI difference. The relative percentage biases can be large for low UVI cases due to clouds or at high SZAs, above 75°, due to the absence of accurate information for clouds. The results show that there is a general tendency of small underestimation of MSG COT that leads to a systematic but small UVIOS overestimation under cloudy conditions. Another possible explanation is the spatial representativeness issues between a satellite and a single point on the ground.

Using climatological surface albedo has little impact at low albedo sites but mainly leads to underestimations in UVIOS simulations for high albedo situations (snow cover). Most of the percentage difference between forecasted and the measured UVI values varied from -30% to 10% for SZA between 20° to 70° (climate albedo), while it was found to vary from -20% to 10% for dynamically changing albedo. Since high surface albedo conditions correspond to winter months (i.e. high SZAs and relatively low UVI) for the stations used in the study, the corresponding absolute differences in the UVI are generally smaller than 2 UVI. However, there was a huge variation in the percentage difference beyond 70 degree SZA with mostly underestimations from the UVIOS simulations. Finally, for uncertainties in elevation inputs, the UVI percentage difference is found to increase almost linearly with the increase in elevation for a particular total ozone column and beyond that, it is seen that the rate of increase in the percentage difference decreases with increase in the total ozone column.

UVIOS system forms a novel tool for widespread estimations of UVI using real-time and forecasted EO inputs. UVIOS utilizes the MSG domain with high spatiotemporal resolution, producing outputs within acceptable limits of accuracy for UV health related applications. It captures basic cloud features and all major atmospheric and geospatial parameters that affect UVI. Under cloudless conditions it performs to within the uncertainty of the ground based measurements to which it has been compared. Further development and improvement of the model can be achieved in the future. Meteosat Third Generation (MTG) satellites are expected to be launched in the following years and give aerosol and cloud products which would improve the performance of nowcast and forecast UV models when used as inputs. A future goal is to compare the UVIOS accuracy under cloudy conditions by using, (i) the current MSG cloud information (5 km, 15 min), (ii) the ECMWF forecast cloud information (4 km, 1 hour) and (iii) the forthcoming MTG cloud information (500m, 5 min), in order to quantify the uncertainties of the forecasted cloud data as compared to the satellite observations, as well as the overall improvement of the MTG data compared to the MSG due to the MTG's higher resolution.

The future plans with the UVIOS system include open access to the operational UVI product through European online map-based user interfaces, data hubs and cloud platforms for Earth Observation data (e.g. GEOSS Portal and NextGEOSS). A real-time correction and quality assurance of the outputs is also scheduled by assimilating ground measurements in collaboration

with the stations used in this study. In addition, the short-term and long-term forecasting horizons will be exploited for further added value as an early warning system that raises awareness among citizens of the health implications of high UVI doses. To this direction, numerical weather prediction models and computer vision techniques (Kosmopoulos et al., 2020) will be utilized as complements to the UVIOS system in order to capture the cloud movement forecast and effect on the UVI levels. Finally, a historical database of UVI will be developed by using climatological input data sources for past years aiming to study climatic trends and to make the system a holistic platform for scientific and social value deployment.

Author contribution

PGK was responsible for the design of the study and the whole analysis, with support from SK, AWS, PIR, KP, IF, AM and JG. PGK and SK are the developers of UVIOS. All authors contributed to editing the paper.

Code/Data availability

All data used as inputs to the UVIOS system are open access, while all data sets produced by the UVIOS for the purposes of this paper can be requested from the corresponding author. The ground-based measurements can be requested from the PIs of the stations. The UVIOS suite of algorithms and LUTs can be used for various applications after consultation with the corresponding author.

Competing interests

The authors declare that they have no conflict of interest.

Acknowledgements

We acknowledge the Eumetsat SAFNWC, the Copernicus and TEMIS services as well as the Aerocom and GOME teams for providing all the necessary data used in this study. We would like to thank the 17 site instrument operators and technical staff that made the ground based measurements feasible.

Financial support

The UVIOS development received no specific grant from any funding agency in the public, commercial, or not-for-profit sectors. The evaluation part of this study has been partly funded by the European Commission project EuroGEO e-shape (grant agreement No 820852).

References

Andrady, A.L., Aucamp, P.J., Austin, A.T., Bais, A.F., Ballare, C.L., Barnes, P.W., Bernhard, G.H., Bornman, J.F., Caldwell, M.M., de Gruijl, F.R., and Erickson, D.J.: Environmental effects of ozone depletion and its interactions with climate change: 2014 assessment executive summary. Photochemical and Photobiological Sciences 14(1), 14-18, 10.1039/c4pp90042a, 2015.

Arola, A., Kazadzis, S., Lindfors, A., Krotkov, N., Kujanpää, J., Tamminen, J., Bais, A., di Sarra, A., Villaplana, J. M., Brogniez, C., Siani, A. M., Janouch, M., Weihs, P., Webb, A., Koskela, T., Kouremeti, N., Meloni, D., Buchard, V., Auriol, F., Ialongo, I., Staneck, M., Simic, S., Smedley, A., and Kinne, S.: A new approach to correct for absorbing aerosols in OMI UV, Geophysical Research Letters, 36, 10.1029/2009gl041137, 2009.

Badosa, J., and Van Weele, M.: Effects of aerosols on UV-index, KNMI Scientific Report WR-2002-07, 2002.

Badosa, J., Calbó, J., McKenzie, R., Liley, B., González, J.-A., Forgan, B., and Long, C. N.: Two Methods for Retrieving UV Index for All Cloud Conditions from Sky Imager Products or Total SW Radiation Measurements, Photochemistry and Photobiology, 90, 941-951, https://doi.org/10.1111/php.12272, 2014.

Bais, A. F., Zerefos, C. S., Meleti, C., Ziomas, I. C., and Tourpali, K.: Spectral measurements of solar UVB radiation and its relations to total ozone, SO2, and clouds, Journal of Geophysical Research: Atmospheres, 98, 5199-5204, 10.1029/92jd02904, 1993.

Bais, A. F., Lucas, R. M., Bornman, J. F., Williamson, C. E., Sulzberger, B., Austin, A. T., Wilson, S. R., Andrady, A. L., Bernhard, G., McKenzie, R. L., Aucamp, P. J., Madronich, S., Neale, R. E., Yazar, S., Young, A. R., de Gruijl, F. R., Norval, M., Takizawa, Y., Barnes, P. W., Robson, T. M., Robinson, S. A., Ballaré, C. L., Flint, S. D., Neale, P. J., Hylander, S., Rose, K. C., Wängberg, S. Å., Häder, D. P., Worrest, R. C., Zepp, R. G., Paul, N. D., Cory, R. M., Solomon, K. R., Longstreth, J., Pandey, K. K., Redhwi, H. H., Torikai, A., and Heikkilä, A. M.: Environmental effects of ozone depletion, UV radiation and interactions with climate change: UNEP Environmental Effects Assessment Panel, update 2017, Photochemical & Photobiological Sciences, 17, 127-179, 10.1039/c7pp90043k, 2018.

Bais, A. F., Bernhard, G., McKenzie, R. L., Aucamp, P. J., Young, P. J., Ilyas, M., Jöckel, P., and Deushi, M.: Ozone–climate interactions and effects on solar ultraviolet radiation, Photochemical & Photobiological Sciences, 18, 602-640, 10.1039/c8pp90059k, 2019.

Bernhard, G., and Stierle, S.: Trends of UV Radiation in Antarctica, Atmosphere, 11, 10.3390/atmos11080795, 2020.

Bieliński, T.: A Parallax Shift Effect Correction Based on Cloud Height for Geostationary Satellites and Radar Observations, Remote Sensing, 12, 10.3390/rs12030365, 2020.

Blumthaler, M., and Ambach, W.: SOLAR UVB-ALBEDO OF VARIOUS SURFACES, Photochemistry and Photobiology, 48, 85-88, https://doi.org/10.1111/j.1751-1097.1988.tb02790.x, 1988.

Blumthaler, M., Ambach, W., and Ellinger, R.: Increase in solar UV radiation with altitude, Journal of Photochemistry and Photobiology B: Biology, 39, 130-134, https://doi.org/10.1016/S1011-1344(96)00018-8, 1997.

Boynard, A., Hurtmans, D., Garane, K., Goutail, F., Hadji-Lazaro, J., Koukouli, M. E., Wespes, C., Vigouroux, C., Keppens, A., Pommereau, J. P., Pazmino, A., Balis, D., Loyola, D., Valks, P., Sussmann, R., Smale, D., Coheur, P. F., and Clerbaux, C.: Validation of the IASI FORLI/EUMETSAT ozone products using satellite (GOME-2), ground-based (Brewer–Dobson, SAOZ, FTIR) and ozonesonde measurements, Atmos. Meas. Tech., 11, 5125-5152, 10.5194/amt-11-5125-2018, 2018.

Carrer, D., Roujean, J.-L., and Meurey, C.: Comparing Operational MSG/SEVIRI Land Surface Albedo Products From Land SAF With Ground Measurements and MODIS, IEEE Transactions on Geoscience and Remote Sensing, 48, 1714-1728, 10.1109/TGRS.2009.2034530, 2010.

Cede, A., Herman, J., Richter, A., Krotkov, N., and Burrows, J.: Measurements of nitrogen dioxide total column amounts using a Brewer double spectrophotometer in direct Sun mode, Journal of Geophysical Research: Atmospheres, 111, https://doi.org/10.1029/2005JD006585, 2006.

Chubarova, N., Zhdanova, Y., and Nezval, Y.: A new parameterization of the UV irradiance altitude dependence for clear-sky conditions and its application in the on-line UV tool over Northern Eurasia. Atmos. Chem. Phys., 16, 11867-11881, 10.5194/acp-16-11867-2016, 2016.

Chubarova, N.E., Pastukhova, A.S., Zhdanova, E.Y., Volpert, E.V., Smyshlyaev, S.P., and Galin, V.Y.: Effects of ozone and clouds on temporal variability of surface UV radiation and UV resources over Northern Eurasia derived from measurements and modeling. Atmosphere, 11(1), 59, 10.3390/atmos11010059, 2020.

Corr, C. A., Krotkov, N., Madronich, S., Slusser, J. R., Holben, B., Gao, W., Flynn, J., Lefer, B., and Kreidenweis, S. M.: Retrieval of aerosol single scattering albedo at ultraviolet wavelengths at the T1 site during MILAGRO, Atmos. Chem. Phys., 9, 5813-5827, 10.5194/acp-9-5813-2009, 2009.

Czerwińska, A. E., Krzyścin, J. W., Jarosławski, J., and Posyniak, M.: Effects of urban agglomeration on surface-UV doses: a comparison of Brewer measurements in Warsaw and Belsk, Poland, for the period 2013–2015, Atmos. Chem. Phys., 16, 13641-13651, 10.5194/acp-16-13641-2016, 2016.

Dahlback, A.: Dahlback, Measurements of biologically effective UV doses, total ozone abundances, and cloud effects with multichannel, moderate bandwidth filter instruments, Appl. Opt. Vol. 35, No. 33, 1996. Further references, see. Eg. Bernhard et al, Johnsen et al. JGR, 2008, Applied Optics, 35, 6514 - 6521, 10.1364/AO.35.006514, 1996.

De Bock, V., De Backer, H., Van Malderen, R., Mangold, A., and Delcloo, A.: Relations between erythemal UV dose, global solar radiation, total ozone column and aerosol optical depth at Uccle, Belgium, Atmos. Chem. Phys., 14, 12251-12270, 10.5194/acp-14-12251-2014, 2014.

Derrien, M., and Le Gléau, H.: MSG/SEVIRI cloud mask and type from SAFNWC, International Journal of Remote Sensing, 26, 4707-4732, 10.1080/01431160500166128, 2005.

Eleftheratos, K., Kazadzis, S., Zerefos, C. S., Tourpali, K., Meleti, C., Balis, D., Zyrichidou, I., Lakkala, K., Feister, U., Koskela, T., Heikkilä, A., and Karhu, J. M.: Ozone and Spectroradiometric UV Changes in the Past 20 Years over High Latitudes, Atmosphere-Ocean, 53, 117-125, 10.1080/07055900.2014.919897, 2015.

Eskes, H., Huijnen, V., Arola, A., Benedictow, A., Blechschmidt, A. M., Botek, E., Boucher, O., Bouarar, I., Chabrillat, S., Cuevas, E., Engelen, R., Flentje, H., Gaudel, A., Griesfeller, J., Jones, L., Kapsomenakis, J., Katragkou, E., Kinne, S., Langerock, B., Razinger, M., Richter, A., Schultz, M., Schulz, M., Sudarchikova, N., Thouret, V., Vrekoussis, M., Wagner, A., and Zerefos, C.: Validation of reactive gases and aerosols in the MACC global analysis and forecast system, Geosci. Model Dev., 8, 3523-3543, 10.5194/gmd-8-3523-2015, 2015.

Eskes, H. J., Velthoven, P. F. J. V., Valks, P. J. M., and Kelder, H. M.: Assimilation of GOME total-ozone satellite observations in a three-dimensional tracer-transport model, Quarterly Journal of the Royal Meteorological Society, 129, 1663-1681, https://doi.org/10.1256/qj.02.14, 2003.

Eskes, H. J., Wagner, A., Schulz, M., Christophe, Y., Ramonet, M., Basart, S., Benedictow, A., Bennouna, Y., Blechschmidt, A.-M., Chabrillat, S., Clark, H., Cuevas, E., Flentje, H., Hansen, K. M., IM, U., Kapsomenakis, J., Langerock, B., Petersen, K., Richter, A., Sudarchikova, N., Thouret, V., Warneke, T., and Zerefos, C.: Validation report of the cams near-real-time global atmospheric composition service: period September-November 2017., Copernicus Atmosphere Monitoring Service (CAMS) Report, CAMS84_2015SC3_D84.1.1.10_2017SON_V1.pdf, February 2018., 2018.

Feister, U., and Grewe, R.: SPECTRAL ALBEDO MEASUREMENTS IN THE UV and VISIBLE REGION OVER DIFFERENT TYPES OF SURFACES, Photochemistry and Photobiology, 62, 736-744, https://doi.org/10.1111/j.1751-1097.1995.tb08723.x, 1995.

Fioletov, V., Kerr, J. B., and Fergusson, A.: The UV Index: Definition, Distribution and Factors Affecting It, Canadian Journal of Public Health, 101, I5-I9, 10.1007/bf03405303, 2010.

Fioletov, V. E., Kerr, J. B., McArthur, L. J. B., Wardle, D. I., and Mathews, T. W.: Estimating UV Index Climatology over Canada, Journal of Applied Meteorology and Climatology, 42, 417-433, 10.1175/1520-0450(2003)042<0417:EUICOC>2.0.CO;2, 2003.

Fioletov, V. E., McArthur, L. J. B., Mathews, T. W., and Marrett, L.: On the relationship between erythemal and vitamin D action spectrum weighted ultraviolet radiation, Journal of Photochemistry and Photobiology B: Biology, 95, 9-16, https://doi.org/10.1016/j.jphotobiol.2008.11.014, 2009.

Fioletov, V.E., Griffioen, E., Kerr, J.B., Wardle, D.I., and Uchino, O.: Influence of volcanic sulfur dioxide on spectral UV irradiance as measured by Brewer spectrophotometers. Geophysical Research Letters, 25(10), 1665-1668, 1998.

Fountoulakis, I., Bais, A. F., Fragkos, K., Meleti, C., Tourpali, K., and Zempila, M. M.: Short- and long-term variability of spectral solar UV irradiance at Thessaloniki, Greece: effects of changes in aerosols, total ozone and clouds, Atmos. Chem. Phys., 16, 2493-2505, 10.5194/acp-16-2493-2016, 2016.

Fountoulakis, I., Zerefos, C. S., Bais, A. F., Kapsomenakis, J., Koukouli, M.-E., Ohkawara, N., Fioletov, V., De Backer, H., Lakkala, K., Karppinen, T., and Webb, A. R.: Twenty-five years of spectral UV-B measurements over Canada, Europe and Japan: Trends and effects from changes in ozone, aerosols, clouds, and surface reflectivity, Comptes Rendus Geoscience, 350, 393-402, https://doi.org/10.1016/j.crte.2018.07.011, 2018.

Fountoulakis, I., Natsis, A., Siomos, N., Drosoglou, T., and Bais, F. A.: Deriving Aerosol Absorption Properties from Solar Ultraviolet Radiation Spectral Measurements at Thessaloniki, Greece, Remote Sensing, 11, 10.3390/rs11182179, 2019.

Fountoulakis, I., Diémoz, H., Siani, A.-M., Laschewski, G., Filippa, G., Arola, A., Bais, A. F., De Backer, H., Lakkala, K., Webb, A. R., De Bock, V., Karppinen, T., Garane, K., Kapsomenakis, J., Koukouli, M.-E., and Zerefos, C. S.: Solar UV Irradiance in a Changing Climate: Trends in Europe and the Significance of Spectral Monitoring in Italy, Environments, 7, 10.3390/environments7010001, 2020a.

Fountoulakis, I., Diémoz, H., Siani, A. M., Hülsen, G., and Gröbner, J.: Monitoring of solar spectral ultraviolet irradiance in Aosta, Italy, Earth Syst. Sci. Data, 12, 2787-2810, 10.5194/essd-12-2787-2020, 2020b.

Gal, S.: Computing elementary functions: A new approach for achieving high accuracy and good performance, Accurate Scientific Computations, Berlin, Heidelberg, 1986, 1-16,

Garane, K., Bais, A. F., Kazadzis, S., Kazantzidis, A., and Meleti, C.: Monitoring of UV spectral irradiance at Thessaloniki (1990–2005): data re-evaluation and quality control, Ann. Geophys., 24, 3215-3228, 10.5194/angeo-24-3215-2006, 2006.

Garane, K., Lerot, C., Coldewey-Egbers, M., Verhoelst, T., Koukouli, M. E., Zyrichidou, I., Balis, D. S., Danckaert, T., Goutail, F., Granville, J., Hubert, D., Keppens, A., Lambert, J. C., Loyola, D., Pommereau, J. P., Van Roozendael, M., and Zehner, C.: Quality assessment of the Ozone_cci Climate Research Data Package (release 2017) – Part 1: Ground-based validation of total ozone column data products, Atmos. Meas. Tech., 11, 1385-1402, 10.5194/amt-11-1385-2018, 2018.

Garane, K., Koukouli, M. E., Verhoelst, T., Lerot, C., Heue, K. P., Fioletov, V., Balis, D., Bais, A., Bazureau, A., Dehn, A., Goutail, F., Granville, J., Griffin, D., Hubert, D., Keppens, A., Lambert, J. C., Loyola, D., McLinden, C., Pazmino, A., Pommereau, J. P., Redondas, A., Romahn, F., Valks, P., Van Roozendael, M., Xu, J., Zehner, C., Zerefos, C., and Zimmer, W.: TROPOMI/S5P total ozone column data: global ground-based validation and consistency with other satellite missions, Atmos. Meas. Tech., 12, 5263-5287, 10.5194/amt-12-5263-2019, 2019.

Giles, D. M., Sinyuk, A., Sorokin, M. G., Schafer, J. S., Smirnov, A., Slutsker, I., Eck, T. F., Holben, B. N., Lewis, J. R., Campbell, J. R., Welton, E. J., Korkin, S. V., and Lyapustin, A. I.: Advancements in the Aerosol Robotic Network (AERONET) Version 3 database – automated near-real-time quality control algorithm with improved cloud screening for Sun photometer aerosol optical depth (AOD) measurements, Atmos. Meas. Tech., 12, 169-209, 10.5194/amt-12-169-2019, 2019.

Gratien, A., Nilsson, E., Doussin, J.F., Johnson, M.S., Nielsen, C.J., Stenstrøm, Y., and Picquet-Varrault, B.: UV and IR absorption cross-sections of HCHO, HCDO, and DCDO. The journal of Physical Chemistry, A, 111(45), 11506-11513, 2007.

Gröbner, J., Schreder, J., Kazadzis, S., Bais, A. F., Blumthaler, M., Görts, P., Tax, R., Koskela, T., Seckmeyer, G., Webb, A. R., and Rembges, D.: Traveling reference spectroradiometer for routine quality assurance of spectral solar ultraviolet irradiance measurements, Applied Optics, 44, 5321-5331, 10.1364/ao.44.005321, 2005.

Gröbner, J., and Sperfeld, P.: Direct traceability of the portable QASUME irradiance scale to the primary irradiance standard of the PTB, Metrologia, 42, 134-139, 10.1088/0026-1394/42/2/008, 2005.

Gröbner, J., Kröger, I., Egli, L., Hülsen, G., Riechelmann, S., and Sperfeld, P.: The high-resolution extraterrestrial solar spectrum (QASUMEFTS) determined from ground-based solar irradiance measurements, Atmos. Meas. Tech., 10, 3375-3383, 10.5194/amt-10-3375-2017, 2017.

Gröbner, J.: Example datasets from PMOD/WRC Davos, Switzerland with the double Brewer B163 and QASUME II compared with the UVIOS model. Atmos. Meas. Tech. (supplement comment), 10.5194/amt-2020506-CC1, 2021.

Heikkilä, A., Kaurola, J., Lakkala, K., Karhu, J. M., Kyrö, E., Koskela, T., Engelsen, O., Slaper, H., and Seckmeyer, G.: European UV DataBase (EUVDB) as a repository and quality analyser for solar spectral UV irradiance monitored in Sodankylä, Geosci. Instrum. Method. Data Syst., 5, 333-345, 10.5194/gi-5-333-2016, 2016.

Henderson-Sellers, A., and Wilson, M. F.: Surface albedo data for climatic modeling, Reviews of Geophysics, 21, 1743-1778, https://doi.org/10.1029/RG021i008p01743, 1983.

Henken, C. C., Schmeits, M. J., Deneke, H., and Roebeling, R. A.: Using MSG-SEVIRI Cloud Physical Properties and Weather Radar Observations for the Detection of Cb/TCu Clouds, Journal of Applied Meteorology and Climatology, 50, 1587-1600, 2011.

Herman, J. R.: Global increase in UV irradiance during the past 30 years (1979–2008) estimated from satellite data, Journal of Geophysical Research: Atmospheres, 115, 10.1029/2009jd012219, 2010.

Holick, M. F.: Vitamin D: the underappreciated D-lightful hormone that is important for skeletal and cellular health, Current Opinion in Endocrinology, Diabetes and Obesity, 9, 2002.

Hülsen, G., Gröbner, J., Bais, A., Blumthaler, M., Disterhoft, P., Johnsen, B., Lantz, K. O., Meleti, C., Schreder, J., Vilaplana Guerrero, J. M., and Ylianttila, L.: Intercomparison of erythemal broadband radiometers calibrated by seven UV calibration facilities in Europe and the USA, Atmos. Chem. Phys., 8, 4865-4875, 10.5194/acp-8-4865-2008, 2008.

Hülsen, G., Gröbner, J., Nevas, S., Sperfeld, P., Egli, L., Porrovecchio, G., and Smid, M.: Traceability of solar UV measurements using the Qasume reference spectroradiometer, Applied Optics, 55, 7265 - 7275, 10.1364/AO.55.007265, 2016.

Hülsen, G., Gröbner, J., Bais, A., Blumthaler, M., Diemoz, H., Bolsee, D., Rodríguez, A. D., Fountoulakis, I., Naranen, E., Schreder, J., Stefania, F., and Vilaplana Guerrero, J. M.: Second solar ultraviolet radiometer comparison campaign UVC-II, Metrologia, 2020.

Johnsen B., Kjeldstad B., Aalerud T.N., Nilsen L.T., Schreder J., Blumthaler M., Bernhard G., Topaloglou C., Meinander O., Bagheri A., Slusser J.R. and Davis J.: Intercomparison and harmonization of UV index measurements from multiband filter radiometers, J. Geophys. Res. 113, D15206. doi:10.1029/2007JD009731, 2008.

Juzeniene, A., Brekke, P., Dahlback, A., Andersson-Engels, S., Reichrath, J., Moan, K., Holick, M. F., Grant, W. B., and Moan, J.: Solar radiation and human health, Reports on Progress in Physics, 74, 066701, 10.1088/0034-4885/74/6/066701, 2011.

Kato, S., and Marshak, A.: Solar zenith and viewing geometry-dependent errors in satellite retrieved cloud optical thickness: Marine stratocumulus case. Journal of Geophysical Research, 114, D01202, 10.1029/2008JD010579, 2009.

Kazadzis, S., Bais, A., Balis, D., Kouremeti, N., Zempila, M., Arola, A., Giannakaki, E., Amiridis, V., and Kazantzidis, A.: Spatial and temporal UV irradiance and aerosol variability within the area of an OMI satellite pixel, Atmos. Chem. Phys., 9, 4593-4601, 10.5194/acp-9-4593-2009, 2009a.

Kazadzis, S., Kouremeti, N., Bais, A., Kazantzidis, A., and Meleti, C.: Aerosol forcing efficiency in the UVA region from spectral solar irradiance measurements at an urban environment, Ann. Geophys., 27, 2515-2522, 10.5194/angeo-27-2515-2009, 2009b.

Kazadzis, S., Raptis, P., Kouremeti, N., Amiridis, V., Arola, A., Gerasopoulos, E., and Schuster, G. L.: Aerosol absorption retrieval at ultraviolet wavelengths in a complex environment, Atmos. Meas. Tech., 9, 5997-6011, 10.5194/amt-9-5997-2016, 2016.

Kerr, J. B., Evans, W. F. J., and Asbridge, I. A.: Recalibration of Dobson Field Spectrophotometers with a Travelling Brewer Spectrophotometer Standard, Atmospheric Ozone, Dordrecht, 1985, 381-386,

Kerr, J. B., and Fioletov, V. E.: Surface ultraviolet radiation, Atmosphere-Ocean, 46, 159-184, 10.3137/ao.460108, 2008.

Kinne, S.: The MACv2 aerosol climatology, Tellus B: Chemical and Physical Meteorology, 71, 1-21, 10.1080/16000889.2019.1623639, 2019.

Koren, I., Remer, L. A., Kaufman, Y. J., Rudich, Y., and Martins, J. V.: On the twilight zone between clouds and aerosols, Geophysical Research Letters, 34, https://doi.org/10.1029/2007GL029253, 2007.

Kosmopoulos, P. G., Kazadzis, S., Taylor, M., Raptis, P. I., Keramitsoglou, I., Kiranoudis, C., and Bais, A. F.: Assessment of surface solar irradiance derived from real-time modelling techniques and verification with ground-based measurements, Atmos. Meas. Tech., 11, 907-924, 10.5194/amt-11-907-2018, 2018.

Kosmopoulos, P.G., Kouroutsidis, D., Papachristopoulou, K., Raptis, P.I., Masoom, A., Saint-Drenan, Y-M., Blanc, P., Kontoes, C. and Kazadzis, S.: Short-Term Forecasting of Large-Scale Clouds Impact on Downwelling Surface Solar Irradiation. Energies, 13(24), 6555. https://doi.org/10.3390/en13246555, 2020.

Kreuter, A., Buras, R., Mayer, B., Webb, A., Kift, R., Bais, A., Kouremeti, N., and Blumthaler, M.: Solar irradiance in the heterogeneous albedo environment of the Arctic coast: measurements and a 3-D model study, Atmos. Chem. Phys., 14, 5989-6002, 10.5194/acp-14-5989-2014, 2014.

Krotkov, N. A., Bhartia, P. K., Herman, J. R., Fioletov, V., and Kerr, J.: Satellite estimation of spectral surface UV irradiance in the presence of tropospheric aerosols: 1. Cloud-free case, Journal of Geophysical Research: Atmospheres, 103, 8779-8793, https://doi.org/10.1029/98JD00233, 1998.

Lacaze, R., Smets, B., Trigo, I., Calvet, J.C., Jann, A., Camacho, F., Baret, F., Kidd, R., Defourny, P., Tansey, K., et al.: The Copernicus Global Land Service: Present and future. In Proceedings of the EGU General Assembly, Vienna, Austria, 7-12 April, 2013.

Lakkala, K., Arola, A., Heikkilä, A., Kaurola, J., Koskela, T., Kyrö, E., Lindfors, A., Meinander, O., Tanskanen, A., Gröbner, J., and Hülsen, G.: Quality assurance of the Brewer spectral UV measurements in Finland, Atmos. Chem. Phys., 8, 3369-3383, 10.5194/acp-8-3369-2008, 2008.

Lakkala, K., Redondas, A., Meinander, O., Thölix, L., Hamari, B., Almansa, A. F., Carreno, V., García, R. D., Torres, C., Deferrari, G., Ochoa, H., Bernhard, G., Sanchez, R., and de Leeuw, G.: UV measurements at Marambio and Ushuaia during 2000–2010, Atmos. Chem. Phys., 18, 16019-16031, 10.5194/acp-18-16019-2018, 2018.

Lakkala, K., Kujanpää, J., Brogniez, C., Henriot, N., Arola, A., Aun, M., Auriol, F., Bais, A. F., Bernhard, G., De Bock, V., Catalfamo, M., Deroo, C., Diémoz, H., Egli, L., Forestier, J. B., Fountoulakis, I., Garcia, R. D., Gröbner, J., Hassinen, S., Heikkilä, A., Henderson, S., Hülsen, G., Johnsen, B., Kalakoski, N., Karanikolas, A., Karppinen, T., Lamy, K., León-Luis, S.

F., Lindfors, A. V., Metzger, J. M., Minvielle, F., Muskatel, H. B., Portafaix, T., Redondas, A., Sanchez, R., Siani, A. M., Svendby, T., and Tamminen, J.: Validation of TROPOMI Surface UV Radiation Product, Atmos. Meas. Tech. Discuss., 2020, 1-37, 10.5194/amt-2020-121, 2020.

Larkin, A., Haigh, J. D., and Djavidnia, S.: The Effect of Solar UV Irradiance Variations on the Earth's Atmosphere, Space Science Reviews, 94, 199-214, 10.1023/a:1026771307057, 2000.

Levelt, P. F., Oord, G. H. J. v. d., Dobber, M. R., Malkki, A., Huib, V., Johan de, V., Stammes, P., Lundell, J. O. V., and Saari, H.: The ozone monitoring instrument, IEEE Transactions on Geoscience and Remote Sensing, 44, 1093-1101, 10.1109/tgrs.2006.872333, 2006.

Levelt, P. F., Joiner, J., Tamminen, J., Veefkind, J. P., Bhartia, P. K., Stein Zweers, D. C., Duncan, B. N., Streets, D. G., Eskes, H., van der A, R., McLinden, C., Fioletov, V., Carn, S., de Laat, J., DeLand, M., Marchenko, S., McPeters, R., Ziemke, J., Fu, D., Liu, X., Pickering, K., Apituley, A., González Abad, G., Arola, A., Boersma, F., Chan Miller, C., Chance, K., de Graaf, M., Hakkarainen, J., Hassinen, S., Ialongo, I., Kleipool, Q., Krotkov, N., Li, C., Lamsal, L., Newman, P., Nowlan, C., Suleiman, R., Tilstra, L. G., Torres, O., Wang, H., and Wargan, K.: The Ozone Monitoring Instrument: overview of 14 years in space, Atmos. Chem. Phys., 18, 5699-5745, 10.5194/acp-18-5699-2018, 2018.

López-Solano, J., Redondas, A., Carlund, T., Rodriguez-Franco, J. J., Diémoz, H., León-Luis, S. F., Hernández-Cruz, B., Guirado-Fuentes, C., Kouremeti, N., Gröbner, J., Kazadzis, S., Carreño, V., Berjón, A., Santana-Díaz, D., Rodríguez-Valido, M., De Bock, V., Moreta, J. R., Rimmer, J., Smedley, A. R. D., Boulkelia, L., Jepsen, N., Eriksen, P., Bais, A. F., Shirotov, V., Vilaplana, J. M., Wilson, K. M., and Karppinen, T.: Aerosol optical depth in the European Brewer Network, Atmos. Chem. Phys., 18, 3885-3902, 10.5194/acp-18-3885-2018, 2018.

Lucas, R., McMichael, T., Smith, W., Armstrong, B. K., Prüss-Üstün, A., and World Health, O.: Solar ultraviolet radiation : global burden of disease from solar ultraviolet radiation / Robyn Lucas ... [et al.] ; editors, Annette Prüss-Üstün ... [et al.]. Environmental burden of disease series ; no. 13, World Health Organization, Geneva, 2006.

Lucas, R. M., Byrne, S. N., Correale, J., Ilschner, S., and Hart, P. H.: Ultraviolet radiation, vitamin D and multiple sclerosis, Neurodegenerative Disease Management, 5, 413-424, 10.2217/nmt.15.33, 2015.

Madronich, S.: Environmental UV Photobiology, Environ. UV Photobiol., 10.1007/978-1-4899-2406-3, 1993.

Mayer, B., Kylling, A., Madronich, S., and Seckmeyer, G.: Enhanced absorption of UV radiation due to multiple scattering in clouds: Experimental evidence and theoretical explanation, Journal of Geophysical Research: Atmospheres, 103, 31241-31254, https://doi.org/10.1029/98JD02676, 1998.

Mayer, B., and Kylling, A.: Technical note: The libRadtran software package for radiative transfer calculations - description and examples of use, Atmos. Chem. Phys., 5, 1855-1877, 10.5194/acp-5-1855-2005, 2005.

McKenzie, R., Bernhard, G., Liley, B., Disterhoft, P., Rhodes, S., Bais, A., Morgenstern, O., Newman, P., Oman, L., Brogniez, C., and Simic, S.: Success of Montreal Protocol Demonstrated by Comparing High-Quality UV Measurements with “World Avoided” Calculations from Two Chemistry-Climate Models, Scientific Reports, 9, 12332, 10.1038/s41598-019-48625-z, 2019.

McKenzie, R. L., Aucamp, P. J., Bais, A. F., Björn, L. O., Ilyas, M., and Madronich, S.: Ozone depletion and climate change: impacts on UV radiation, Photochemical & Photobiological Sciences, 10, 182-198, 10.1039/c0pp90034f, 2011.

Meinander, O., Kazadzis, S., Arola, A., Riihelä, A., Räisänen, P., Kivi, R., Kontu, A., Kouznetsov, R., Sofiev, M., Svensson, J., Suokanerva, H., Aaltonen, V., Manninen, T., Roujean, J. L., and Hautecoeur, O.: Spectral albedo of seasonal snow during

intensive melt period at Sodankylä, beyond the Arctic Circle, Atmos. Chem. Phys., 13, 3793-3810, 10.5194/acp-13-3793-2013, 2013.

MétéoFrance: Algorithm theoretical basis document for cloud products (CMa-PGE01 v3.2, CT-PGE02 v2.2 & CTTH-PGE03 v2.2), Technical Report SAF/NWC/CDOP/MFL/SCI/ATBD/01, Paris: MétéoFrance, 2013.

Mok, J., Krotkov, N. A., Torres, O., Jethva, H., Li, Z., Kim, J., Koo, J. H., Go, S., Irie, H., Labow, G., Eck, T. F., Holben, B. N., Herman, J., Loughman, R. P., Spinei, E., Lee, S. S., Khatri, P., and Campanelli, M.: Comparisons of spectral aerosol single scattering albedo in Seoul, South Korea, Atmos. Meas. Tech., 11, 2295-2311, 10.5194/amt-11-2295-2018, 2018.

Myhre, G., and Myhre, A.: Uncertainties in Radiative Forcing due to Surface Albedo Changes Caused by Land-Use Changes, Journal of Climate, 16, 1511-1524, 10.1175/1520-0442(2003)016<1511:uirfdt>2.0.co;2, 2003.

NOAA: Data Announcement 88-MGG-02, Digital relief of the surface of the Earth. NOAA, National Geopgysical Data Center, Boulder, Colorado, 1988.

Noël, S., Mieruch, S., Bovensmann, H., and Burrows, J. P.: Preliminary results of GOME-2 water vapour retrievals and first applications in polar regions, Atmos. Chem. Phys., 8, 1519-1529, 10.5194/acp-8-1519-2008, 2008.

Peeters, P., Simon, P. C., Hansen, G., Meerkoetter, R., Verdebout, J., Seckmeyer, G., Taalas, P., and Slaper, H.: MAUVE: A European Initiative for Developing and Improving Satellite Derived Ultraviolet Maps, Radiation Protection Dosimetry, 91, 201-202, 10.1093/oxfordjournals.rpd.a033200, 2000.

Pfeifroth, U., Kothe, S., and Trentmann, J.: Validation report: Meteosat solar surface radiation and effective cloud albedo climate data record (Sarah 2), EUMETSAT SAF CM Validation report with reference number SAF/CM/DWD/VAL/METEOSAT/HEL, 2.1, https://doi.org/10.5676/EUM_SAF_CM/SARAH/V002, 2016.

Probst, P., Rizzi, R., Tosi, E., Lucarini, V., and Maestri, T.: Total cloud cover from satellite observations and climate models, Atmospheric Research, 107, 161-170, https://doi.org/10.1016/j.atmosres.2012.01.005, 2012.

Raptis, I.-P., Kazadzis, S., Eleftheratos, K., Amiridis, V., and Fountoulakis, I.: Single Scattering Albedo's Spectral Dependence Effect on UV Irradiance., Atmosphere, 9, 10.3390/atmos9090364, 2018.

Reda, I., and Andreas, A.: Solar position algorithm for solar radiation applications. NREL Technical Report, NREL/TP-560-34302, Prepared under Task No. WU1D5600, 2008.

Renaud, A., Staehelin, J., Fröhlich, C., Philipona, R., and Heimo, A.: Influence of snow and clouds on erythemal UV radiation: Analysis of Swiss measurements and comparison with models, Journal of Geophysical Research: Atmospheres, 105, 4961-4969, https://doi.org/10.1029/1999JD900160, 2000.

Rimmer, J. S., Redondas, A., and Karppinen, T.: EuBrewNet – A European Brewer network (COST Action ES1207), an overview, Atmos. Chem. Phys., 18, 10347-10353, 10.5194/acp-18-10347-2018, 2018.

Schmalwieser, A., and Siani, A.: Review on Non-Occupational Personal Solar UV Exposure Measurements, Photochemistry and Photobiology, 94, 10.1111/php.12946, 2018.

Schmalwieser, A. W., Gröbner, J., Blumthaler, M., Klotz, B., De Backer, H., Bolsée, D., Werner, R., Tomsic, D., Metelka, L., Eriksen, P., Jepsen, N., Aun, M., Heikkilä, A., Duprat, T., Sandmann, H., Weiss, T., Bais, A., Toth, Z., Siani, A.-M., Vaccaro, L., Diémoz, H., Grifoni, D., Zipoli, G., Lorenzetto, G., Petkov, B. H., di Sarra, A. G., Massen, F., Yousif, C., Aculinin, A. A., den Outer, P., Svendby, T., Dahlback, A., Johnsen, B., Biszczuk-Jakubowska, J., Krzyscin, J., Henriques, D., Chubarova, N.,

Kolarž, P., Mijatovic, Z., Groselj, D., Pribullova, A., Gonzales, J. R. M., Bilbao, J., Guerrero, J. M. V., Serrano, A., Andersson, S., Vuilleumier, L., Webb, A., and O'Hagan, J.: UV Index monitoring in Europe, Photochemical & Photobiological Sciences, 16, 1349-1370, 10.1039/c7pp00178a, 2017.

Schmalwieser, A. W.: Possibilities to estimate the personal UV radiation exposure from ambient UV radiation measurements, Photochemical & Photobiological Sciences, 19, 1249-1261, 10.1039/d0pp00182a, 2020.

Seckmeyer, G., Erb, R., and Albold, A.: Transmittance of a cloud is wavelength-dependent in the UV-range, Geophysical Research Letters, 23, 2753-2755, https://doi.org/10.1029/96GL02614, 1996.

Seckmeyer, G., Pissulla, D., Glandorf, M., Henriques, D., Johnsen, B., Webb, A., Siani, A.-M., Bais, A., Kjeldstad, B., Brogniez, C., Lenoble, J., Gardiner, B., Kirsch, P., Koskela, T., Kaurola, J., Uhlmann, B., Slaper, H., Den Outer, P., Janouch, M., Werle, P., Gröbner, J., Mayer, B., De La Casiniere, A., Simic, S., and Carvalho, F.: Variability of UV Irradiance in Europe, Photochemistry and Photobiology, 84, 172-179, 10.1111/j.1751-1097.2007.00216.x, 2008.

Siani, A. M., Casale, G. R., Diémoz, H., Agnesod, G., Kimlin, M. G., Lang, C. A., and Colosimo, A.: Personal UV exposure in high albedo alpine sites, Atmos. Chem. Phys., 8, 3749-3760, 10.5194/acp-8-3749-2008, 2008.

Slaper, H., Reinen, H. A. J. M., Blumthaler, M., Huber, M., and Kuik, F.: Comparing ground-level spectrally resolved solar UV measurements using various instruments: A technique resolving effects of wavelength shift and slit width, Geophysical Research Letters, 22, 2721-2724, 10.1029/95gl02824, 1995.

Smedley, A. R. D., Rimmer, J. S., Moore, D., Toumi, R., and Webb, A. R.: Total ozone and surface UV trends in the United Kingdom: 1979–2008, International Journal of Climatology, 32, 338-346, 10.1002/joc.2275, 2012.

Taylor, M., Kosmopoulos, P. G., Kazadzis, S., Keramitsoglou, I., and Kiranoudis, C. T.: Neural network radiative transfer solvers for the generation of high resolution solar irradiance spectra parameterized by cloud and aerosol parameters, Journal of Quantitative Spectroscopy and Radiative Transfer, 168, 176-192, https://doi.org/10.1016/j.jqsrt.2015.08.018, 2016.

Vanicek, K., Frei, T., Litynska, Z., and Schmalwieser, A.: UV-Index for the Public, European Union, 2000.

Verdebout, J.: Amethod to generate surface UV radiation maps over Europe using GOME, Meteosat and ancillary geophysical data. Journal of Geophysical Research: Atmospheres, 105(D4), 5049-5058, 2000.

Vitt, R., Laschewski, G., Bais, A. F., Diémoz, H., Fountoulakis, I., Siani, A.-M., and Matzarakis, A.: UV-Index Climatology for Europe Based on Satellite Data, Atmosphere, 11, 10.3390/atmos11070727, 2020.

Webb, A. R., and Engelsen, O.: Ultraviolet Exposure Scenarios: Risks of Erythema from Recommendations on Cutaneous Vitamin D Synthesis, in: Sunlight, Vitamin D and Skin Cancer, edited by: Reichrath, J., Springer New York, New York, NY, 72-85, 2008.

Webb, A. R., Slaper, H., Koepke, P., and Schmalwieser, A. W.: Know Your Standard: Clarifying the CIE Erythema Action Spectrum, Photochemistry and Photobiology, 87, 483-486, 10.1111/j.1751-1097.2010.00871.x, 2011.

WHO: Global Solar UV Index: A Pratical Guide, No. WHO/SD., Geneva, Switzerland, 2002.

WMO: Report of the WMO Meeting of Experts on UVB Measurements, Data Quality and Standardization of UV Indices, 1994, 1995.

Zempila, M.-M., Koukouli, M.-E., Bais, A., Fountoulakis, I., Arola, A., Kouremeti, N., and Balis, D.: OMI/Aura UV product validation using NILU-UV ground-based measurements in Thessaloniki, Greece, Atmospheric Environment, 140, 283-297, https://doi.org/10.1016/j.atmosenv.2016.06.009, 2016.

Zerefos, C. S., Tourpali, K., Eleftheratos, K., Kazadzis, S., Meleti, C., Feister, U., Koskela, T., and Heikkilä, A.: Evidence of a possible turning point in solar UV-B over Canada, Europe and Japan, Atmos. Chem. Phys., 12, 2469-2477, 10.5194/acp-12-2469-2012, 2012.

Table 1: UVIOS model input parameters

Parameter	Description (spatial – temporal resolution)	Source	Reference
Cloud microphysics	Nowcast cloud optical thickness (COT), cloud phase (CPH) (5 km – 15 minutes)	Meteosat Second Generation (MSG4) NOA Antenna	(MétéoFrance, 2013)
Aerosol optical depth	1-day forecast aerosol optical depth (AOD) (40 km – 3 hours)	Copernicus Atmosphere Monitoring Service (CAMS) – FTP access	(Eskes et al., 2015)
Aerosol optical properties	Single scattering albedo (SSA), Angstrom exponent (AE) (1 x 1 degrees – 1 month)	Aerosol Comparisons between Observations and Models (Aerocom)	(Kinne, 2019)
Solar elevation	Solar zenith angle (SZA) (5 km – 15 minutes)	Astronomical model In-house software (NOA)	(Reda and Andreas, 2008)
Surface albedo	Surface albedo (ALB) (1 km – 12 days)	Copernicus Global Land Service (CGLS)	(Carrer et al., 2010)
Water vapor	H_2O observation (40 x 80 km – 1day)	Global Ozone Monitoring Experiment 2 Level 2 data (GOME-2 L2)	(Noël et al., 2008)
Surface elevation	Elevation observation (ELE) (1 m – fixed)	Digital Elevation Model (DEM) In-house database (NOAA)	(NOAA, 1988)
Ozone	1-day forecast total ozone column (TOC) (1 x 1 degrees – 1 day)	Tropospheric Emission Monitoring Internet Service (TEMIS) with Assimilated Ozone Fields from GOME-2 (METOP-B)	(Eskes et al., 2003)

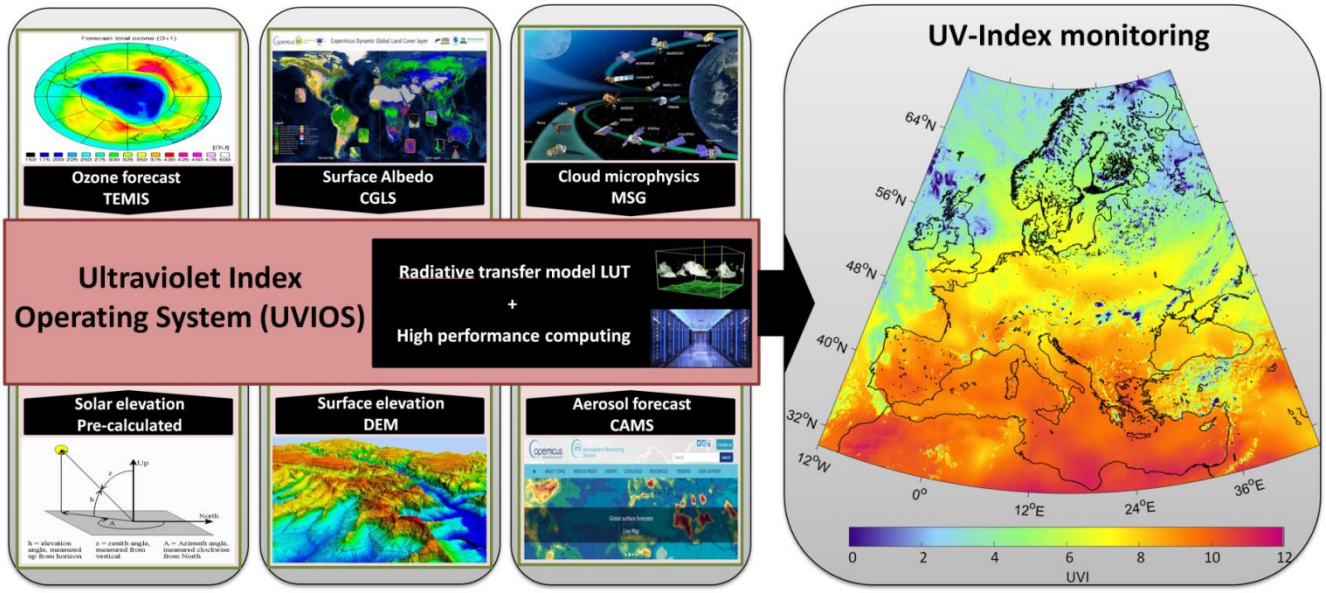

Figure 1: Flowchart illustration of the UVIOS modelling technique scheme. The pre-calculated effects of solar and surface elevation and albedo followed by the aerosol and ozone forecasts and the real-time cloud observations to the UVIOS solver result in the spectrally weighted output of UVI for the European region.

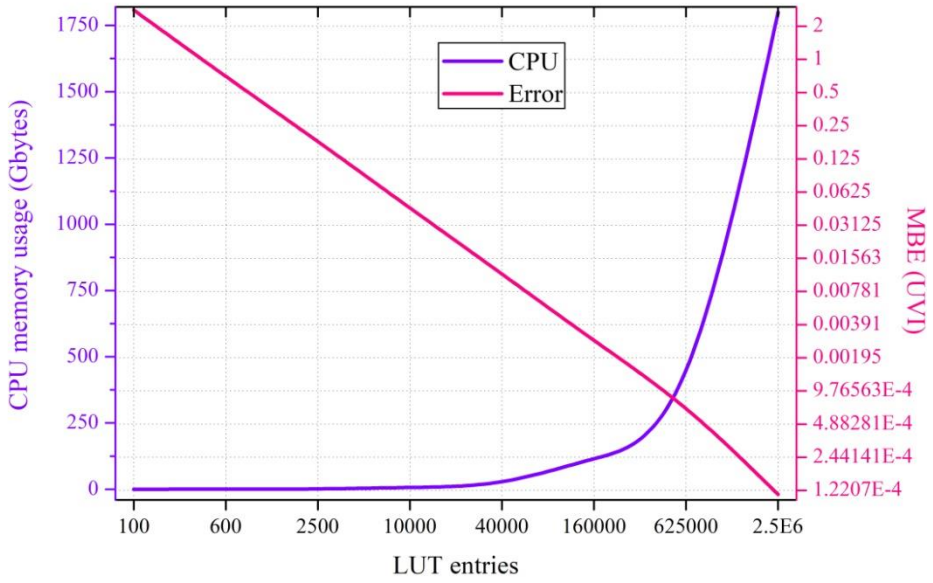

Figure 2: UVIOS memory usage and error statistics in terms of mean bias error (MBE) for a range of different LUT sizes.

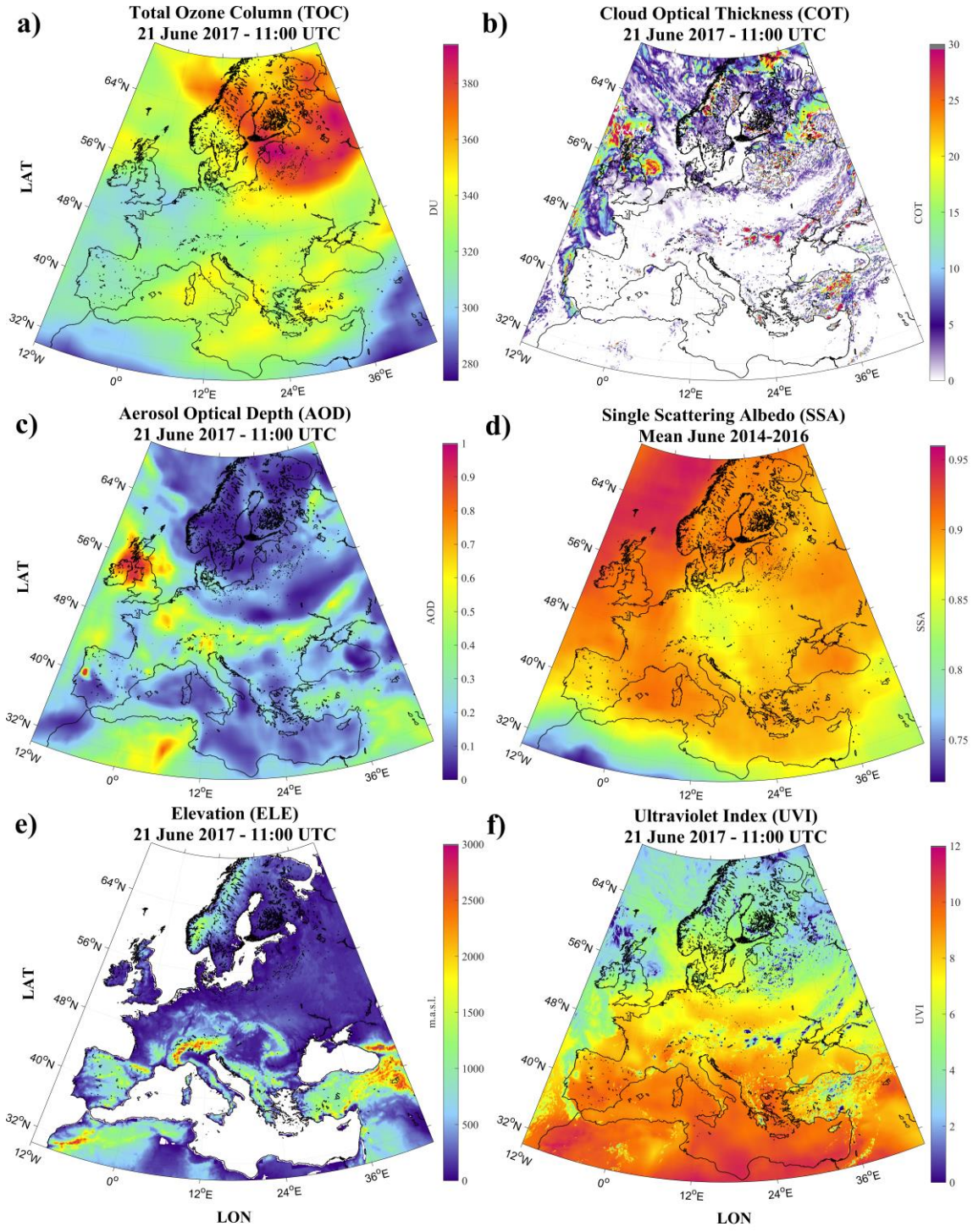

Figure 3: An example of the input TOC (a), COT (b), AOD (c), SSA (d), ELE (e) and output UVI (f) maps based on the UVIOS modelling technique applied for the 21st of June 2017 at 11:00 UTC.

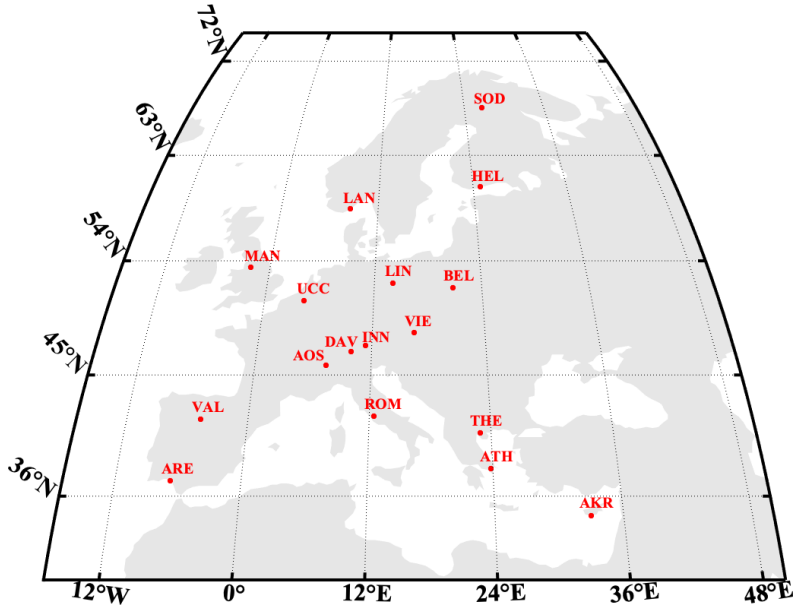

Figure 4: Study region and UVI ground measurement locations.

Table 2: Coordinates (degrees), instrument type, height (metres above sea level) and maximum UVI measured levels of the European stations used for the comparison.

Station	Country	Code	Latitude (ºN)	Longitude (ºE)	Instrument	Height (m.a.s.l.)	UVImax	Reference
Akrotiri	Cyprus	**AKR**	34.59	32.99	SL501	23	9.14	
Aosta	Italy	**AOS**	45.74	7.36	Bentham DTMc300	570	9.60	(Fountoulakis et al., 2020b)
El Arenosillo	Spain	**ARE**	37.10	-6.73	Brewer MKIII	52	9.78	
Athens	Greece	**ATH**	37.99	23.78	Brewer MKIV	180	10.20	
Belsk	Poland	**BEL**	51.84	20.79	Brewer MKIII	176	7.54	(Czerwińska et al., 2016)
Davos	Switzerland	**DAV**	46.81	9.84	Brewer MKIII	1590	10.57	
Helsinki	Finland	**HEL**	60.20	24.96	Brewer MKIII	48	5.68	(Lakkala et al., 2008)
Innsbruck	Austria	**INN**	47.26	11.38	SL501	577	8.35	(Hülsen et al., 2020)
Landvik	Norway	**LAN**	58.33	8.52	GUV-541	10	6.65	(Johnsen et al., 2008)
Lindenberg	Germany	**LIN**	52.21	14.11	Bentham DTMc300	127	8.86	
Manchester	United Kingdom	**MAN**	53.47	-2.23	Brewer MKII	76	7.30	(Smedley et al., 2012)
Rome	Italy	**ROM**	41.90	12.50	Brewer MKIV	75	8.38	
Sodankyla	Finland	**SOD**	67.37	26.63	Brewer MKIII	179	4.51	(Heikkilä et al., 2016; Lakkala et al., 2008)
Thessaloniki	Greece	**THE**	40.63	22.96	Brewer MKIII	60	10.40	(Fountoulakis et al., 2016; Garane et al., 2006)
Uccle	Belgium	**UCC**	50.80	4.35	Brewer MKIII	100	8.99	(De Bock et al., 2014)
Valladolid	Spain	**VAL**	41.66	-4.71	YES	705	10.32	(Hülsen et al., 2020)
Vienna	Austria	**VIE**	48.26	16.43	SL501	153	8.09	(Hülsen et al., 2020)

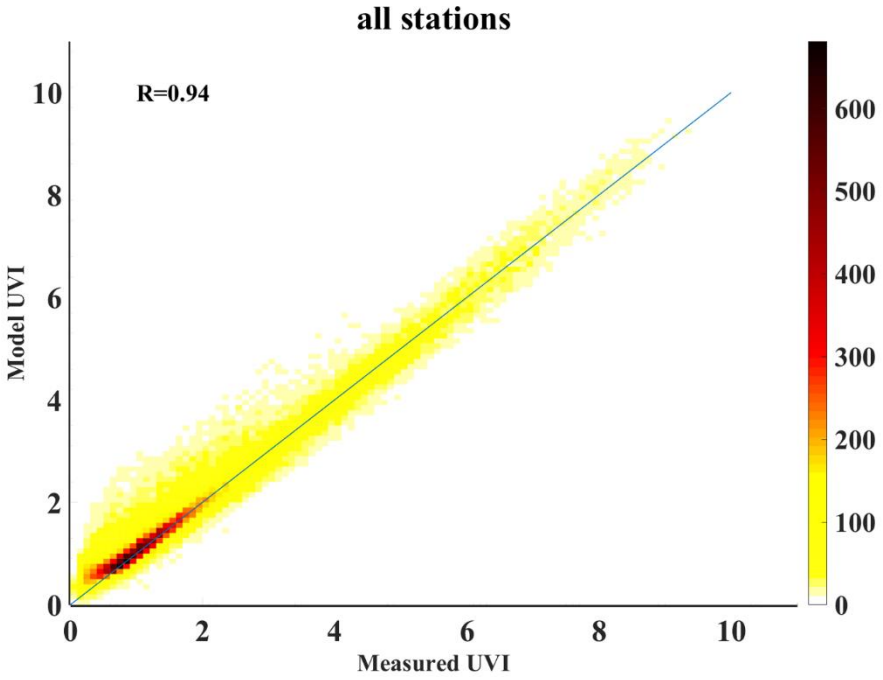

Figure 5: Density scatterplot of the overall UVIOS performance for all stations. The analytical statistics for each station can be found in the Appendix A.

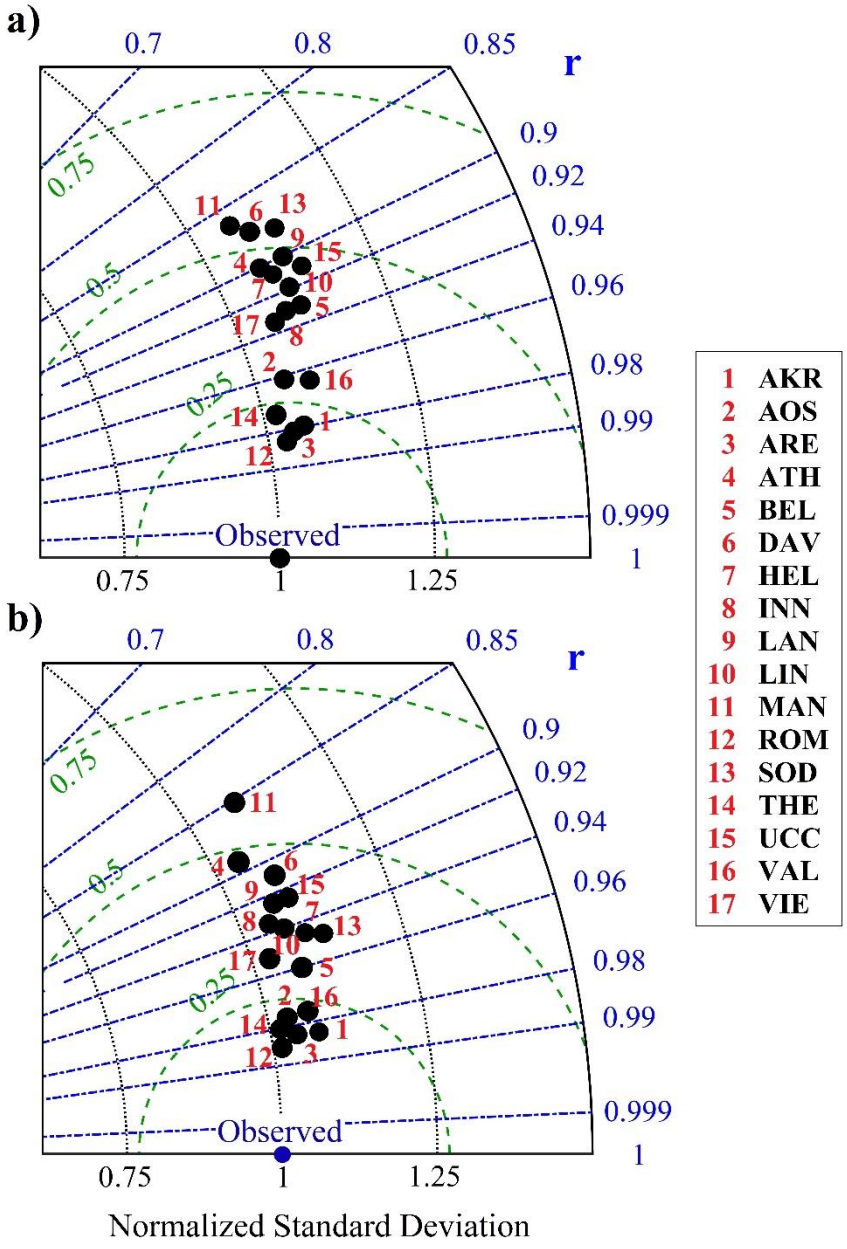

Figure 6: Taylor diagram for the overall UVIOS accuracy for all ground-stations under all sky (a) and clear sky (b) conditions.

Table 3: Absolute difference between UVIOS and ground-based UVI measurements in terms of percentages (%) of data that are within 0.5 and 1 UVI of difference (U0.5 and U1.0, respectively) as well as the correlation coefficient (r) for all sky and clear sky conditions.

STATION	ALL SKY			CLEAR SKY		
	U0.5	U1.0	r	U0.5	U1.0	r
AKR	82.25	96.02	0.980	84.57	97.48	0.987
AOS	86.81	94.40	0.961	92.23	97.07	0.978
ARE	85.15	95.73	0.981	87.99	96.86	0.986
ATH	84.99	94.29	0.902	88.98	96.35	0.891
BEL	83.07	93.28	0.933	91.30	96.50	0.960
DAV	74.20	86.43	0.873	76.19	87.06	0.912
HEL	86.53	94.79	0.909	94.13	97.70	0.944
INN	79.96	92.17	0.932	87.09	95.23	0.937
LAN	84.94	93.46	0.900	92.34	96.52	0.925
LIN	81.58	91.86	0.919	90.95	96.31	0.941
MAN	77.72	90.44	0.862	87.85	94.27	0.852
ROM	87.69	96.19	0.985	89.55	97.00	0.991
SOD	90.86	97.26	0.883	95.69	98.94	0.947
THE	88.98	95.91	0.974	92.51	97.35	0.981
UCC	71.18	87.68	0.913	83.23	92.15	0.926
VAL	85.86	93.93	0.962	86.61	95.22	0.976
VIE	76.65	91.53	0.936	83.37	94.42	0.952

Table 4: Mean bias error of the TEMIS TOC as compared to the WOUDC ground-based measurements.

Station	AOS	ATH	DAV	MAN	ROM	SOD	THE	UCC
MBE TOC (DU)	7.6	-0.9	1.9	5.0	-9.9	-5.4	-2.2	2.9
RMSE TOC (DU)	15.8	10.0	9.1	11.3	12.5	13.1	6.2	7.8
r	0.92	0.95	0.97	0.97	0.94	0.97	0.99	0.98

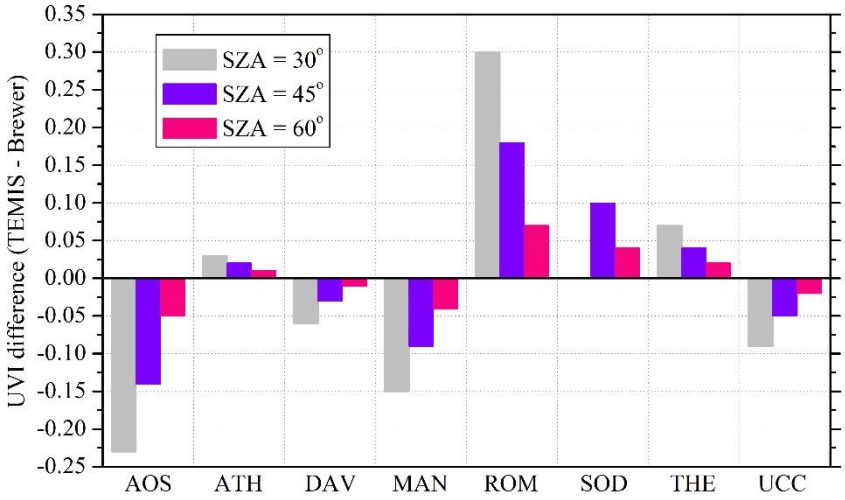

Figure 7: Differences of UVI derived by the UVIOS using as input the TEMIS and the Brewer TOC respectively at all stations with available data. (lower possible SOD SZA is 44 degrees).

Table 5: Comparison results between CAMS forecasted AOD values used as UVIOS input and AERONET ground-based AOD measurements. The AOD MBE and RMSE statistical scores are shown in absolute units, along with correlation coefficient.

Station	AKR	ARE	ATH	DAV	HEL	LIN	ROM	SOD	THE	UCC	VAL	VIE
MBE	0.037	0.042	0.030	0.029	0.062	0.026	0.017	0.047	0.008	-0.007	0.024	0.071
RMSE	0.074	0.070	0.074	0.053	0.078	0.074	0.056	0.065	0.066	0.150	0.073	0.157
r	0.77	0.91	0.80	0.73	0.70	0.69	0.80	0.63	0.76	0.50	0.78	0.10

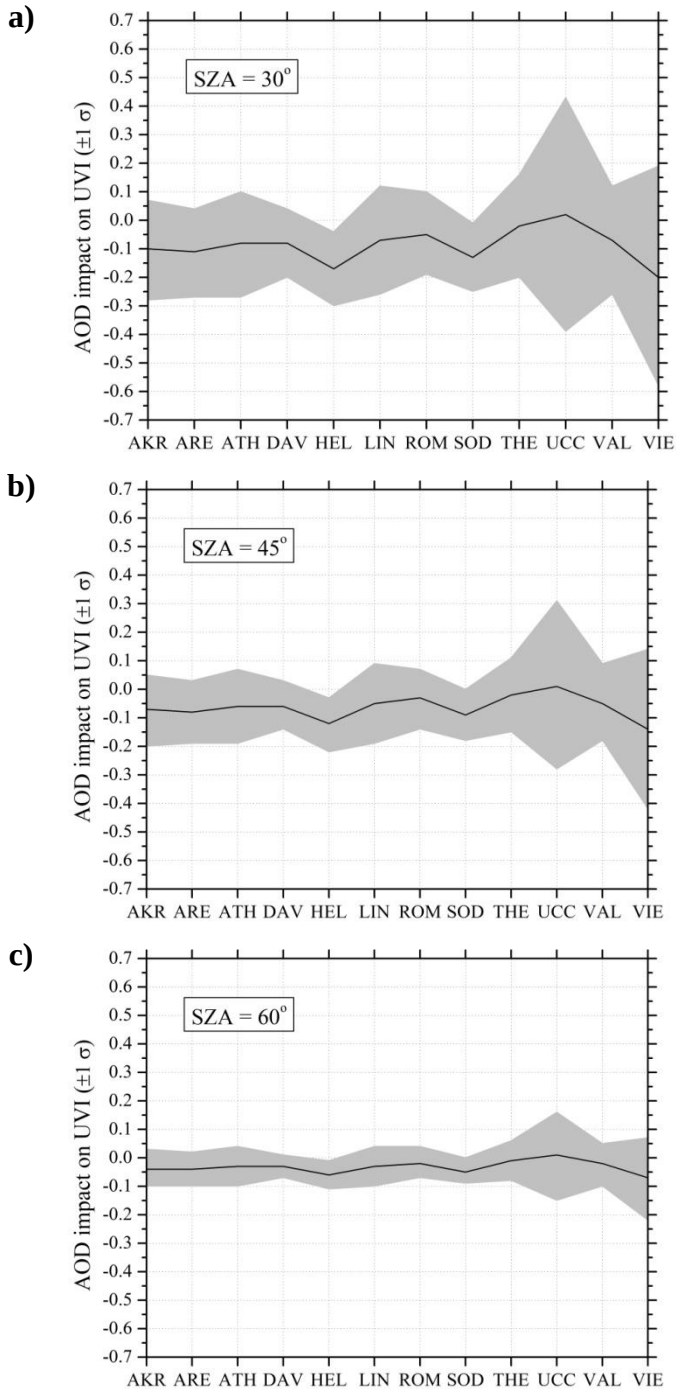

Figure 8: The mean bias error of the CAMS – AERONET AOD impact on UVI for all stations with available data as a function of SZA at 30 (a), 45 (b) and 60 (c) degrees together with the uncertainty range (± 1 σ).

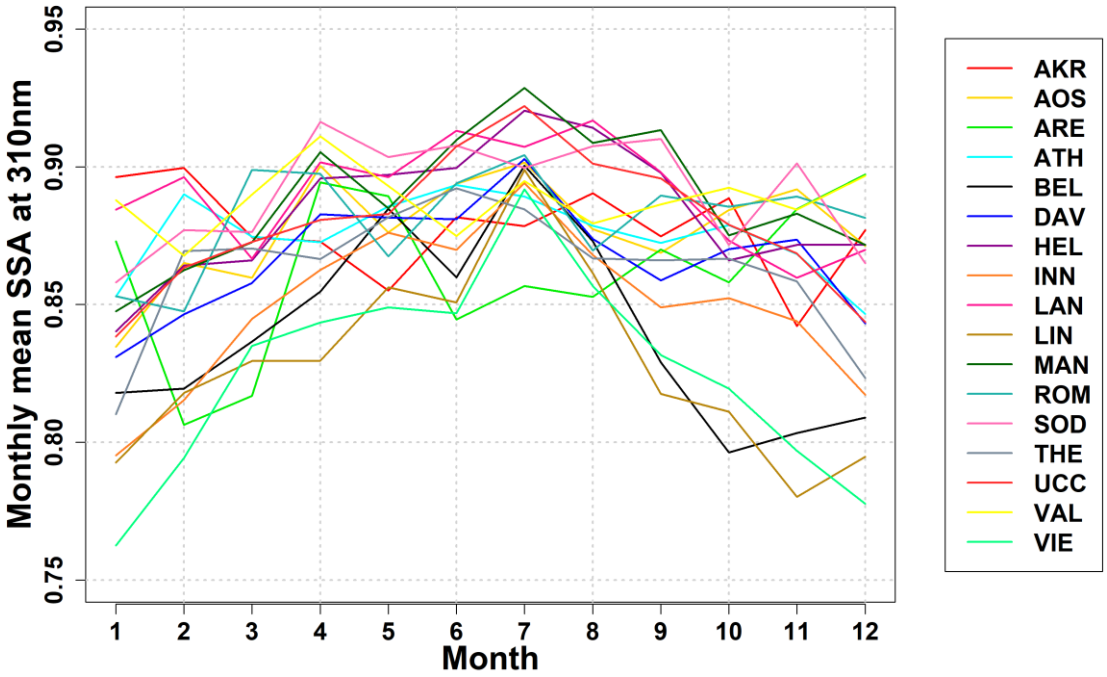

Figure 9: The monthly mean (i.e. 1-12 = Jan-Dec) SSA levels for all ground stations as derived by the MACv2 database.

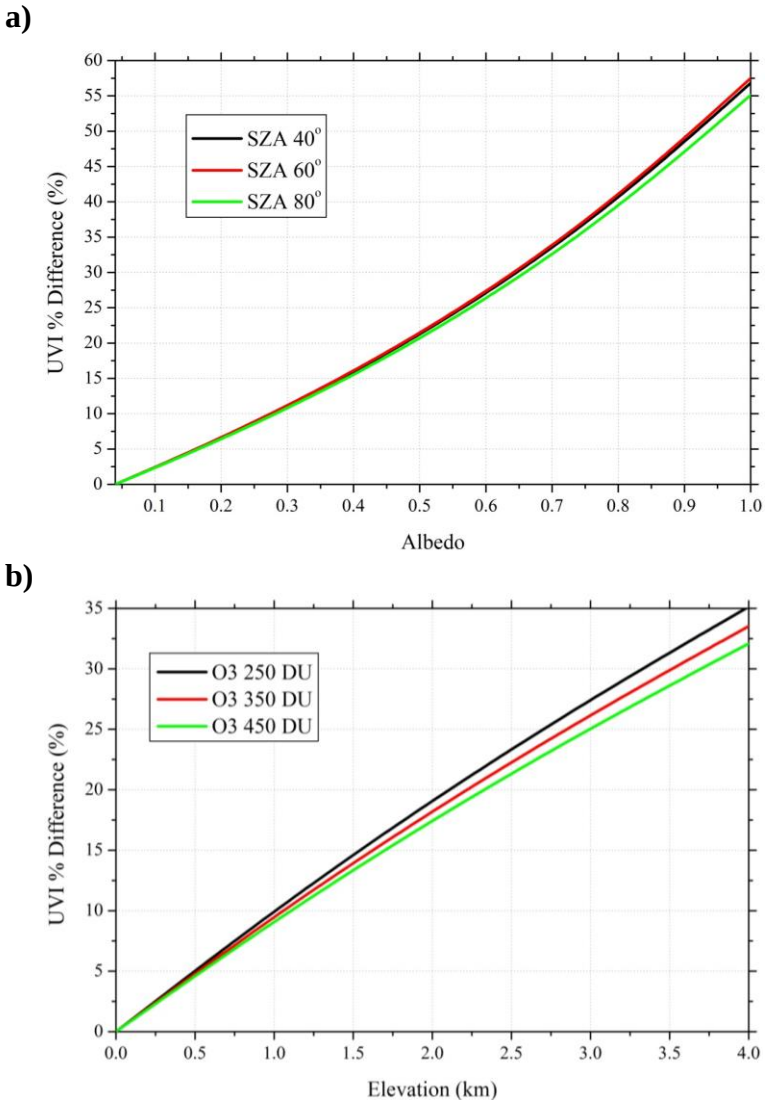

Figure 10: The surface albedo effect on UVI as a function of percentage difference for various SZAs (a). The surface elevation effect on UVI as a function of percentage difference for various total ozone columns (b).

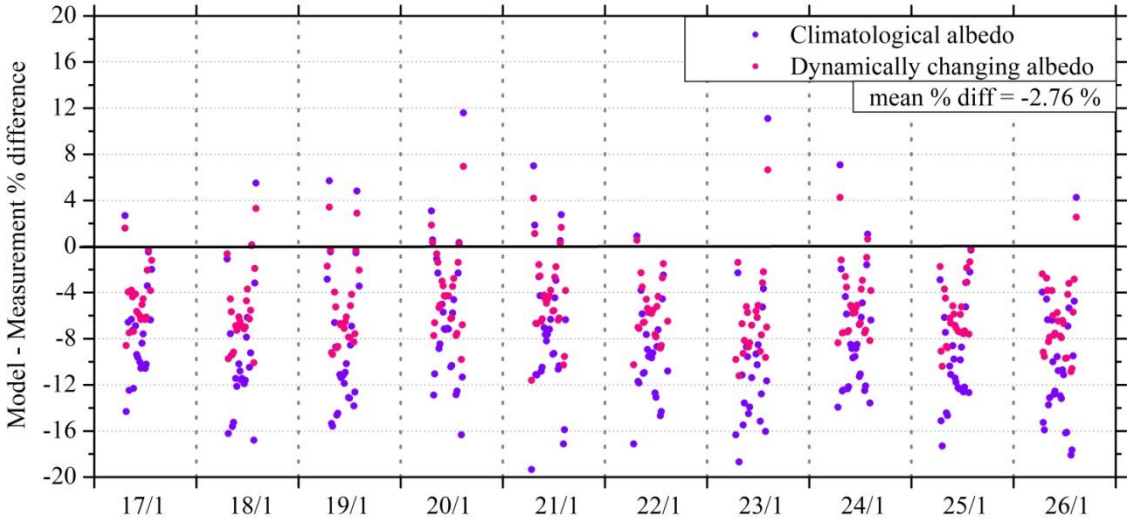

Figure 11: The effect of surface albedo correction on UVI for the Davos station. The climatological and the dynamically changing albedo in terms of percentage differences of modelled and ground measurements during a snow covered period (17/1 - 26/1) under clear sky conditions.

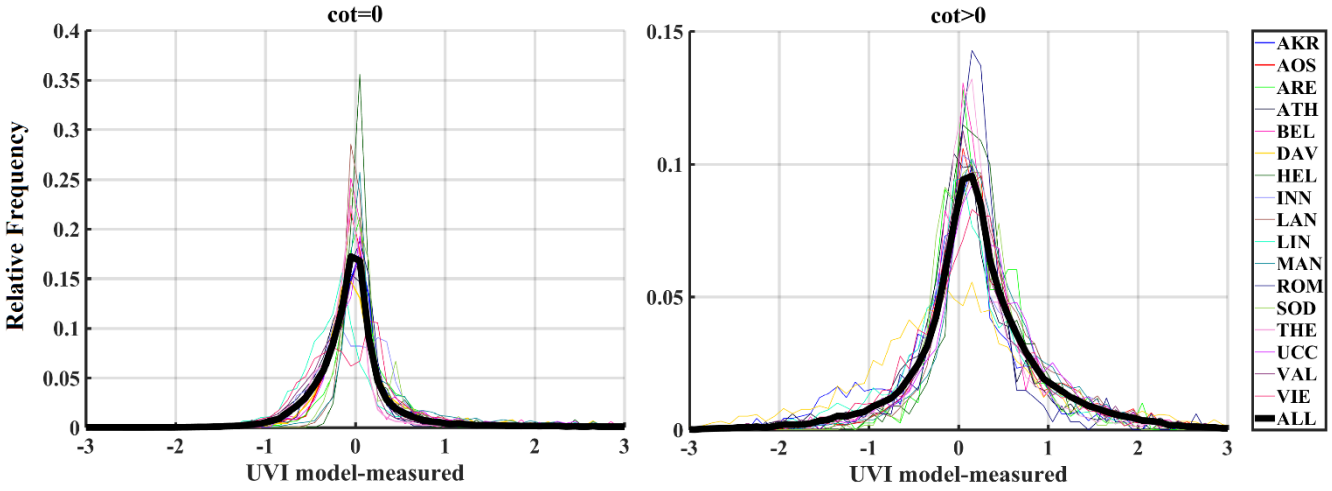

Figure 12: Relative frequency distribution of UVI residuals for all stations (coloured lines) and the mean (bold black line) for cloudless (left plot) and cloudy (right plot) conditions.

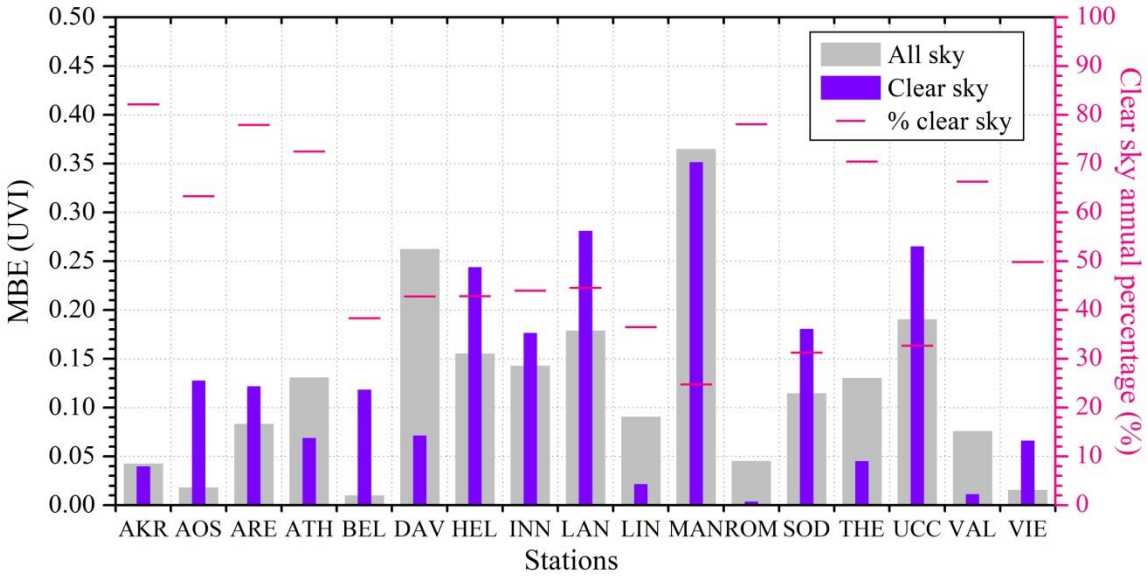

Figure 13: Mean bias error of the modelled UVI as compared to the ground-based measurements for all and clear sky conditions. The percentage of clear sky data time steps was also plotted with red lines.

Table 6: Percentage of data for UVIOS underestimation (A1-A3) and overestimation (B1-B3) under clear and cloudy sky conditions for various UVI difference (modelled-ground) classes.

Difference of UVI	< -1.0 (A1)	< -0.5 (A2)	< 0.0 (A3)	> 0.0 (B3)	> 0.5 (B2)	> 1.0 (B1)
% of data COT > 0	3.6	11.5	37.5	62.5	24.8	11.1
% of data COT = 0	0.9	10.2	45.4	54.6	11.4	4.2

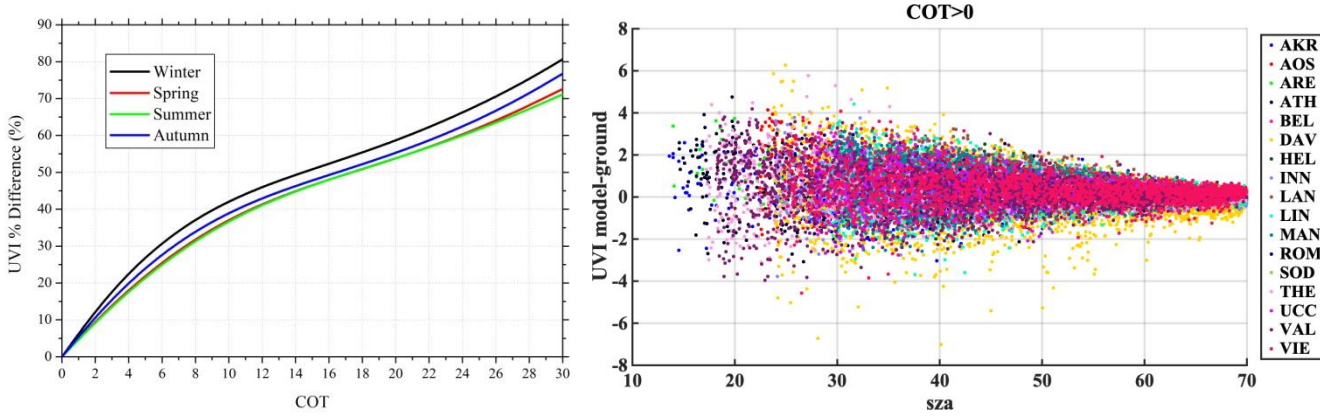

Figure 14: The average COT effect on UVI as a function of percentage difference for all seasons (left) and scatterplot of the UVI difference under cloudy sky conditions for all stations (right).

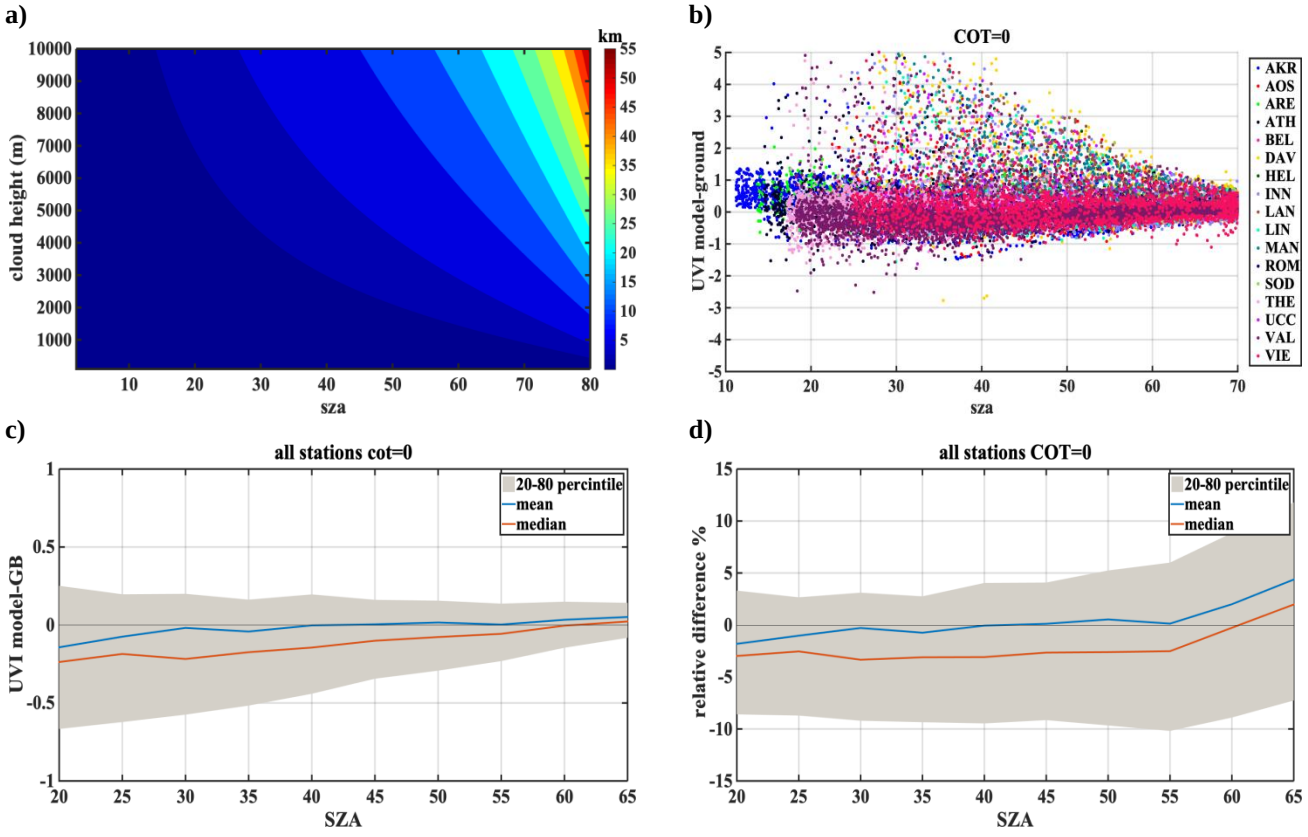

Figure 15: The shadow volume at the surface level of a cloud relative to the SEVIRI angle view, as a function of cloud height and SZA (a). Scatterplot of the UVI difference under clear sky conditions for all stations (b). UVI mean, median and 20-80 percentile differences (c) and percentage differences (d) derived by the UVIOS as compared to the ground-based measurements for clear sky conditions as a function of SZA.

Appendix A

The following set of Figures (A.1 – A.17) show for all stations, in the upper row, density scatterplots of measured and modeled UVI for all sky and clear sky conditions, followed by the correlation coefficient (R) and the number of data points (N) used in the analysis. In the middle row, the normalized probability histogram of differences is depicted, while the lower row presents the boxplot of differences as a function of SZA, representing median (red lines), mean (blue dotted lines), 25-75 percentiles (blue boxes) and 5-95 whiskers (dotted lines).

We have categorized the stations mostly based on cloud cover as Mediterranean, Central Europe, High altitude and High latitude. Each of the station has its own characteristics in terms of atmospheric conditions and parameters affecting the UVI reaching the ground. A summary of the results with possible explanation of the differences observed are shown here. The Mediterranean region includes the stations THE, ATH, AKR, ROM, VAL and ARE. Analysis of TOC showed that in most of the cases UVI mean differences are less than 0.1 in general while a negative bias between TOC and the ground measurements was seen to be highest for ROM (-9.9) that corresponds to the UVI difference of 0.3. Impact of AOD uncertainty showed the correlation coefficient between the modelled and the measured UVI values above 0.7 for most of the stations while it was as high as 0.91 for ARE. The mean bias between the modelled and measured UVI for clear sky condition was found to be less than that for the all sky condition for the stations AKR, ATH and THE that had most days of the year as cloud-free (the clear sky percentage is above 70%). The mean bias between the modelled and measured UVI for clear sky condition was more than the all sky condition for ARE even though it had mostly clear skies throughout the year. The analysis of the combined effect of the aerosol and ozone at Thessaloniki revealed that the model showed a slight underestimation with real inputs (AERONET and Brewer) while overestimations for forecasted inputs (CAMS and TEMIS). However, the coefficient of correlation was found to be as 0.989 and 0.992 for the model with forecasted and real inputs, respectively. Stations of this classification have the single scattering albedo ranging from 0.76 to 0.93, with most of them having SSA values between 0.83 to 0.93 except stations ARE and THE that had relatively smaller SSA values (0.76-0.9) and greater variability, and large MBE. AKR station comparison showed some UVIOS calculated UVI at higher levels than the ground-based measurements especially in low SZA's. However, ground-based UVI measurements seem more unrealistic than the UVIOS calculated UVI for summer local noon conditions as modeled UVIs with real AOD and TOC measurements at the area tend to agree with UVIOS outputs.

The second classification is the Central European regions including AOS, UCC, BEL, MAN, LIN, VIE and INN. The median of the absolute UVI differences between the model and the measurement for all sky condition were higher for MAN and UCC while for others it was close to zero. Larger UVI difference of -0.22 due to TOC uncertainty impact was observed for AOS which might be due to large values of UVI at higher altitude as the positive bias is highest for AOS station (7.6). The UVIOS MBE and RMSE statistical scores for analyzing AOD uncertainty impact showed a mean positive bias up to 0.071 for all the stations except UCC which is showed a mean negative bias of 0.007. The mean bias between the modelled and measured UVI for clear sky condition was more than the all sky condition for AOS even though it had mostly clear skies throughout the year. BEL, UCC and VIE showed more MBE for clear sky condition than the all sky condition as they have mostly cloudy skies

throughout the year (clear sky annual percentage less than 50%). However, stations LIN and MAN also have more MBE for clear sky condition even though they have most days of the year as cloudy (clear sky annual percentage less than 45%). Analysis of AOD uncertainty showed that UVI difference was highest for VIE than the other stations. The monthly values of the single scattering albedo used in UVIOS ranged from 0.76 to 0.93 for stations AOS, UCC and MAN, with most of them having SSA values between 0.83 to 0.93, and relatively small variability. While, the stations BEL, INN, LIN and VIE had relatively smaller SSA values (0.76-0.9) and greater variability than the other stations and most of these stations have shown large MBE.

The high altitude station is DAV and high latitude stations include LAN, HEL and SOD. DAV have less MBE for clear sky condition even though they have most days of the year as cloudy (clear sky annual percentage less than 45%). DAV and MAN show worse statistical behavior for clear sky, which is probably caused by misclassification of cloudy pixels. For DAV this could be explained by the complex mountainous topography of the area. Large UVI differences in SOD and HEL indicate higher introduced uncertainties over higher latitudes. Higher aerosol levels in the atmosphere tend to lower the UVI. Highest difference in UVI is observed for the stations HEL, SOD and VIE. Since, the aerosol level at the stations HEL and SOD is very low this leads to higher UVI which can be the reason for the small UVI differences observed for these stations. The stations of this classification have mostly cloudy skies throughout the year (clear sky annual percentage less than 50%) and have more MBE for clear sky condition than the all sky condition. This might be due the fact that the clouds are not captured well at a point station and a cloudy sky might have been considered as a clear sky. Higher UVI difference was observed for HEL and SOD as a result of AOD uncertainty analysis which might be due to the low aerosol content of these stations due to higher latitude that leads to higher UVI values.

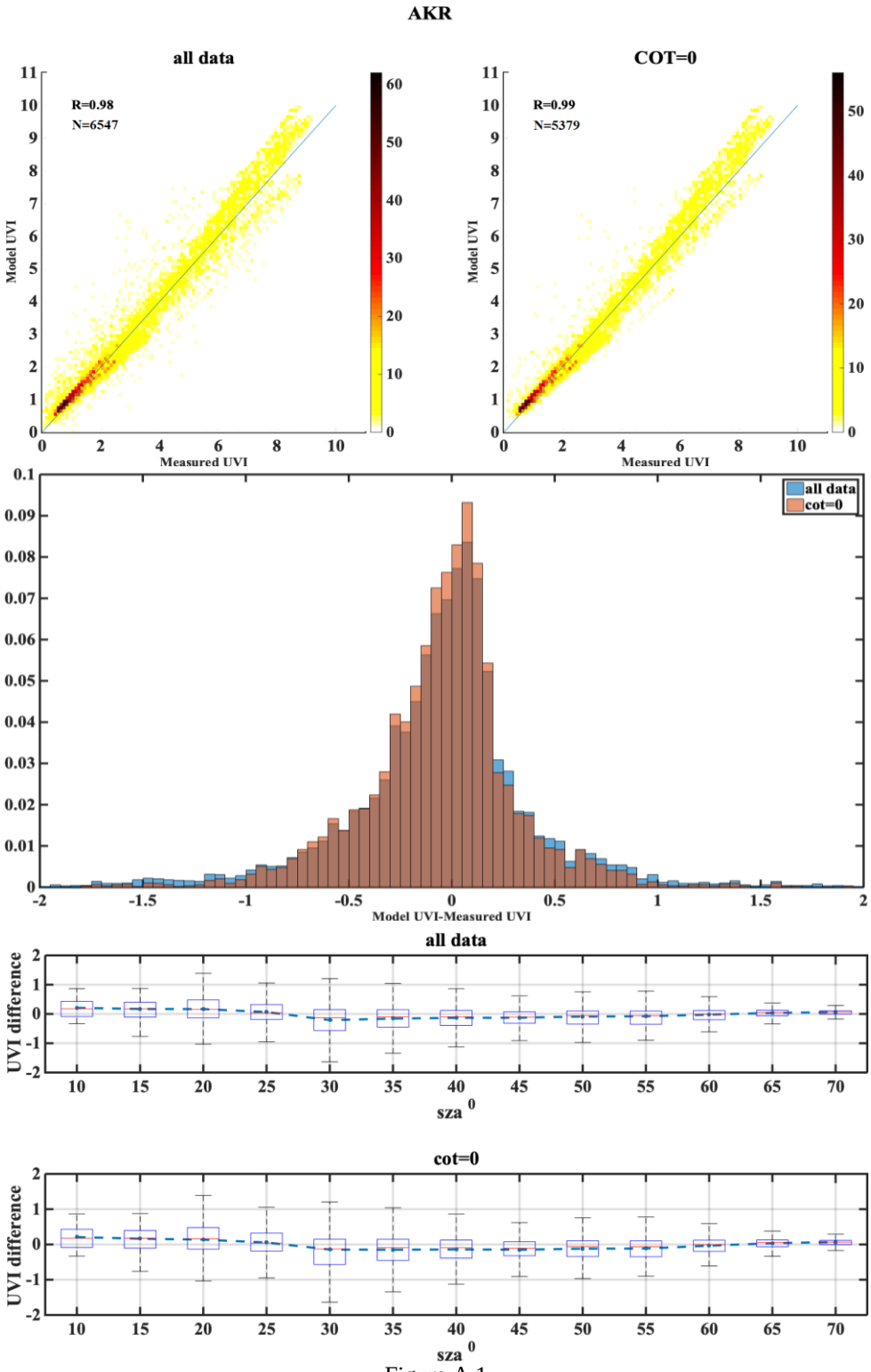
AKR
all data
R=0.98
N=6547
Model UVI
Measured UVI
COT=0
R=0.99
N=5379
Model UVI
Measured UVI
all data
cot=0
Model UVI-Measured UVI
all data
UVI difference
sza 0
cot=0
UVI difference
sza 0

Figure A.1

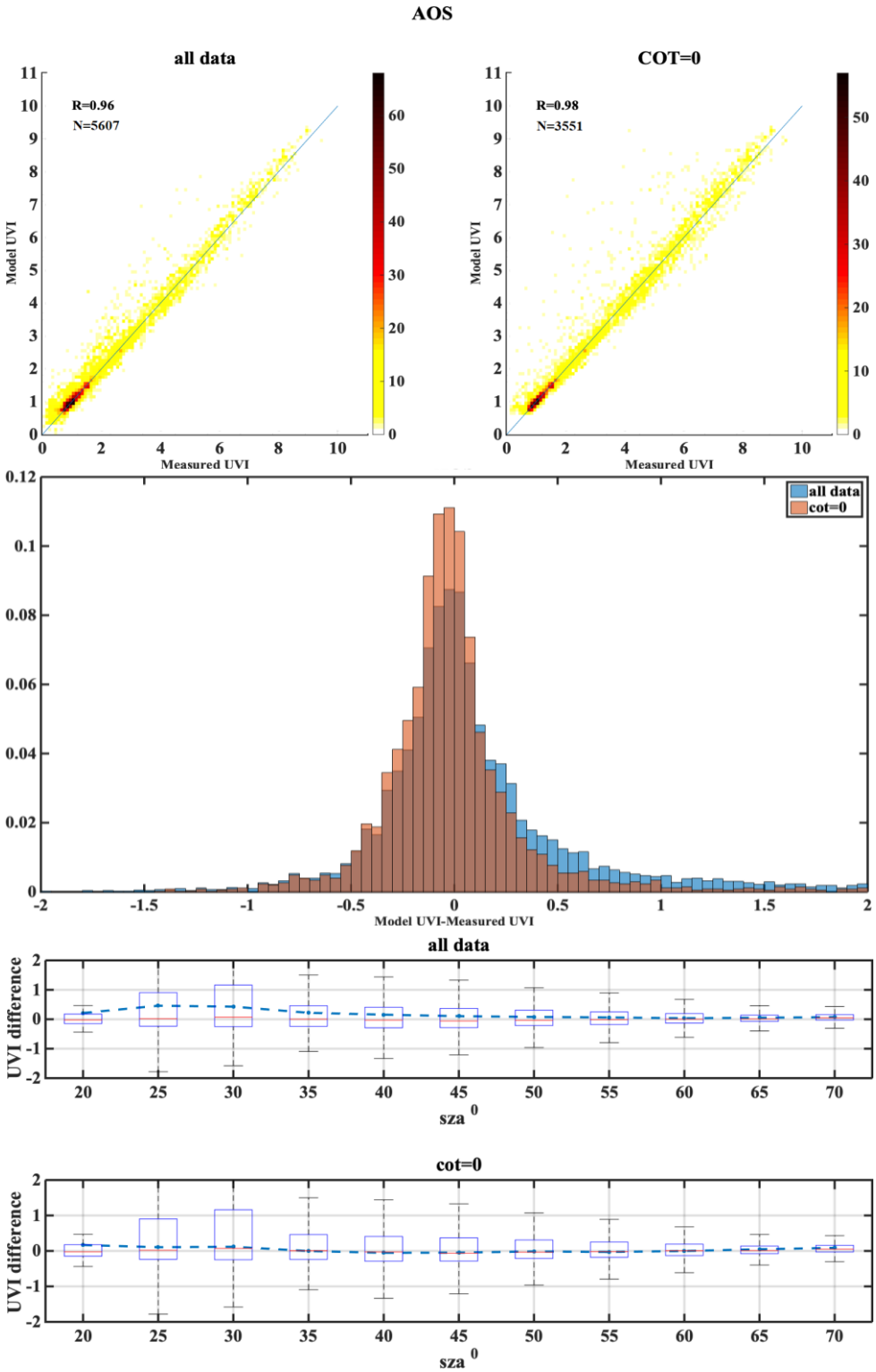
AOS
all data
R=0.96
N=5607
Model UVI
Measured UVI
COT=0
R=0.98
N=3551
Model UVI
Measured UVI
all data
cot=0
Model UVI-Measured UVI
all data
UVI difference
sza 0
cot=0
UVI difference
sza 0

Figure A.2

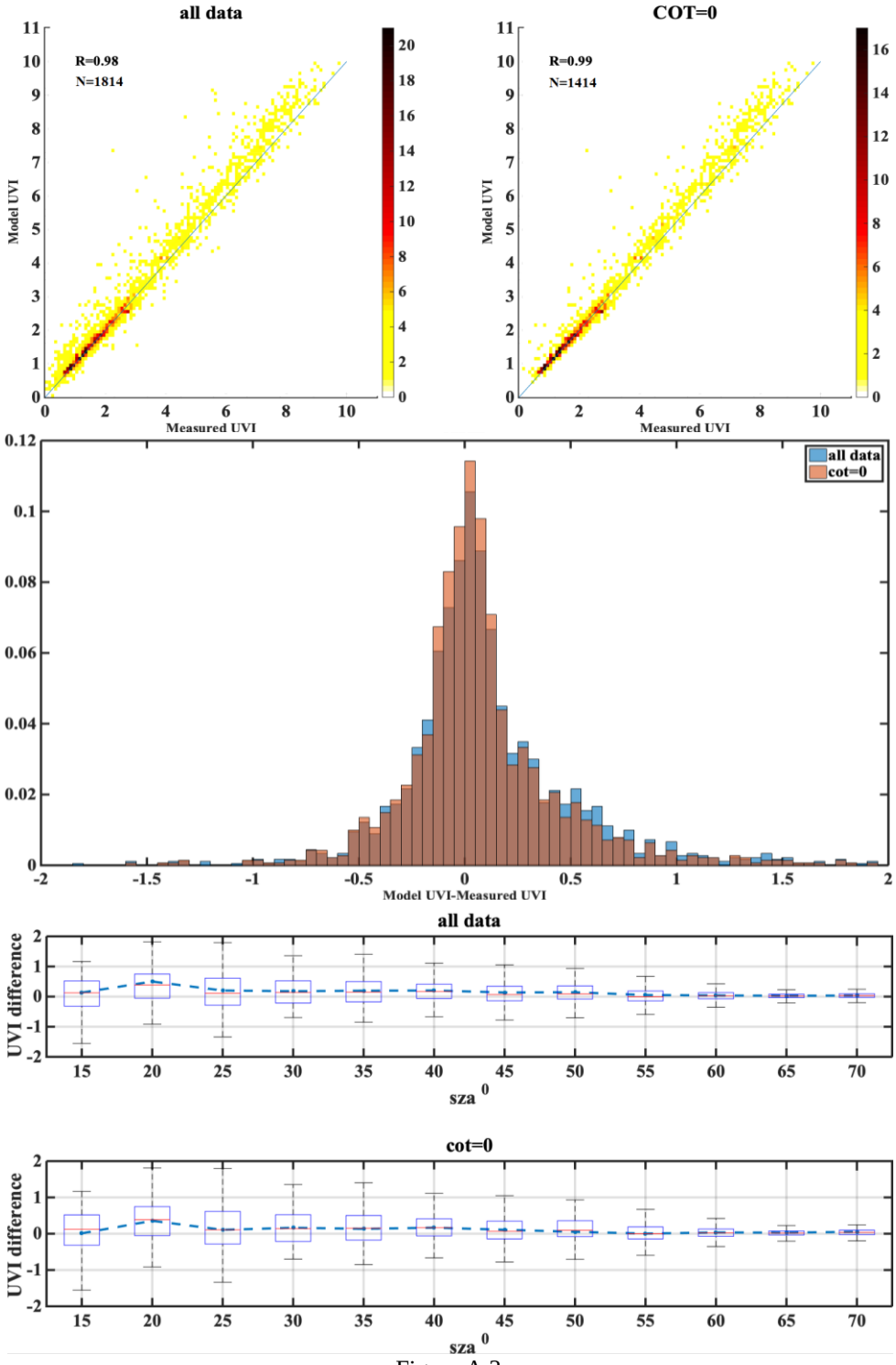
all data
R=0.98
N=1814
Model UVI
Measured UVI
COT=0
R=0.99
N=1414
Model UVI
Measured UVI
all data
cot=0
Model UVI-Measured UVI
all data
UVI difference
sza 0
cot=0
UVI difference
sza 0

Figure A.3

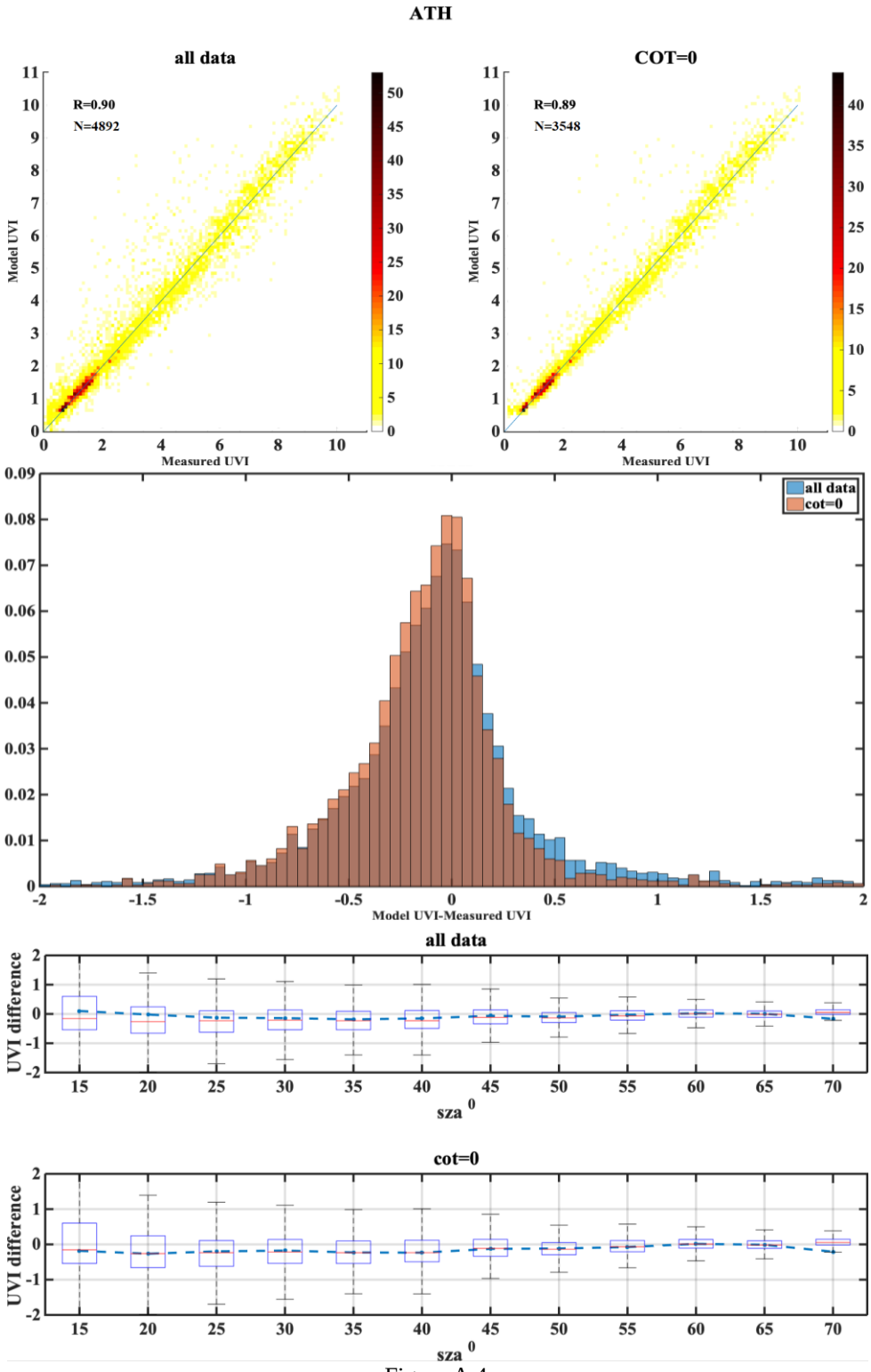
ATH
all data
R=0.90
N=4892
Model UVI
Measured UVI
COT=0
R=0.89
N=3548
Model UVI
Measured UVI
all data
cot=0
Model UVI-Measured UVI
all data
UVI difference
sza 0
cot=0
UVI difference
sza 0

Figure A.4

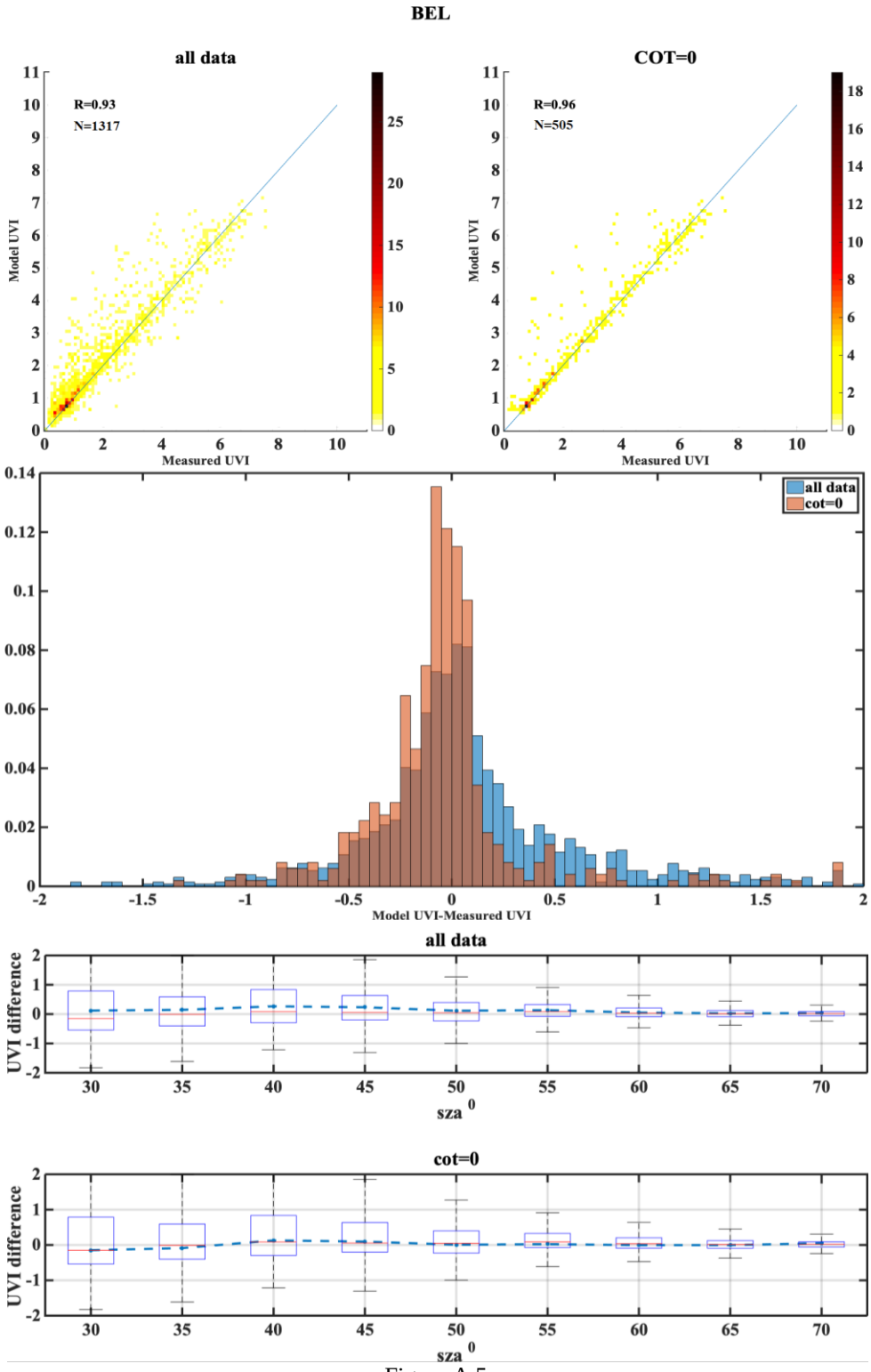
BEL
all data
R=0.93
N=1317
Model UVI
Measured UVI
COT=0
R=0.96
N=505
Model UVI
Measured UVI
all data
cot=0
Model UVI-Measured UVI
all data
UVI difference
sza 0
cot=0
UVI difference
sza 0

Figure A.5

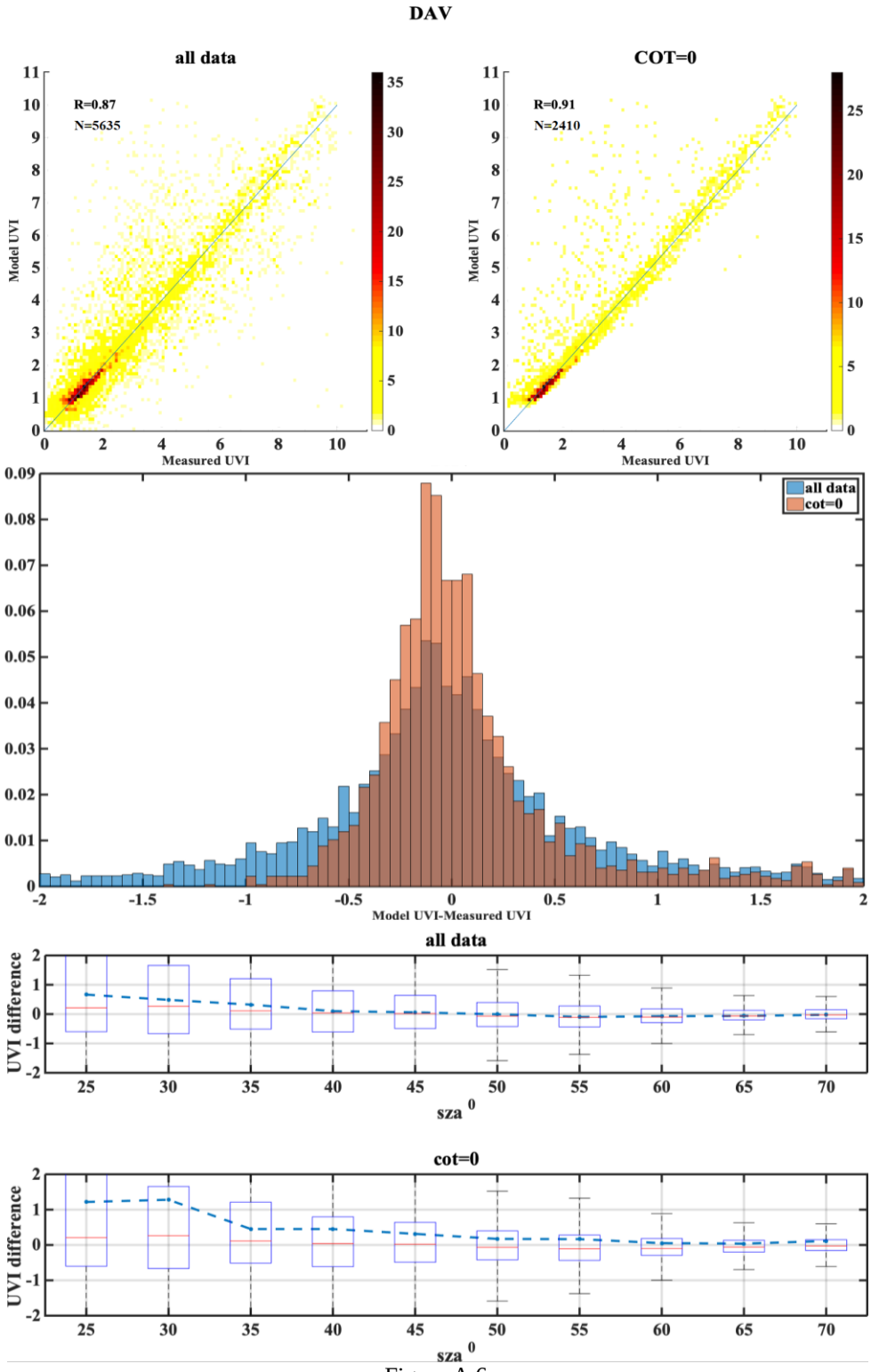
DAV
all data
R=0.87
N=5635
Model UVI
Measured UVI
COT=0
R=0.91
N=2410
Model UVI
Measured UVI
all data
cot=0
Model UVI-Measured UVI
all data
UVI difference
sza 0
cot=0
UVI difference
sza 0

Figure A.6

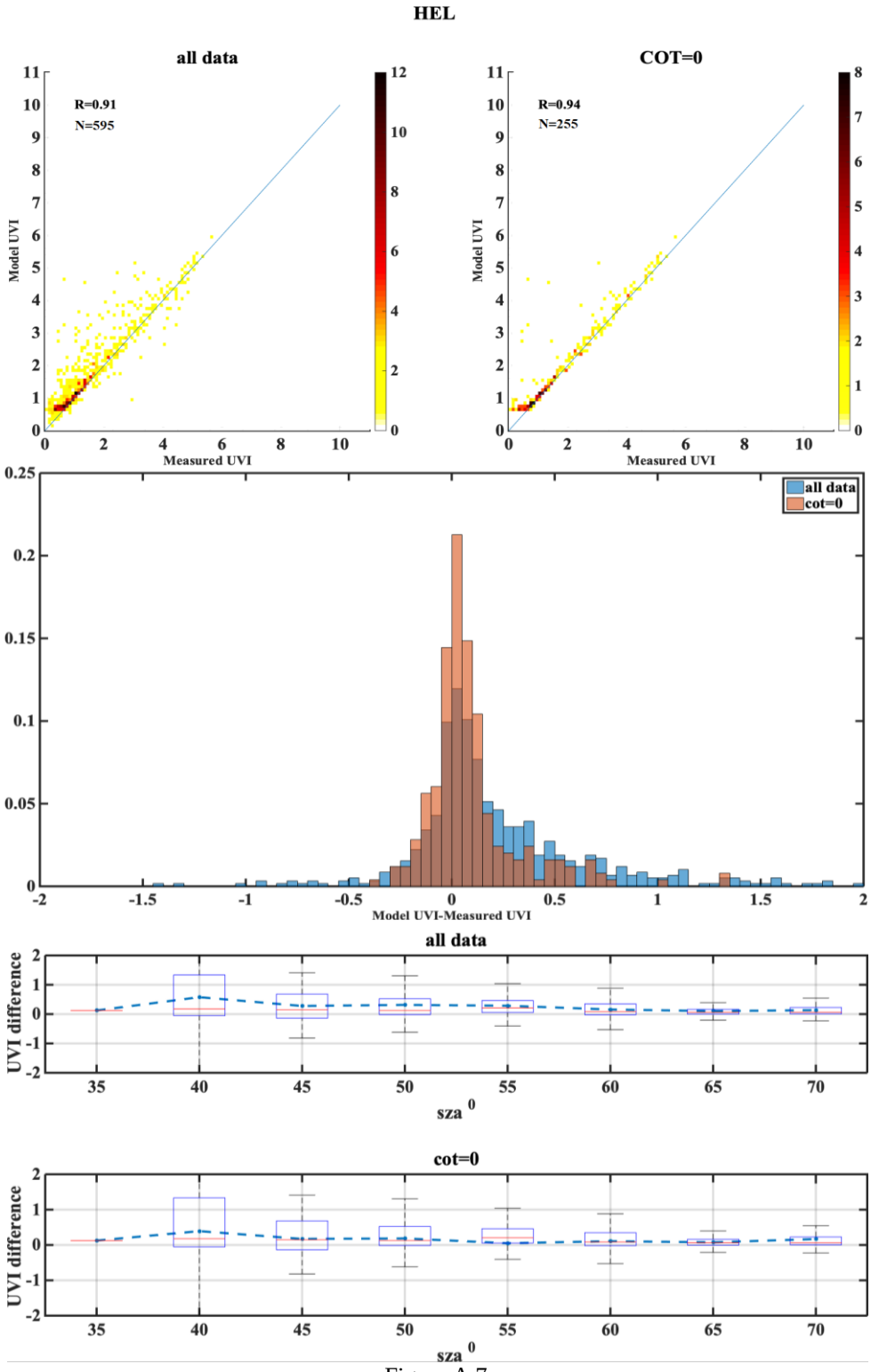
HEL
all data
R=0.91
N=595
Model UVI
Measured UVI
COT=0
R=0.94
N=255
Model UVI
Measured UVI
all data
cot=0
Model UVI-Measured UVI
all data
UVI difference
sza 0
cot=0
UVI difference
sza 0

Figure A.7

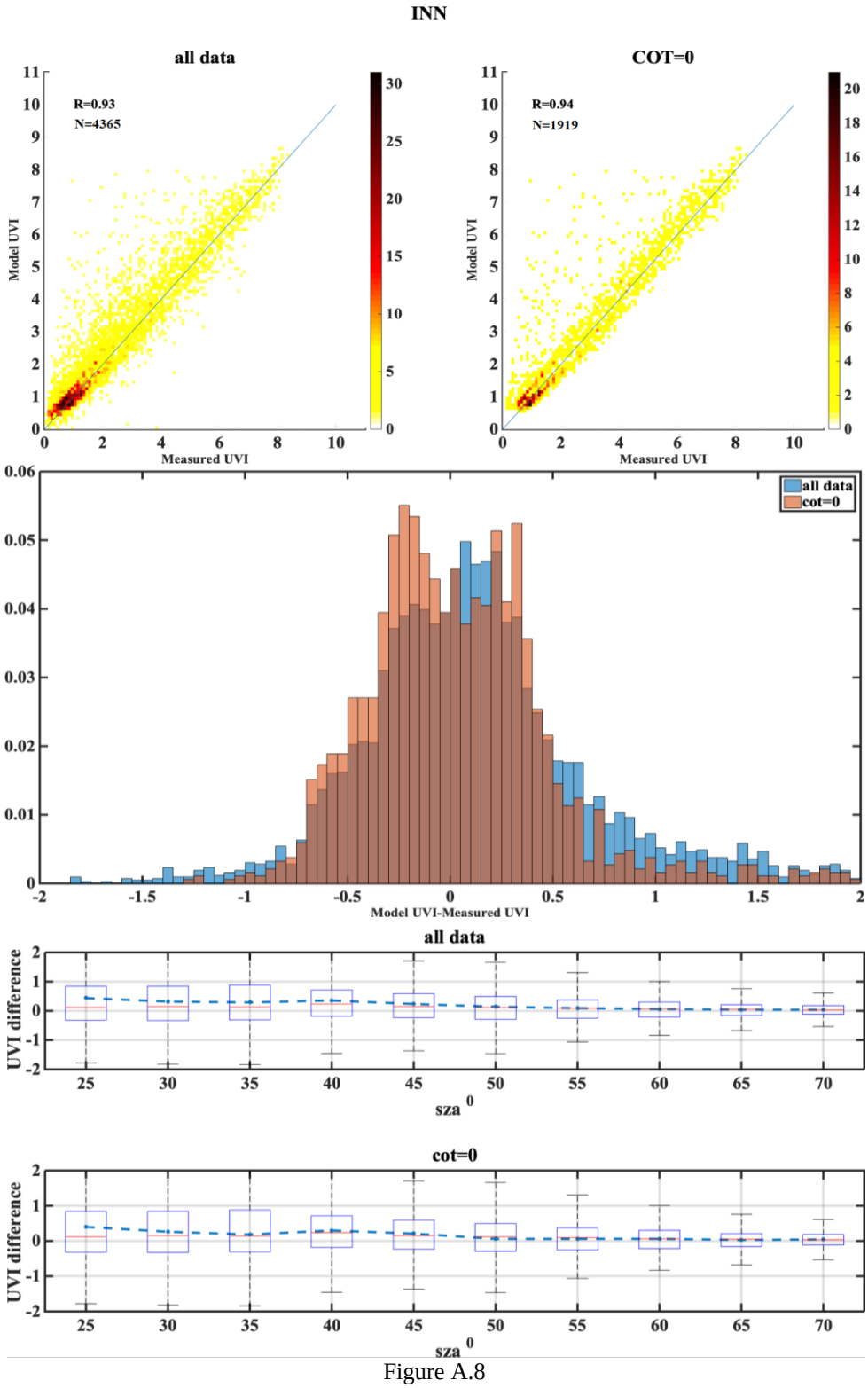
INN
all data
R=0.93
N=4365
Model UVI
Measured UVI
COT=0
R=0.94
N=1919
Model UVI
Measured UVI
all data
cot=0
Model UVI-Measured UVI
all data
UVI difference
sza 0
cot=0
UVI difference
sza 0

Figure A.8

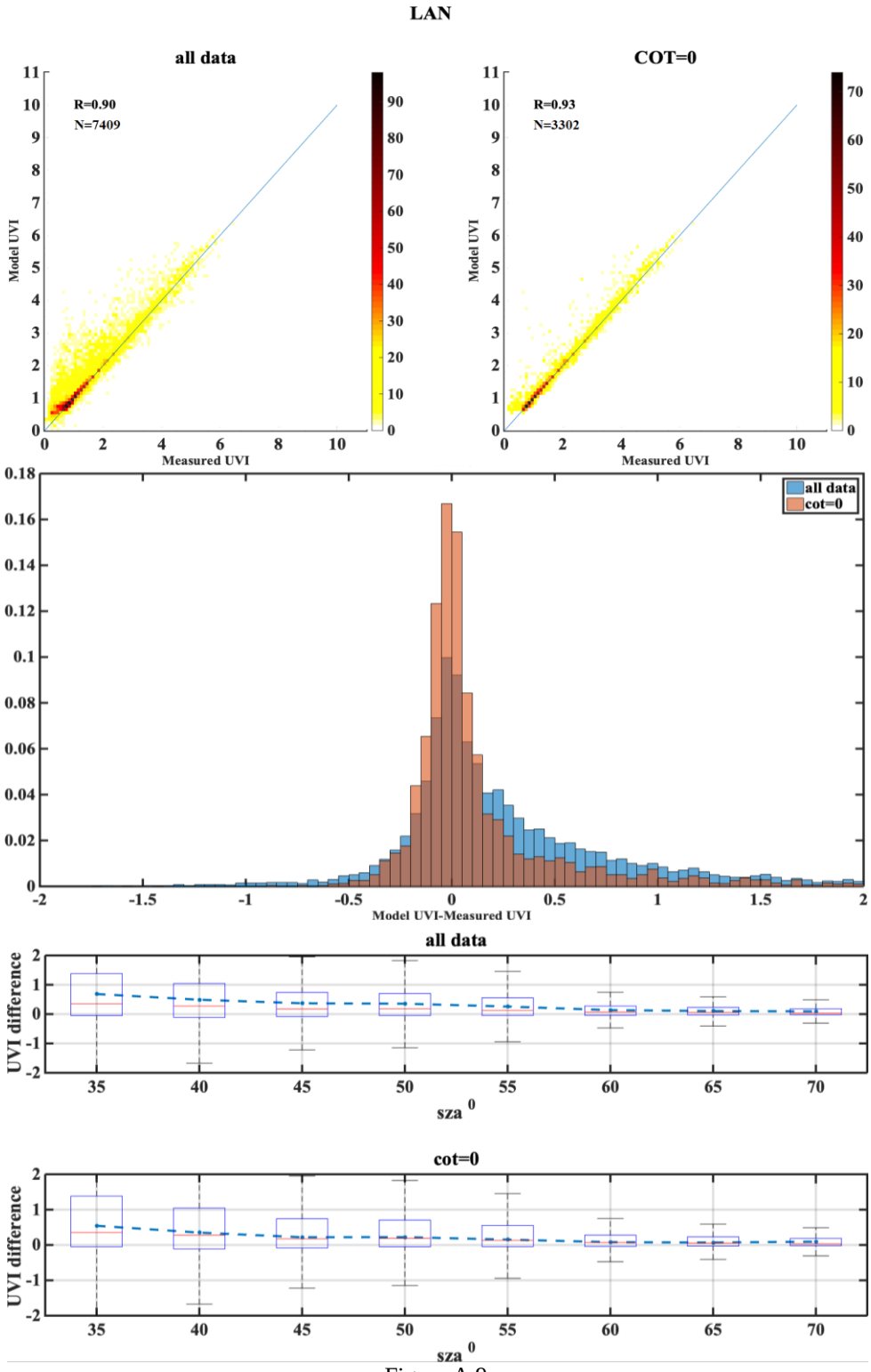
LAN
all data
R=0.90
N=7409
Model UVI
Measured UVI
COT=0
R=0.93
N=3302
Model UVI
Measured UVI
all data
cot=0
Model UVI-Measured UVI
all data
UVI difference
sza 0
cot=0
UVI difference
sza 0

Figure A.9

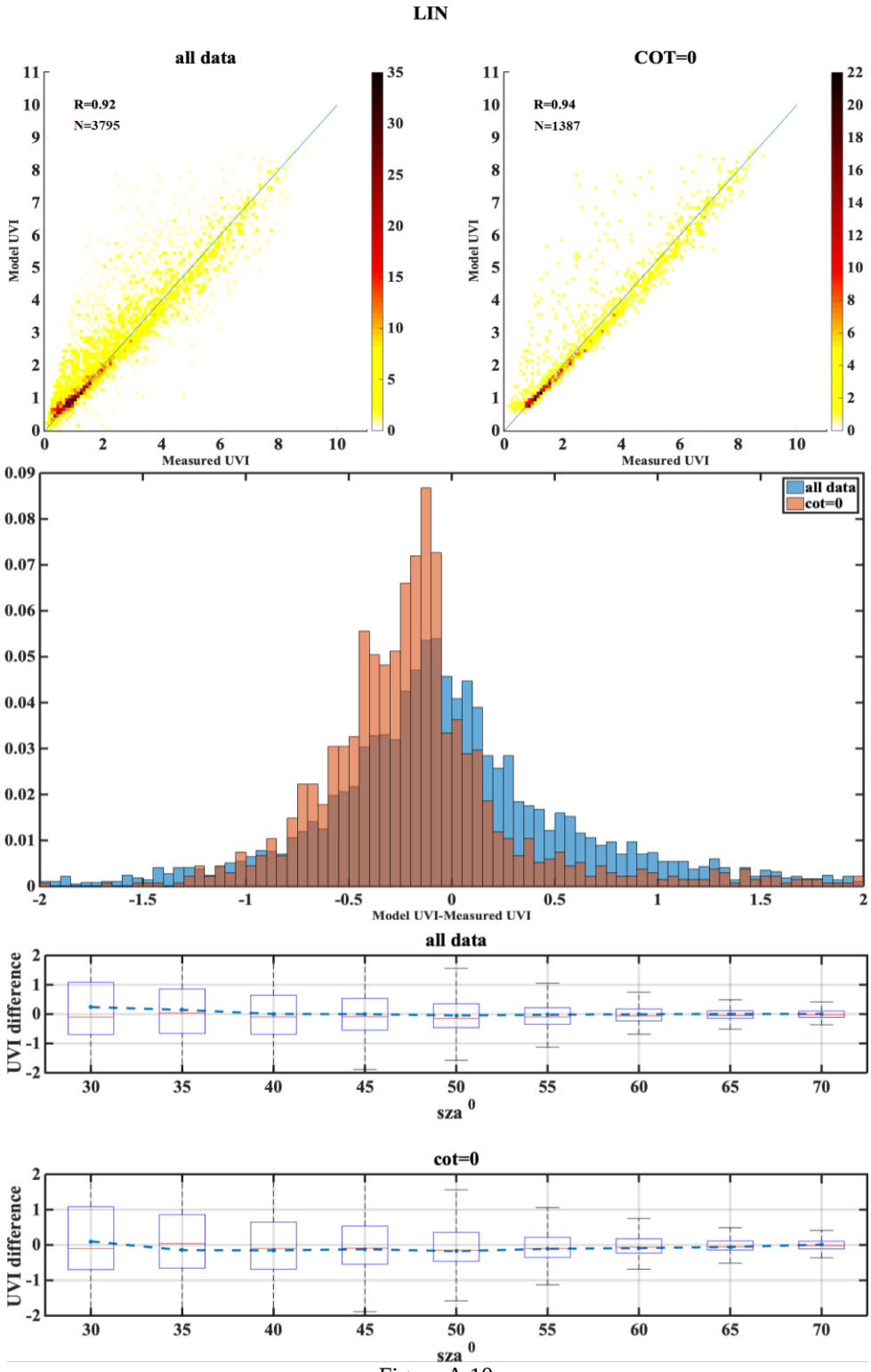
LIN
all data
R=0.92
N=3795
Model UVI
Measured UVI
COT=0
R=0.94
N=1387
Model UVI
Measured UVI
all data
cot=0
Model UVI-Measured UVI
all data
UVI difference
sza 0
cot=0
UVI difference
sza 0

Figure A.10

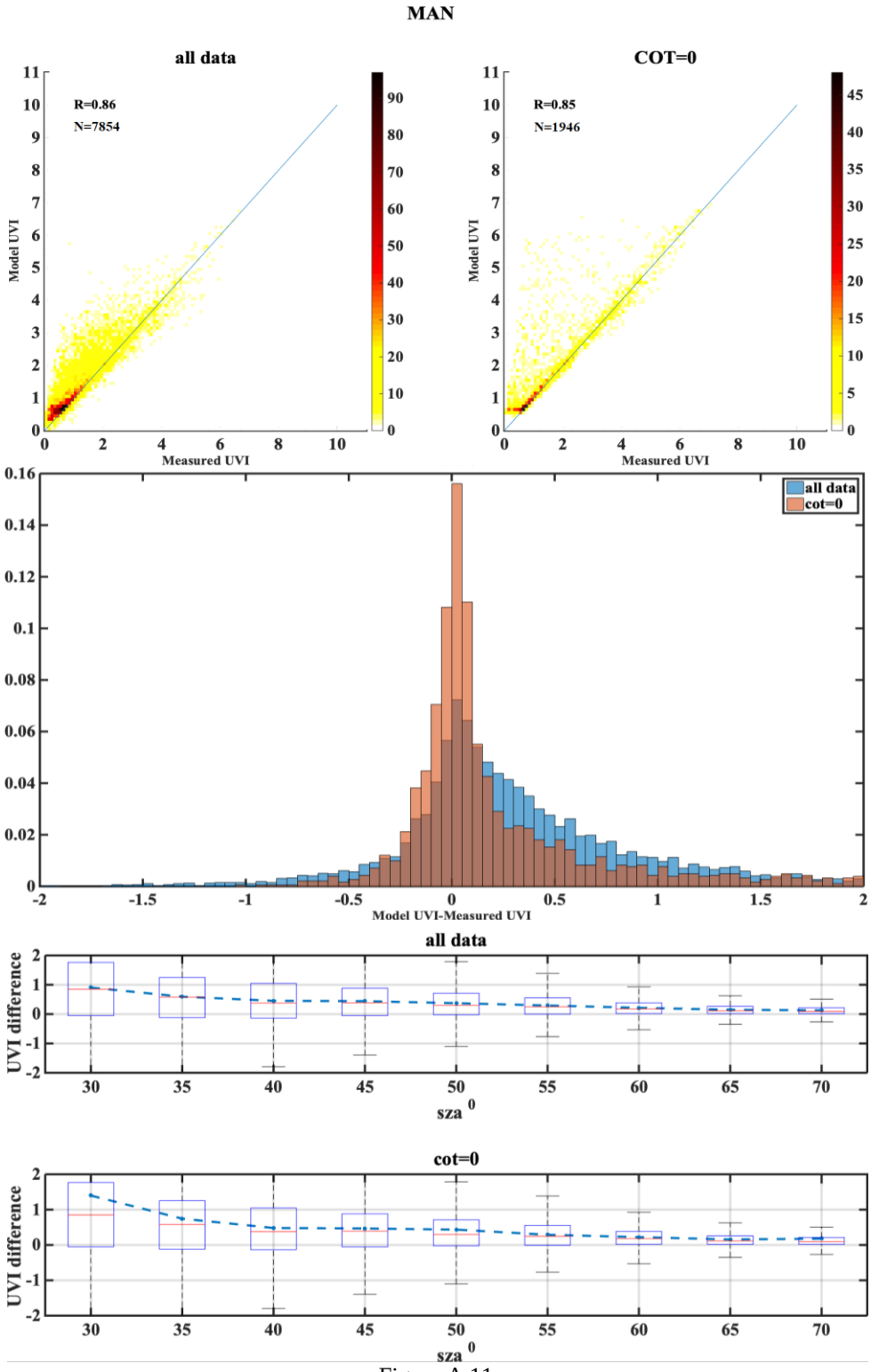
MAN
all data
R=0.86
N=7854
Model UVI
Measured UVI
COT=0
R=0.85
N=1946
Model UVI
Measured UVI
all data
cot=0
Model UVI-Measured UVI
all data
UVI difference
sza 0
cot=0
UVI difference
sza 0

Figure A.11

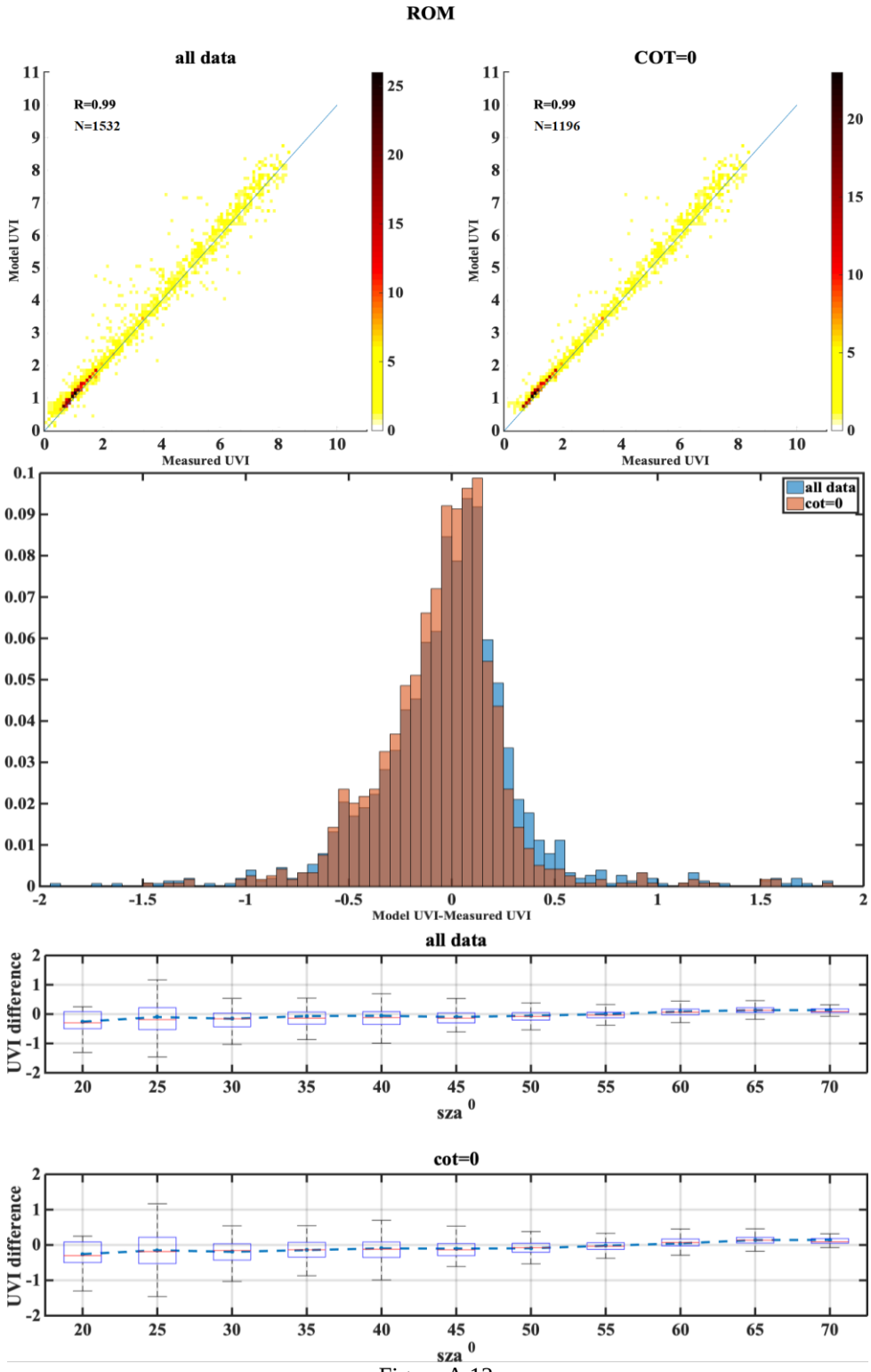
ROM
all data
R=0.99
N=1532
Model UVI
Measured UVI
COT=0
R=0.99
N=1196
Model UVI
Measured UVI
all data
cot=0
Model UVI-Measured UVI
all data
UVI difference
sza 0
cot=0
UVI difference
sza 0

Figure A.12

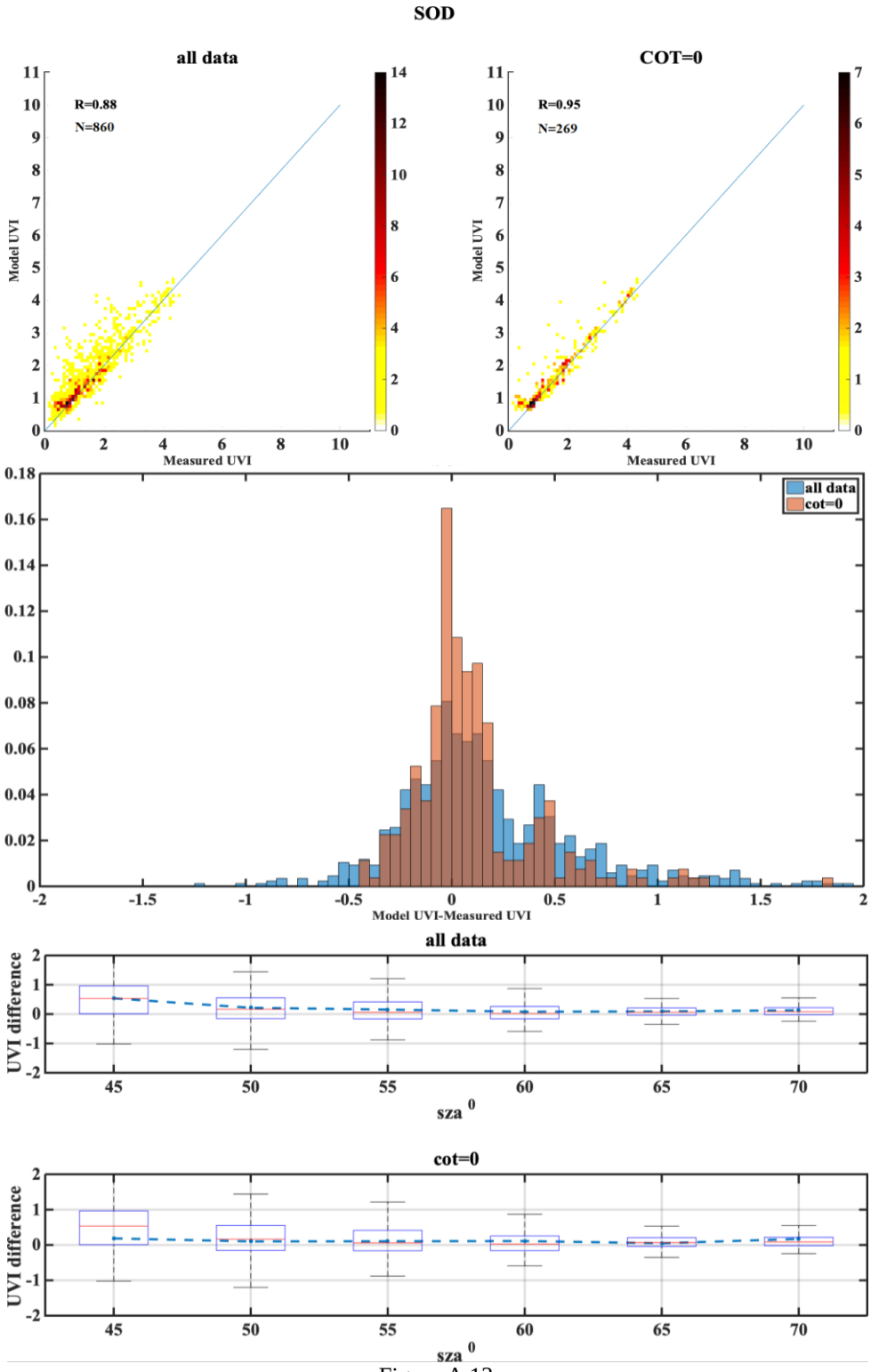
SOD
all data
R=0.88
N=860
Model UVI
Measured UVI
COT=0
R=0.95
N=269
Model UVI
Measured UVI
all data
cot=0
Model UVI-Measured UVI
all data
UVI difference
sza 0
cot=0
UVI difference
sza 0

Figure A.13

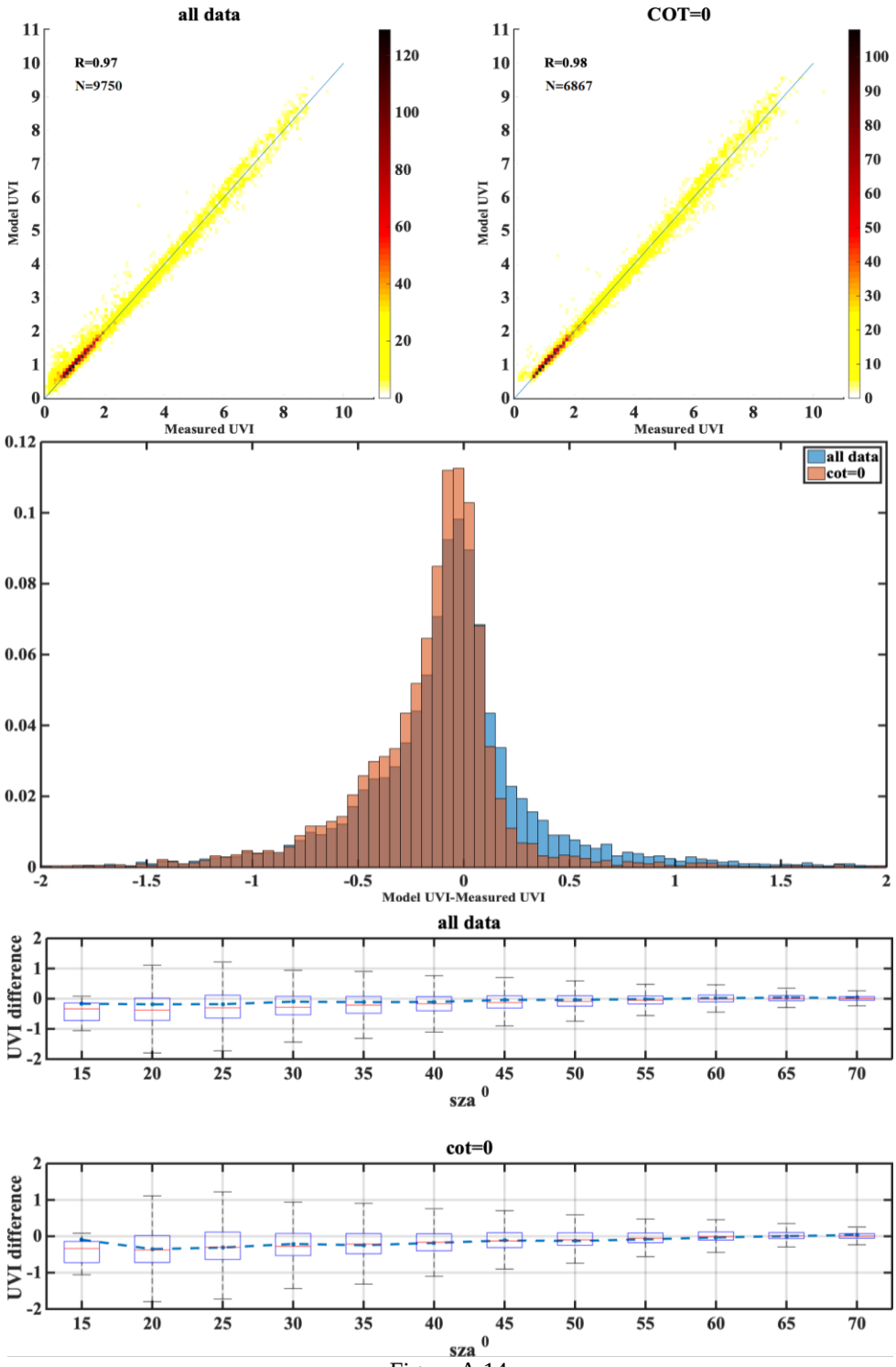
all data
R=0.97
N=9750
Model UVI
Measured UVI
COT=0
R=0.98
N=6867
Model UVI
Measured UVI
all data
cot=0
Model UVI-Measured UVI
all data
UVI difference
sza 0
cot=0
UVI difference
sza 0

Figure A.14

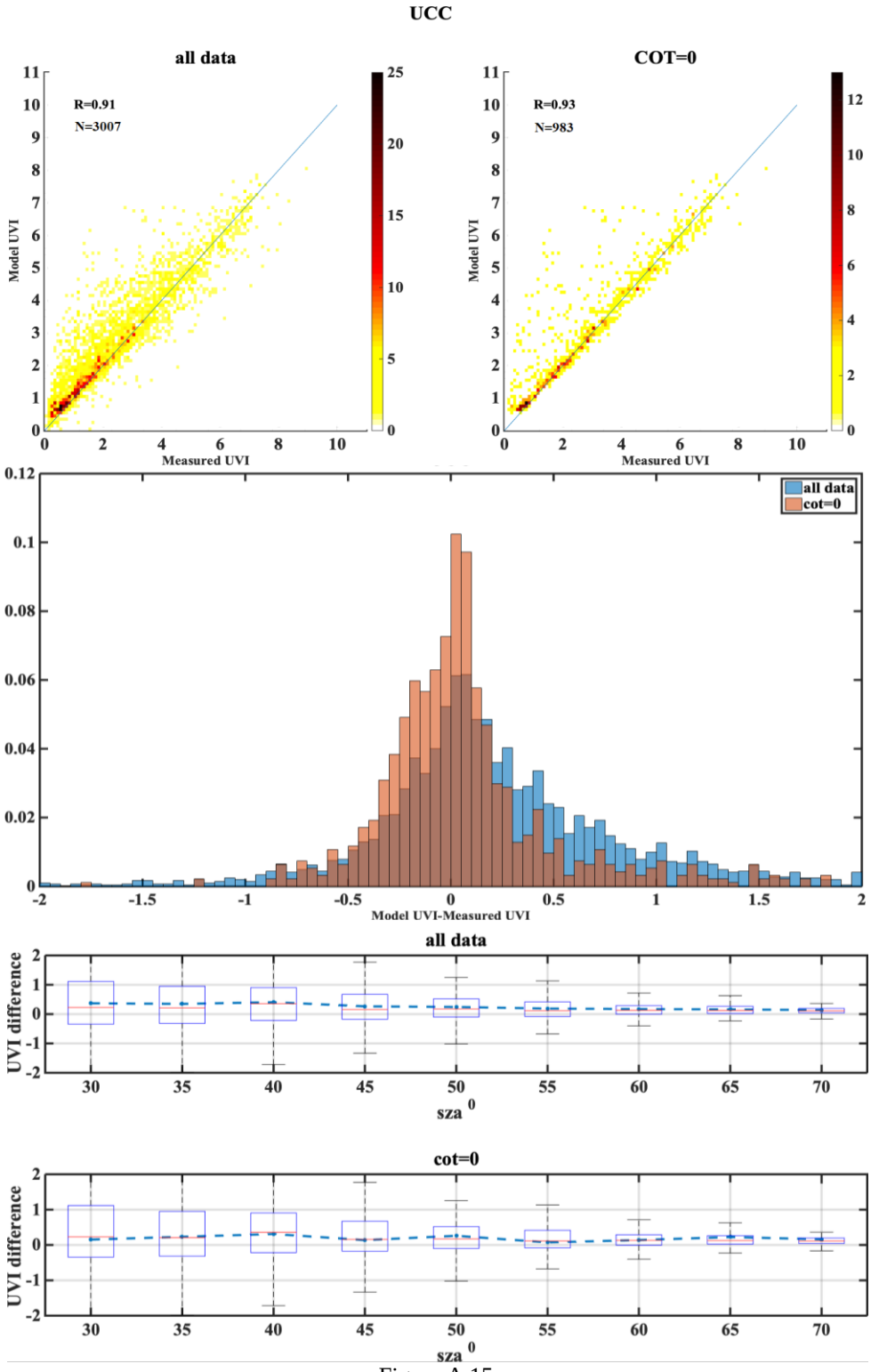
UCC
all data
R=0.91
N=3007
Model UVI
Measured UVI
COT=0
R=0.93
N=983
Model UVI
Measured UVI
all data
cot=0
Model UVI-Measured UVI
all data
UVI difference
sza 0
cot=0
UVI difference
sza 0

Figure A.15

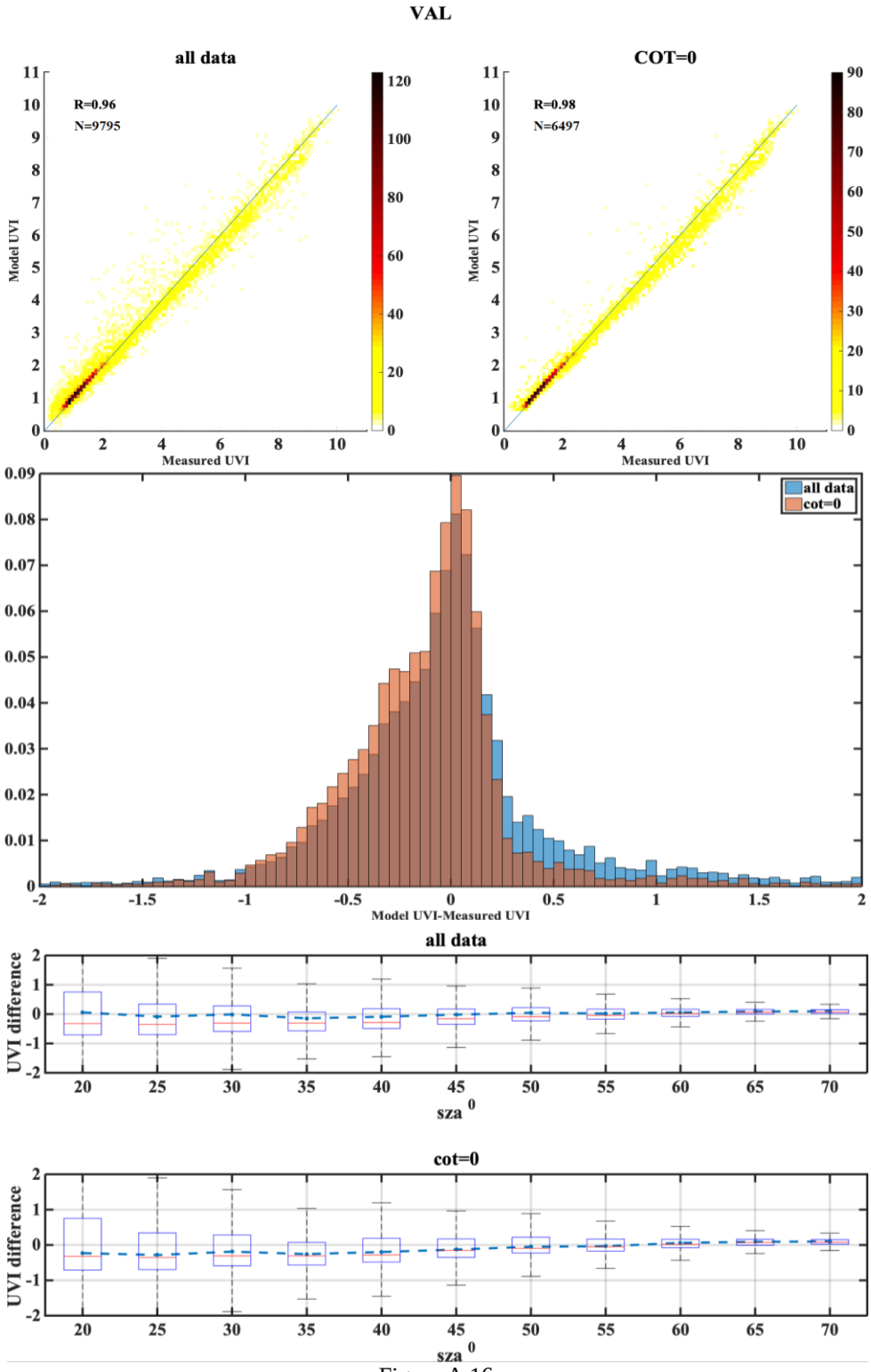
VAL
all data
R=0.96
N=9795
Model UVI
Measured UVI
COT=0
R=0.98
N=6497
Model UVI
Measured UVI
all data
cot=0
Model UVI-Measured UVI
all data
UVI difference
sza 0
cot=0
UVI difference
sza 0

Figure A.16

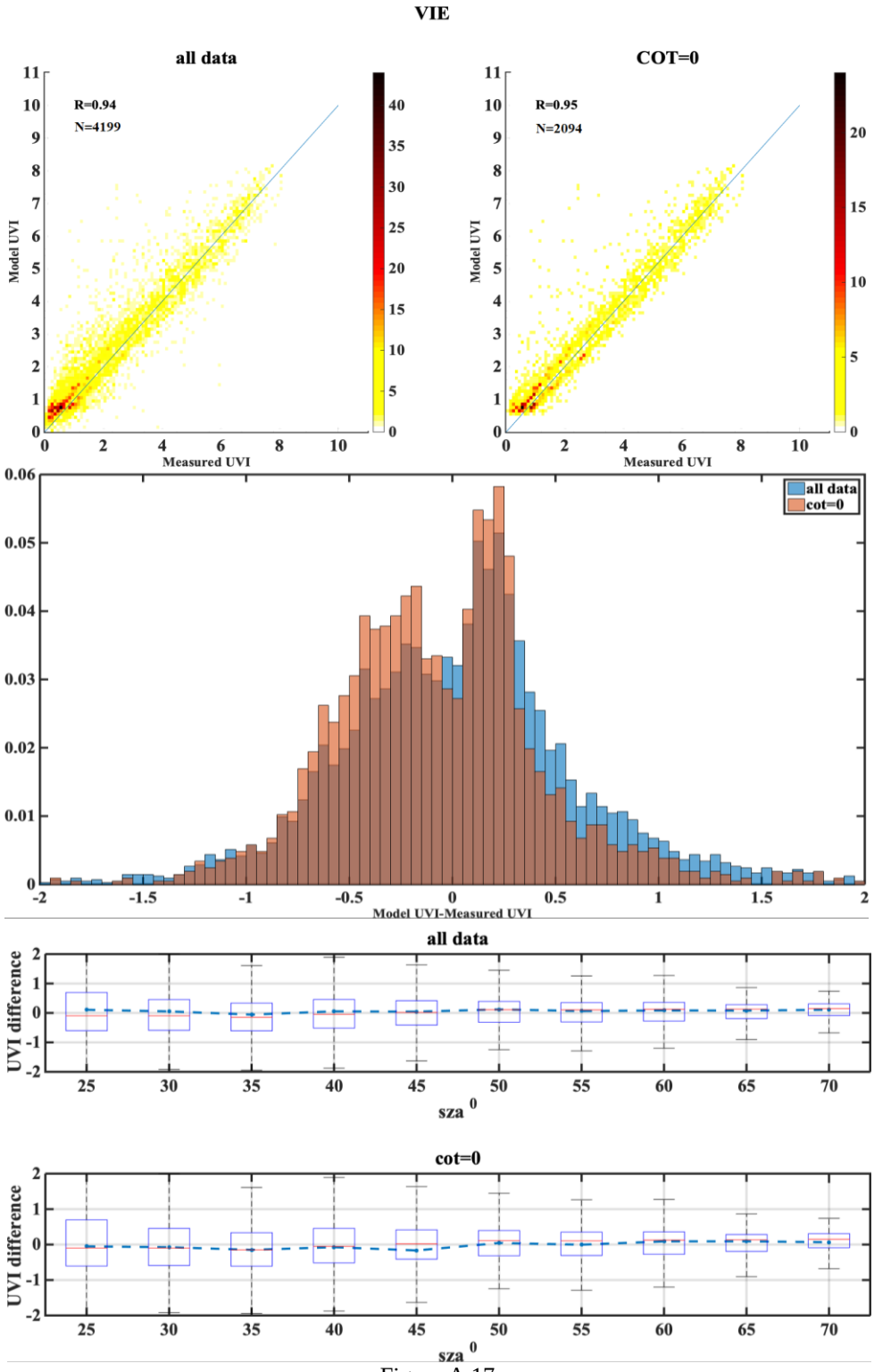
VIE
all data
R=0.94
N=4199
Model UVI
Measured UVI
COT=0
R=0.95
N=2094
Model UVI
Measured UVI
all data
cot=0
Model UVI-Measured UVI
all data
UVI difference
sza 0
cot=0
UVI difference
sza 0

Figure A.17